Finger-Joint Optimization of Spruce Lumber using Finite Element and Statistical Modelling

By

Mohamed Essam Abdelazim Ahmed Said

A Thesis Submitted to the School of Graduate
Studies in Partial Fulfillment of the
Requirements for the Degree of
Master of Engineering

Faculty of Engineering and Applied Science

Memorial University of Newfoundland

October 2018

St. John's Newfoundland and Labrador Canada

ABSTRACT

The primary objective of this thesis was to investigate and explore the feasibility of using a numerical 3-D finite element analysis (FEA) and statistical design of experiment methodology (DOE) to optimize finger-joint (FJ) configuration. This thesis provides guidelines to achieve structural behaviour of finger-joined elements that approaches non-finger-joined (NFJ) lumber. The optimum configurations will improve strength, save time, and money.

A numerical 3-D finite element model was established using Abaqus FEA to simulate the interface between the two FJ adherent parts. The model was verified with experimental tests of actual FJ samples which showed a close agreement with the corresponding numerical model.

An optimization of FJ lumber in horizontal, vertical and slope orientations were carried out to obtain the FJ geometry that achieves maximum structural performance of such lumber. A Reduced Quadratic Response Surface Model (RSM) and a Modified Two-Factor Interaction (2FI) experimental design were then used for both Normal and Inclined FJ categories, respectively. The statistical model were set up to assess the effect of the main factors: FJ-length, FJ-pitch, and FJ-tip width (tip thickness) and their interactions values on the stiffnesses. One additional parameter, FJ-Slope of three-levels was added with the Inclined FJ category. The obtained results showed clearly the potential of increasing FJ resistance by optimizing its geometry. In addition, it was observed that FJ in vertical orientation achieved higher structural performance close to the NFJ lumber comparing to the FJ in the horizontal orientation.

Regression analysis was used to develop a design equations per each joint orientation (horizontal and vertical). The predicted equations will be useful to determine the optimum FJ geometry directly without the need to use a trial and error approach to achieve structural behaviours close to the NFJ lumber.

Finally, enhancing these properties impact the behaviour and capacity of finger-joined elements at the serviceability and ultimate limit states.

ACKNOWLEDGEMENTS

All praises and thanks are due to Allah for providing me the opportunity and strength as well as showing me the way during the work on this thesis.

This thesis was completed at Memorial University of Newfoundland funded by the Center for Forest Science and Innovation (CFSI) under the Forestry and Agrifoods Agency of Newfoundland, Canada. Funding in the form of graduate fellowship and graduate supplement from Memorial University is gratefully acknowledged.

At this moment of accomplishment, I would like to give my sincere thanks to Drs. Amgad Hussein and Leonard Lye, Department of Civil Engineering, for their financial support, keen supervision, immense knowledge and effort during the program.

Sincere thanks are due to the technical staff who made their services available at every stage of this project, especially Jason P. Murphy. I express my appreciation to the Technical Services of Memorial University for their help when it was needed. Sincere gratitude extends to my brother Mahmoud E. Said, for his great help, support and advices to this research program. I also would not forget to thank Sexton Lumber Co Limited in Bloomfield, NL for providing their support with the samples needed for the experimental program.

Finally, I would like to express my profound gratitude and appreciation to all my family members for their support, encouragement, patience, affection and deep understanding during the tenure of this thesis.

TABLE OF CONTENTS

ABSTRACT i

ACKNOWLEDGEMENTS ii

TABLE OF CONTENTS iii

LIST OF TABLES vi

LIST OF FIGURES vii

LIST OF SYMBOLS AND ABBREVIATIONS xii

Chapter 1 1

Introduction 1

1.1. General 1

1.2. Background 1

1.3. Scope 2

1.4. Objectives 4

1.5. Thesis Outline 5

Chapter 2 7

Review of Literature 7

2.1. Finger Joint (FJ) 7

2.2. Glued-Laminated Lumber (Glulam) 15

2.3. Modeling 16

Chapter 3 20

Numerical 3-D finite element model of finger-joined spruce lumber 20

3.1. Finite element methodology 20

3.1.1. Properties and modeling of adherent 21

3.1.2. Properties and modeling of adhesive 24

3.2. Verification and validation 27

3.2.1. Validation of adherent properties 27

3.2.2. Validation of adhesive properties 32

Chapter 4 37

Optimization of finger-joined spruce lumber 37

4.1. Optimization of normal finger-joined spruce lumber 39

4.1.1. Optimization of Hz-finger-joint spruce lumber at normal position 42

4.1.1.1. DOE for normal FJ in Hz orientation (N-FJ-Hz) 42

4.1.1.2. ANOVA for normal FJ in Hz orientation (N-FJ-Hz) 45

4.1.2. Optimization of VL-finger-joint spruce lumber at normal position 56

4.1.2.1. DOE for normal FJ in VL orientation (N-FJ-VL) 56

4.1.2.2. ANOVA for normal FJ in VL orientation (N-FJ-VL) 59

Chapter 5 69

Optimization of inclined finger-joined spruce lumber 69

5.1. Optimization of Finger-Joint in slope position 69

5.1.1. Optimization of Hz-FJ spruce lumber at different slope positions 71

5.1.1.1. DOE for inclined FJ in Hz orientation (I-S-FJ-Hz) 71

5.1.1.2. ANOVA for for inclined FJ in Hz orientation (I-S-FJ-Hz) 76

5.1.2. Optimization of VL FJ spruce lumber at different slope positions 83

5.1.2.1. DOE for inclined FJ in VL orientation (I-S-FJ-VL) 83

5.1.2.2. ANOVA for inclined FJ in VL orientation (I-S-FJ-VL) 88

Chapter 6 94

6.1. Conclusions 94

6.2. Recommendations 98

REFERENCES 99

LIST OF TABLES

Table 1 Mechanical properties used for the analysis of the specimens 28

Table 2 Melamine-urea-formaldehyde (MUF) properties for modes I, II and III 32

Table 3 Summarized the Models used for obtaining the optimal FJ-Configurations 38

Table 4 Run parameters of 20-models design variables for N-FJ-Hz.....42

Table 5 ANOVA for RSM second-order model for N-FJ-Hz 46

Table 6 Model summary statistics for N-Hz.....48

Table 7 Optimization for N-FJ-Hz.....53

Table 8 Stiffnesses from predicted equation versus model – N-FJ-Hz.....54

Table 9 Run parameters of 20-models design variables for N-FJ-VL.....56

Table 10 ANOVA for RSM second-order model for N-FJ-VL.....60

Table 11 Model summary statistics for N-VL 60

Table 12 Optimization for N-FJ-VL 65

Table 13 Stiffnesses from predicted equation versus model – N-FJ-VL.....66

Table 14 Run parameters of 24-models design variables – I-S-FJ-Hz 72

Table 15 ANOVA for RSM for I-S-FJ-Hz 76

Table 16 Model summary statistics for I-S-FJ-Hz.....77

Table 17 Optimization for I-S-FJ-Hz.....82

Table 18 Run parameters of 24-models Design variables – I-S-FJ-VL.....84

Table 19 ANOVA for RSM for I-S-FJ-VL.....88

Table 20 Model summary statistics for I-S-FJ-VL 88

Table 21 Optimization for I-S-FJ-VL 93

LIST OF FIGURES

Figure 1 Schematic for mixed-mode response.....21

Figure 2 Stress components and material directions.....23

Figure 3 Schematic illustration of the control specimen used in the test.....28

Figure 4 Experimental test of control spruce specimen (without FJ).....29

Figure 5 Failure of the experimental control spruce specimen (without FJ).....30

Figure 6 Typical numerical analysis of the control specimen (without FJ).....30

Figure 7 Typical contour showed numerical analysis for the control specimen from upper, side and lower views.....31

Figure 8 Comparison between experimental and numerical load-displacement curves for control spruce specimens (without FJ).....31

Figure 9 Schematic illustration of the test specimen with FJ at mid-span.....33

Figure 10 Cross-section showed the FJ specimen geometry dimensions.....33

Figure 11 Experimental test of spruce specimen with FJ.....33

Figure 12 Failure of the experimental spruce specimen with FJ.....34

Figure 13 Failure profile of the spruce specimen with FJ.....34

Figure 14 Typical numerical analysis of the spruce specimen with FJ.....35

Figure 15 Typical contour showed numerical failure for the spruce specimen with FJ from upper, side and lower views.....36

Figure 16 Comparison between experimental and numerical load-displacement curves for spruce specimen with FJ.....36

Figure 17 FJ in the Normal horizontal orientation.....39

Figure 18 FJ in the normal vertical orientation.....39

Figure 19 Typical meshed FE model of spruce specimen in N-FJ-Hz.....43

Figure 20 Typical meshed cross-section of the N-FJ-Hz before interlocking.....44

Figure 21 Typical FEA stress contour for failure of FJ spruce specimen in N-FJ-Hz.....44

Figure 22 Numerical load-displacement curves show comparison between the control and different FJs geometries of spruce specimens in N-Hz orientation.....45

Figure 23 Normal probability plot of residuals for N-FJ-Hz.....49

Figure 24 Plot between residuals and predicted for N-FJ-Hz.....49

Figure 25 Plot between residuals and run for N-FJ-Hz.....50

Figure 26 Contour shows interaction between A and B at min C = 0.5 mm.....52

Figure 27 Contour shows interaction between A and B at mid C = 1.0 mm.....52

Figure 28 Contour shows interaction between A and B at max C = 1.5 mm.....52

Figure 29 Contour shows interaction between A and C at min B = 3.8 mm.....52

Figure 30 Contour shows interaction between A and C at mid B = 5.7 mm.....52

Figure 31 Contour shows interaction between A and C at max B = 7.6 mm.....52

Figure 32 Contour shows interaction between B and C at min A = 7.0 mm.....52

Figure 33 Contour shows interaction between B and C at mid A = 21.0 mm.....52

Figure 34 Contour shows interaction between B and C at max A = 35.0 mm.....52

Figure 35 Schematic diagram for optimal predicted maximum N-FJ-Hz value.....53

Figure 36 Graph showed predicted stiffnesses versus model values – N-FJ-Hz.....54

Figure 37 Cube simulate the second-order model – N-FJ-Hz.....55

Figure 38 3-D surface simulated the statistical second-order model –N-FJ-Hz.....55

Figure 39 Typical meshed FE model of Spruce Specimen in N-FJ-VL.....57

Figure 40 Typical meshed Cross-section of the N-FJ-VL before interlocking.....58

Figure 41 Typical FEA stress contour for failure of FJ spruce specimen in N-FJ-VL.....58

Figure 42 Numerical load-displacement curves show comparison between the control and different FJs geometries of spruce specimens in N-VL orientation.....59

Figure 43 Normal probability plot of residuals for N-FJ-VL 61

Figure 44 Plot between residuals and predicted for N-FJ-VL 62

Figure 45 Plot between residuals and run for N-FJ-VL.....62

Figure 46 Contour shows interaction between A and B at min C = 0.5 mm 64

Figure 47 Contour shows interaction between A and B at mid C = 1.0 mm 64

Figure 48 Contour shows interaction between A and B at max C = 1.5 mm 64

Figure 49 Contour shows interaction between A and C at min B = 4.45 mm 64

Figure 50 Contour shows interaction between A and C at mid B =11.13 mm 64

Figure 51 Contour shows interaction between A and C at max B = 17.8 mm 64

Figure 52 Contour shows interaction between B and C at min A = 7.0 mm 64

Figure 53 Contour shows interaction between B and C at mid A = 21.0 mm 64

Figure 54 Contour shows interaction between B and C at max A = 35.0 mm 64

Figure 55 Schematic diagram for optimal predicted maximum N-FJ-VL value 65

Figure 56 Graph showed predicted stiffnesses versus model values – N-FJ-VL 67

Figure 57 Cube simulate the second-order model – N-FJ-VL.....68

Figure 58 3-D surface simulated the statistical second-order model – N-FJ-VL 68

Figure 59 FJ at α^{o} slope position – Hz orientation 69

Figure 60 FJ at α^{o} slope position – VL orientation.....69

Figure 61 Numerical load-displacement curves for I-S-30°-FJ-Hz 73

Figure 62 Numerical load-displacement curves for I-S-45°-FJ-Hz 73

Figure 63 Numerical load-displacement curves for I-S-60°-FJ-Hz 74

Figure 64 Typical meshed FE of Hz-FJ specimen at α^{o} slope 74

Figure 65 Typical meshed cross-section of Hz-FJ at α^{o} slope before interlocking 75

Figure 66 Typical FEA stress contour for failure at α^{o} of Hz-FJ spruce specimen 75

Figure 67 Normal probability plot of residuals for I-S-FJ-Hz 78

Figure 68 Plot between residuals and predicted for I-S-FJ-Hz 78

Figure 69 Plot between residuals and run for I-S-FJ-Hz 79

Figure 70 Contour shows interaction between A and D at C=0.5mm and B=3.8mm 81

Figure 71 Contour shows interaction between A and D at C=0.5mm and B=5.7mm 81

Figure 72 Contour shows interaction between A and D at C=0.5mm and B=7.6mm 81

Figure 73 Contour shows interaction between A and D at C=1.0mm and B=3.8mm 81

Figure 74 Contour shows interaction between A and D at C=1.0mm and B=5.7mm 81

Figure 75 Contour shows interaction between A and D at C=1.0mm and B=7.6mm 81

Figure 76 Contour shows interaction between A and D at C=1.5mm and B=3.8mm 81

Figure 77 Contour shows interaction between A and D at C=1.5mm and B=5.7mm 81

Figure 78 Contour shows interaction between A and D at C=1.5mm and B=7.6mm 81

Figure 79 Schematic diagram for optimal predicted maximum I-S-FJ-Hz value 82

Figure 80 Numerical load-displacement curves at I-S-30°-FJ-VL 85

Figure 81 Numerical load-displacement curves at I-S-45°-FJ-VL 85

Figure 82 Numerical load-displacement curves at I-S-60°-FJ-VL 86

Figure 83 Typical meshed FE of VL-FJ specimen at α^{o} slope.....86

Figure 84 Typical meshed cross-section of VL-FJ at α^{o} slope before interlocking 87

Figure 85 Typical FEA stress contour for failure at slope of VL-FJ Spruce Specimen 87

Figure 86 Normal probability pot of residuals for I-S-FJ-VL 90

Figure 87 Plot between residuals and predicted for I-S-FJ-VL 90

Figure 88 Plot between residuals and run for I-S-FJ-VL.....91

Figure 89 Contour shows interaction between A and B at min C=0.5mm and D=30° 92

Figure 90 Contour shows interaction between A and B at min C=0.5mm and D=45° 92

Figure 91 Contour shows interaction between A and B at min C=0.5mm and D=60° 92

Figure 92 Contour shows interaction between A and C at mid C=1.0mm and D=30° 92

Figure 93 Contour shows interaction between A and C at mid C=1.0mm and D=45° 92

Figure 94 Contour shows interaction between A and C at mid C=1.0mm and D=60° 92

Figure 95 Contour shows interaction between B and C at max C=1.5mm and D=30° 92

Figure 96 Contour shows interaction between B and C at max C=1.5mm and D=45° 92

Figure 97 Contour shows interaction between B and C at max C=1.5mm and D=60° 92

Figure 98 Schematic diagram for optimal predicted maximum I-S-FJ-VL value 93

LIST OF SYMBOLS AND ABBREVIATIONS

ASTM	American Society for Testing and Materials
2FI	Two-Factor Interaction Technique
ANOVA	Analysis of Variance
BS	Black Spruce
COST	Changing-One-Single-Thing Technique
CZM	Cohesive Zone Model
DOE	Design of Experimental Methodology
D-VTKA	Desmodur-VTKA Adhesive
EWPs	Engineered Wood Products
FEA	Finite Element Analysis
FEM	Finite Element Method
FJ	Finger Joint
GB/T	Guobiao standard - Chinese national standards
Glulam	Glued-laminated timber

Hz	Horizontal orientation
I-S	Inclined - Slope
LBLB	Laminated Bamboo Lumber Beam
MDI	Methylene Diphenyl Diisocyanate Adhesive
MOE	Modulus of Elasticity
MOR	Modulus of Rupture
N	Normal (0° Slope)
NFJ	Non-Finger-Jointed / un-jointed wood
NLGA	National Lumber Grades Authority
OFAT	One-Factor-at-a-time Technique
psi	Pound per Square Inch
PUR or PU	Polyurethane Adhesive
PVAc	Polyvinyl Acetate Adhesive
RF	Resorcinol Formaldehyde Resin Adhesive
RPF	Resorcinol Phenol Formaldehyde Adhesive

RSM	Response Surface Model technique
RSM	Response Surface Model Methodology
SEM	Scanning Electron Microscopy
SPS	Special Products Standard
TS EN	Turkish Standard England
UF	Urea Formaldehyde Adhesive
UTS	Ultimate Tensile Strength
VL	Vertical Orientation

Chapter 1

Introduction

1.1. General

Currently, despite the importance of forests, we are still allowing them to disappear. We depend on this renewable resource for our survival, from the air we breathe to the wood we use. In addition, forests provide habitats for animals, protect watersheds, prevent soil erosion, and mitigate climate change by reducing global warming by using carbon dioxide in photosynthesis (Tollefson, 2017). Forests also offer a source of economic growth from timber and non-timber products, and various recreational options. Wood as a natural resource is unique as it is considered a 100% renewable building material. Yet, each year, countless acres of forests are lost which may lead to dire consequences for all of us (FAO, 2015) Therefore, the proper exploitation of forests is paramount. One area of research is to improve our understanding and enhance the performance of engineered wood products. Engineered wood products contribute to the economy, and play an important role in increasing the export revenue to Canada. The modelling of FJ using FE and statistical analysis considered in this thesis will lead to the improved exploitation of timber resources.

1.2. Background

Finger jointing (FJ) is the technique of joining the ends of two pieces of wood to make a longer piece. Essentially, FJ is a modification of the plain scarf joint; it can be considered as a series of scarfs separated by a fingertip. FJ can be classified as structural or non-

structural depending on the intended use and on its profile. Structural FJs are longer with sharper tips unlike the non-structural FJs which are short with blunt tips. There are five steps which should be considered when manufacturing engineered finger-joined wood products: material selection, FJ profile, adhesive used, assembly procedure, and adhesive curing. These steps vary according to factory conditions and system used (Jokerst, 1981).

Spruce timber is straight grained characterized by long fibre length and finely textured. It is lightweight but nonetheless strong. It is classified as medium in strength, but above average in stiffness. It is easy to glue, holds nails well, and holds paint well. It is used for lumber and plywood manufacture (Tree Canada - Arbres Canada, no date). Therefore, it is increasingly being used for making cross laminated timber due to its preferable properties as high density and good mechanical properties in structural application that would make the wood products more competitive.

1.3. Scope

The scope of the current research was to develop an effective and systematic methodology for optimization of FJ spruce lumber. The scope was divided into five-main stages as outlined below. The research covers an investigation for the evaluation of the spruce wood mechanical properties for both the adherent and the adhesive to be used as a reference for the other stages. A numerical 3-D FE model was developed using Abaqus FEA to simulate the interface between the two FJ adherent parts. The model was verified with experimental tests of actual finger-joined samples. An optimization of FJ in different orientations (horizontal and vertical) at both normal and slope degree positions were carried out to

obtain the FJ geometry that achieves maximum structural performance of such lumber. Regression analysis were used to develop prediction equations for the different FJ orientations. The five-stages are summarized as follows:

Stage 1: Investigation to evaluate the mechanical properties of spruce adherent wood.

Stage Objectives and Outcomes: examine and evaluate the material stiffness parameters which could be defined by the engineering constants for an orthotropic material. The nine-elastic stiffness parameters were comprised of the 3-Young's moduli (E_L, E_R, E_T), 6-Poisson's ratios $(\nu_{LR}, \nu_{LT}, \nu_{RT}, \nu_{TR}, \nu_{RL}, \nu_{TL})$, and 3-Shear moduli (G_{LR}, G_{RT}, G_{TL}).

Stage 2: Investigation to evaluate the mechanical properties of the adhesive.

Stage Objectives and Outcomes: examine and evaluate the three-cohesive parameters which characterize the traction-separation relationship. The initial stiffness coefficients (K_{nn}, K_{ss}, K_{tt}) in normal, and two local shear directions, respectively are required.

Stage 3: Establish the numerical 3-D finite element using Abaqus FEA

Stage Objectives and Outcomes: establish the FE model based on Cohesive Zone Models (CZM) in Abaqus software.

Stage 4: Establish experimental testing program for the verification of the numerical 3-D finite element model.

Stage Objectives and Outcomes: validate and verify the numerical 3-D model using the experimental data obtained from testing actual FJ spruce lumber specimens in the lab and compare it to the numerical results.

Stage 5: Optimization of FJ at different orientations (horizontal and vertical) with normal and slope degree positions.

Stage Objectives and Outcomes: optimize the FJ geometry towards the improvement of its mechanical properties that approaches NFJ lumber. Develop regression equations to predict the stiffness for FJ-geometry of spruce specimen that will make it easy to use in structural applications.

1.4. Objectives

In this study, the structural performance of finger-joined spruce elements were evaluated using an experimental program, 3-D finite element analysis, and statistical design of experiment methodology.

The main objectives of this thesis could be summarized as follows:

- To numerically investigate the structural properties of spruce FJ lumber especially stiffness which impacts the behaviour and capacity of FJ elements at serviceability and ultimate limit states.
- To use statistical design of experiments methodology as a powerful and systematic approach to optimize FJ geometry configurations. This includes :

- Designing a set of different FJ geometry to provide adequate and reliable measure of the mean responses.
- Obtaining prediction equations for various FJ categories.
- Obtaining optimal combination of the FJ geometry configurations using the fitted mathematical statistical models.

Therefore, this study is a significant contribution to the development of FJs techniques with a potential for structural applications. Hence, this will enable the engineering wood industry to produce a larger variety of the pieces of wood with optimal mechanical properties.

To the best of my knowledge, the proposed work has not been reported in the literature. The results and models obtained from the research will provide engineers with the optimal FJ geometry that will achieve mechanical behaviours close to the non-finger joined (NFJ) lumber, which can be used to enhance the performance of structural members.

1.5. Thesis Outline

Chapter 2 contain the literature review, pertaining to the area of FJ technique in wood applications and EWPs especially glulam beams.

Chapter 3 describe the methodology of the numerical 3-D FE of FJ configuration for spruce lumber. In addition it describe the details of the experimental program testing setup procedure used to validate the numerical FEA model according to Standard tests set-up in NLGA-SPS 1. The results are described, analysed and discussed.

Chapter 4 provide detailed procedure undertaken to design and optimize the first categories of Normal 0° slope FJ spruce wood lumber based on FE and DOE methodology. Moreover, prediction equations are fitted to the measured FJ properties, and are validated using numerical models.

Chapter 5 provide detailed procedure undertaken to design and optimize the second categories of Inclined (30°, 45°, 60°) slope FJ spruce wood lumber based on FE and DOE methodology.

Chapter 6 provide a summary of the overall research work and conclusion. Recommendations for future work are also provided.

Chapter 2

Review of Literature

2.1. Finger Joint (FJ)

Spruce timber is characterized by high density and good mechanical properties in structural application. (Bustos *et al.*, 2003) investigated the tensile strength behaviour of FJ black spruce lumber due to the effects of both curing time and end pressure. In addition to observing typical failure modes due to the tensile test. The FJ length was 28.27 mm, the pitch was 6.69 mm, and finger-tip width (tip thickness) was 0.76 mm. FJs were assembled with a one face glue of an isocyanate adhesive which consisted of a two-component system, an ISOSET UX-100 polyurethane (PUR) pre-polymer mixed with an ISOSET WD3-A322 emulsion polymer. To study the effect of end pressure, The FJ pieces were pressed at 20°C with an applied end pressure ranging from 1.38 N/mm^2 to 4.90 N/mm^2 for 20 seconds. The specimens then were tested after 24 hours of curing at room temperature. FJ pieces were pressed at 3.75 N/mm^2 to study the effect of curing time. The specimens then were tested after 1, 2, 5, and 24 hours of curing time. The results demonstrated that both end pressure and curing time of structural FJs had a significant effect on ultimate tensile strength (UTS). The tensile strength was affected by the end pressure applied. It was observed that UTS increased from applied end pressure at 1.35 N/mm^2 (196 psi) until reached to 3.43 N/mm^2 (498 psi) then UTS decreased. The specimens had adequate strength for handling after 1 hour of curing time. In addition, high strength values were observed after 5 and 24 curing hours. Moreover, failure modes were used to evaluate the glue line quality through

determining the percent of wood failure occurred in the FJs. It was noticed that the excess of applied end pressure of more than 3.43 N/mm^2 (498 psi) will decrease UTS and causing splitting failure at the finger root due to compression, even if there was no gap spacing between finger-tip and root. This study indicated that using isocyanate adhesive in assembly of FJ black spruce was appropriate to structural applications. Furthermore, FJ black spruce had high tensile strength compared to the requirements of special products standard (SPS 1).

(Bustos *et al.*, 2011) investigated the influence of end pressure on FJ black spruce using microscopic analysis technique by the scanning electron microscopy (SEM). They also found the optimal range of end pressure needed to produce high strength FJs through having a better understanding of the effect of end pressure on the FJs. This was done by measuring the depth of damage, glue-line thickness, and the tip gap at five chosen points from each SEM micrograph. A feather FJ profile was used with 28.27 mm in length, the pitch was 6.69 mm, finger-tip width (tip thickness) was 0.76 mm. FJs were assembled with a one face glue of an isocyanate adhesive which was consisted of a two-component system, an ISOSET UX-100 polyurethane (PUR) pre-polymer mixed with an ISOSET WD3-A322 emulsion polymer. A total of twelve blocks of about 1 cm^2 were cut from the FJ transverse glue-line face, whereas another seven blocks of about 1 cm^2 were cut from the FJ longitudinal glue-line face. Six levels of end pressure were applied for 20 seconds each, ranging from 1.3 N/mm^2 to 4.9 N/mm^2. The results demonstrated that increasing the end pressure caused more damage in the wood cell depth. It was observed that at low end pressure, joints had some air bubbles within the glue-line which decreased the tensile

strength. However, it was noticed that 90 % more cell damaged occur at high end pressure. Moreover, results indicated that gap at tip of fingers decreased by increasing the end pressure until reaching to 4.9 N/mm^2, then a crack occurred. Three failure modes were indicated microscopically, inter-cell failure (IC) which represented the split of cells, intra-wall failure (IW) which represented failure within the secondary wall, and trans-wall failure (TW) which represented failure across the wall. FJ black spruce with isocyanate adhesive had a good potential for structural applications. In addition to the using of various end pressures treatments in the manufacture of FJs attain the tensile strength requirements according to national lumber grades authority (NLGA) – SPS 1.

(Hernández, Coman and Beauregard, 2011) investigated the influence of two machining parameters, cutting speed and chip load on the ultimate tensile strength (UTS) of finger-joined black spruce lumber. Statistical analysis was performed to determine the effect of the two machining parameters and their interactions on UTS. In addition to observing the typical failure modes due to the tensile test. The variables were four cutting speeds and three chip loads. A total of 960 specimens of cross-section 38 x 51 mm^2 each were tested. An isocyanate adhesive was used which consisted of a two-component system of an ISOSET UX-200 polyurethane (PUR) pre-polymer mixed with an ISOSET WD3-A300 emulsion polymer using a manual glue gun. A feather FJ profile was chosen and an end pressure of 3.45 N/mm^2 was applied. The results from statistical analysis showed that both parameters had a significant effect on the UTS within the ranges of the studied limit, cutting speed 1860 – 3960 m/min and chip load (0.51 – 1.27 mm). It was observed that FJ black spruce specimens which were manufactured within the previous ranges exceeding the UTS

requirement of SPS 4. Moreover, more than 89 % of the specimens failed in failure modes 2, 3, 4, and 5, which were an indicative of good adhesive in accordance with SPS 4. This study indicated that both machining parameters were important and did not consider a limiting factor because maximum could be used for both cutting speed of 3960m/min and maximum chip load of 1.27 mm. In addition, the study showed that isocyanate adhesive could be successfully used for manufacturing structural FJ high density black spruce.

(Barboutis, Vassiliou and Karastergiou., 2005) studied the behaviour of non-structural FJ lumber which were manufactured from small dimensions of steamed and un-steamed beech wood. Both MOE and MOR due to the effect of finger lengths were evaluated. In addition to investigating the effect of finger orientation on bending strength of steamed and un-steamed beech wood. Three different parameters of two variables each were studied, wood handling (steamed and un-steamed), FJ orientation (horizontal and vertical), and two FJs geometry. A total of 120 specimens of dimensions 50 x 30 x 400 mm^3 were tested. Two FJs profiles were employed in that investigation where, the FJ lengths were 4 and 10 mm, the pitches were 1.6 and 3.8 mm, finger-tip widths were 0.4 and 0.16 mm, and slopes were 12º and 11º respectively. PVA based glue with three durability classes (D1, D2, and D3) were used for the assembly of the FJs. FJs were assembled manually with a one face glued by a brush, then a constant end pressure was applied for 60 seconds. The results demonstrated that specimens with 10 mm finger length appeared higher MOR than 4 mm. Furthermore, horizontal FJ orientation showed higher MOR than vertical FJ orientation in both steamed and un-steamed samples. It was observed that MOE affected by the handling of wood. MOE of steamed specimens showed slightly higher than the control solid wood.

On the contrary, MOE of un-steamed specimens showed approximately the same compared to the control solid wood. D3 glue class achieved the higher MOR followed by D2, then D3 which achieved lower values of MOR. The study indicated that steamed wood specimens achieved higher MOR than the un-steamed specimens.

(Özçifçi and Yapıcı, 2008) evaluated the structural behaviour of the FJ due to the effect of FJ geometry, adhesive type, and wood species. In addition, MOE and MOR were calculated. Four different wood species were used: oriental beech, oak, poplar, and Uludag fir. Two adhesive types were used: polyvinyl acetate (PVAc), and Desmodur-VTKA (D-VTKA). Based on TS EN 310 standard, TS 2471 and BS EN 204 standard for wood species, 300 samples with a 12% average moisture content were tested. The dimensions of the specimens were 320 x 20 x 20 mm^3. The FJ-lengths were 7, 14, and 21 mm, the FJ-pitch was 6 mm, tip gap was 0.5 mm, FJ-tip width (tip thickness) was 4 mm, and slope was 8°. FJs were assembled manually with a one face glued by a brush for PVAc or D-VTKA, then a constant end pressure was applied. The applied pressure was 25 N/mm^2 and the adhesive curing of the PVAc was at $50^{\circ}C$ for 2 hours, whereas D-VTKA curing was at $50^{\circ}C$ for 20 minutes. Statistical analysis was performed to determine the differences between the bending strength of FJ surfaces of the samples. The results demonstrated that when the length of FJ was increased from 7 to 21 mm, the bending strength increased. The PVAc gave a high quality bonding surface compared to D-VTKA based on MOE and MOR test results. Furthermore, FJ samples gave approximately same MOE such as the control NFJ samples for this wood species. Eventually, this study advised that the structural behaviour

of FJ depends on: wood type, adhesive type, the compatibility between adhesive and wood, and FJ profile.

(Zhou and Ren, 2012) investigated the effect of grading lumber according to MOE. In addition to evaluating the effect of the spacing between finger-tip and finger-root with different FJ-lengths on the structural behaviour of FJ Chinese fir lumber. Static bending tests and tensile tests were done to determine the structural behaviour of FJ Chinese fir lumber, and comparing the results to the structural properties of un-jointed lumber from the same lot. Furthermore, observing typical failure modes due to both bending test and tensile test. The FJ-lengths were 20, 25, and 35 mm, finger-tip and root thickness was varied from 0.1 to 0.5 mm, and slope was 1 in 10. Methylene diphenyl diisocyanate (MDI) adhesive was used. The results demonstrated that FJ Chinese fir lumber could be used in structural application and giving approximately the same results of un-jointed Chinese fir lumber. The grading process before the manufacture of FJ enhanced the strength performance. Six-failure modes were observed. In addition, failure occurred in the weaker areas near finger-tip or root depending on the space between fingers for side locking assembly. This study advised that using longer FJ-lengths taking into consideration the space between FJ-tip and root to be smaller would enhance the strength performance.

(Yeh and Lin, 2012) investigated the structural behaviour of FJ for two different laminated bamboo species. The two bamboo species were moso bamboo and ma bamboo. There were five parameters considered in the study: FJ-length, profile orientation, lamination direction, culm growth height, and mechanical properties of bamboo materials. The study was divided

into two stages. At the first stage, the standard tests, a total of 288 specimens were used to determine the basic mechanical properties of each bamboo species in both static bending test and tensile test. At the second stage, a total of 360 laminated bamboo specimens were used for compression test, shearing test, bonding test and bending test. The dimension of each laminated bamboo beam specimens was 30 x 30 x 1000 mm^3. The FJ lengths were 12, 15, and 18 mm, the pitch was 4 mm, and FJ-tip thickness was 0.65 mm. Resorcinol phenol formaldehyde (RPF) adhesive of 55 % solid content was used with paraformaldehyde hardener in a 72 % solution during the lamination. Glue was applied at rate of 250 g/cm^2 and then constant end pressure was applied at 1.47 N/mm^2 for 4 hours. The results demonstrated that by increasing the finger length from 12 to 18 mm, the flexural behaviour improved. MOR for the FJ bamboo members laminated vertically was slightly higher than MOR for the others laminated horizontally. Furthermore, MOR of the FJ profile shown on the width face was higher than MOR of the others shown on the thickness face of the bamboo beam for all finger lengths and lamination directions. In addition, the significant strength properties when making laminated bamboo was the bonding strength. The bending strength was less sensitive to the existence of nodes than the tensile strength. Based on FJ efficiency, moso bamboo was superior to ma bamboo.

(Kumar, Sharma and Gupta, 2015) investigated MOE and MOR under static bending. In addition to determining the crushing strength and MOE under compression parallel to grain of FJ sections. The results then were compared with the un-jointed wood sections (NFJ) from the same lot. Two types of non-structural adhesives were used, PVAc and Urea Formaldehyde (UF). All samples cross-section were 50 x 50 mm^2, whereas the length of

750 mm long each used for bending tests, and 200 mm long each used for compression tests. The FJ length was 15 mm, the pitch was 5 mm, and tip thickness was 1 mm. The results demonstrated that FJ mango wood sections was used for non-structural applications like furniture. It was observed that MOE of FJ sections for the two adhesives had better values than NFJ sections under both bending and compression. However, from bending tests, MOR of FJ sections using UF were approximately the same to the NFJ sections, whereas FJ sections using PVAc obtained lower MOR than that of NFJ sections. This study advised that using UF would be more efficient than PVAc when used in the application of FJ mango wood sections.

(Habipi and Ajdinaj, 2015) investigated the effect of both finger-tips slope positions and finger length on bending strength of poplar and silver fir FJ lumbers. In addition, MOE and MOR were calculated. A total of 384 specimens were tested. The specimen dimensions were 20 x 20 x 320 mm^3 each, and the FJ-tips slope angles were 0° (vertical position), 10°, 20°, and 30°. The FJ lengths were 6, 10, and 14 mm, the pitch was 6 mm, and slope was 17° at the vertical position of the FJ-tips, then slope was changed according to the slope angle of the finger-tips. FJs were assembled manually with a one face glued of polyvinyl adhesive by a brush, then a constant end pressure was applied manually through hand vice grip for 24 hours. The quality of gluing process was verified by weighing the pieces before and after the gluing process. The results demonstrated that longer FJs perform higher bending strength than shorter FJs within the rate of (FJ-length / FJ-pitch) from (1 to 2.3). Moreover, FJ-tips slope positions 10°, and 20° performed better results than 0° (vertical position), whereas slope position 30° of 14 mm FJ-length produced lower strength.

Furthermore, MOE showed no influence neither by FJ-tips slope angle nor by the FJ-length. The slope angle 10° was the best slope position of the FJ-tips which performed the best values for strength for all three FJ-lengths.

2.2. Glued-Laminated Lumber (Glulam)

Both MOE and MOR are predominant properties of glulam. From this concept, (Gao *et al.*, 2015) predicted and estimated MOE and MOR of Cathay poplar FJ glulam through finite element models and experimental investigations. In addition to observing typical failure modes of FJ glulam specimens due to bending. Furthermore, examining and comparing the bending strength of Cathay poplar glulam with Douglas fir glulam in order to simulating the results between them. Based on GB/T 26899-2011, all of the specimens were 3000 mm long each and cross-section of 60 x 120 mm^2, half of the specimens were four-layered glulam whereas the other half were six-layered glulam. FJ length was 21.5 mm and the pitch was 8 mm. FJs were positioned at least 300 mm away from each adjacent layer. Two adhesive types were used, one-component polyurethane (PU) adhesive and resorcinol formaldehyde resin (RF) adhesive. The results demonstrated that bending strength of glulam depended on both laminate strength and FJ strength. In addition, the specimen capacity increased when the number of layers increased within the same specimen thickness. The RF was shown to be less effective than PU when used with Cathay poplar glulam specimens. Three-typical failure modes were observed, first type was shear failure of FJ, second type was shear failure of FJ with splitting of timber, and the third failure type was splitting of timber that did not describe the bonding strength of FJ with adhesives. This study demonstrated that Cathay poplar glulam had a lower stiffness,

however, marginally higher strength compared to Douglas fir glulam. Eventually, the study indicated that Cathay poplar had the potential to be a glulam material in china.

(Li *et al.*, 2016) examined the flexural behavior of 20 laminated bamboo lumber beam (LBLB) specimens. In addition, observing typical failure modes. MOE and MOR were calculated. Furthermore, bending strength, stress-strain relationship and load-displacement relationship of specimens were examined. Based on ASTM D198 (2010) and GB/T 50329-2012, all of the 20 LBLB specimens were (2400 mm long x 100 mm depth x 2100 mm span) each. The specimens were divided to five groups according to their widths (45, 50, 60, 70, and 80 mm) to determine any width effect. The specimens had no joints through the span length where the selected bamboo strips were 2100 mm long. Phenol resin glue was used to manufacturing the specimens. The results demonstrated that all the specimens showed an initial elastic phase until relatively half the ultimate load, followed by non-linear deformation, then accompanied by brittle failure initiated by rupture on the tension side of the beam. The strain was linear across the cross-section of the LBLB throughout the test. The width had no obvious effects on MOE, bending strength and the ultimate tensile strain of the LBLB specimens. The study indicated that the deflection was the critical design criteria for LBLB rather than strength. Eventually, the study recommended that improving the beam stiffness would reduce the deflection and enhance the strength.

2.3. Modeling

(Fortino *et al.*, 2012) presented a numerical 3-D finite element model for the simulation of the cohesive short-term crack propagation (Mode I) in timber structures. The Mode I crack

growth in solid wood and across the bond-lines of glulam was modelled using the cohesive elements of Abaqus FEA software and exponential damage laws. To simulate the cohesive crack growth in wood, a damage initiation criterion of maximum stress, a damage evolution of displacement with exponential softening, and a traction type mixed mode ratio were used. Experimental work of modified double cantilever beam (DCB) specimens was established. Two types of modified DCB glulam specimens with two different adhesives, hyper-branched polyurethane (HBPU) and melamine urea formaldehyde adhesives (MUF), were tested. The load-displacement curves were then calculated for both experimentally and numerically in order to compare the data. The results showed a close agreement between the experimental and numerical load-displacement curves data with the notice of some influence of different adhesives on fracture response of the tested specimens. The numerical modeling was suitable for solid wood and glulam cracked specimens under short-term fracture tests where the crack propagates in a known direction.

(Sandhaas and Van de Kuilen, 2013) developed a numerical 3-D finite elements material model for wood based on the concepts of Continuum Damage Mechanics (CDM). The determination of the necessary mechanical properties were considered the major point in the model, whereas both model performance and prediction capacity were dependent on these properties. A material subroutine was created containing the developed finite element model. Eight stress-based failure criteria (or damage initiation functions) were derived to formulate piecewise defined failure surfaces. The eight stress-based failures criteria were defined by the material strengths in tension, compression, and shear (longitudinal and tangential) in parallel and perpendicular directions. The damage development of wood was

controlled by nine damage variables (or nine stiffness parameters). Three-different wood species (spruce, beech, azobé) were tested experimentally in order to compare the results with modelling outcomes. The results showed a close agreement between experimental and numerical load-displacement curves data. Wood is a highly anisotropic material, hence, the results also showed ductile behaviour in compression and brittle behaviour in tension and shear, where both failure modes could occurred simultaneously. The constitutive model was used to predict the results of embedment tests to assess the load carrying capacity and mechanical behaviour of timber joints.

(Tran, Oudjene and Meausoone, 2014) presented experimental and numerical 2-D finite element data on the mechanical behavior of finger-joined timber beech wood. Numerical simulations based on the Cohesive Zone Model (CZM) of Abaqus FEA software were developed to simulate the progressive failure. Two and three-layers glued beams with and without FJs from laminations of 42 mm thickness were constructed. The FJ lengths were 22 mm, the pitch was 6 mm, and finger-tip width (tip thickness) was 1 mm. FJs were assembled with a one face glue of melamine urea formaldehyde (MUF) adhesive. The bi-linear traction separation law was used to simulate the progressive failure of the FJ. The created numerical model assumed initially linear elastic behavior followed by the initiation and evolution of the damage. The results showed that glued-solid beech timber beams without FJ behave better and present greater MOR than beams with FJ. Inspection of failure modes revealed that beams with FJ in the maximum tension zone showed premature failure. The failure was propagated by steps: it taken place, first, at the FJ and then propagates to the inter-layer bond-line. Therefore, from the obtained results, the actual FJ was the weak

links of glued-solid beech timber beams. The constitutive finite element model could predict the non-linear behavior of timber beech material with brittle failure in shear, tension parallel and perpendicular to grain. The model could also predict the damage and crack propagation across the glue-lines with in FJ. An Optimization using the Response Surface Method (RSM) and the Kriging interpolation were performed. The geometry of FJ configuration was defined as the design variables, the FJ-length, the pitch, and the tip-width. The objective function (response) was defined in terms of the maximum bending force, obtained from four-point bending tests. Eventually, the results demonstrated the potential in increasing the FJ resistance by optimizing its geometry.

Chapter 3

Numerical 3-D finite element model of finger-joined spruce lumber

3.1. Finite element methodology

Finger-joined lumber is a composite material which consists of timber as the adherent and glue as the adhesive. To develop a finite element model (FE) to simulate finger-joined lumber, the mechanical properties of both materials need to be specified. This is very essential so that the model simulates the true structural behaviour of the element. The adherent properties can be determined from standard tests according to NLGA-SPS-1 for finger-joined structural lumber (NLGA-SPS-1, 2014). Also, the adhesive's properties (glue-line) can be determined through two tests for mode I (pure tension) and mode II (pure shear). For glue-line properties in mode I, the Double Cantilever Beam (DCB) test can be set up similar to that presented in (Fortino *et al.*, 2012; Tran, Oudjene and Meausoone, 2014; Tran, Oudjene and Méausoone, 2015). Subsequently, the pure shear test can be set up for mode II similar to that presented in (Tran, Oudjene and Meausoone, 2014; Tran, Oudjene and Méausoone, 2015). According to Tran et al (2014) the FJ fracture process was often caused by a combination of the two modes together in Mixed-Mode behaviour as shown in Figure 1 (Tran, Oudjene and Meausoone, 2014; Tran, Oudjene and Méausoone, 2015).

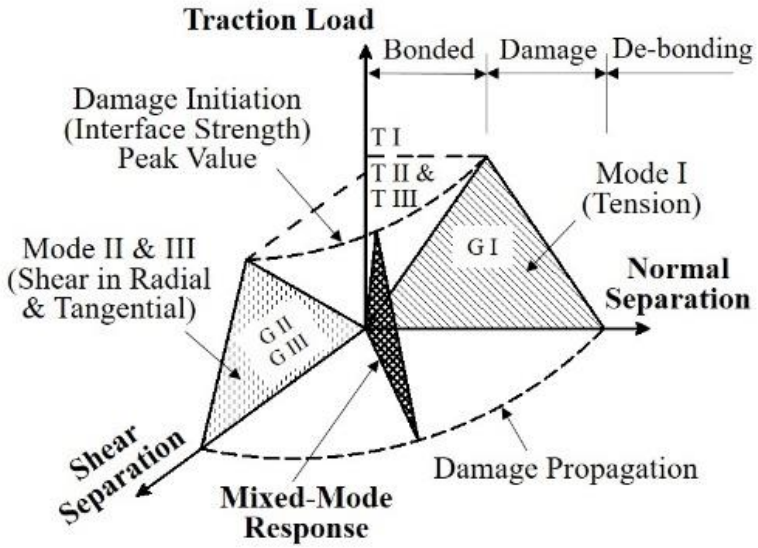

Figure 1 Schematic for mixed-mode response

The tension modes and shear modes may have to be combined. For instance, splitting parallel to longitudinal-radial-plane can be caused by tension perpendicular-to-grain (mode I), shear (mode II) or a combination of both (mixed mode). The separate failure modes may be defined for each stress component as degradation of one component that leads to the degradation of the other components. This means that failure due to longitudinal shear may induces failure in tension perpendicular-to-grain even the tension stress component is still less than its strength (Sandhaas and Van de Kuilen, 2013).

3.1.1. Properties and modeling of adherent

Wood microstructure is the main characteristic to determine its mechanical behaviour. The wood cell-wall consists mainly of the primary wall and the secondary wall which can be considered as fibre-reinforced composites. Both cell-wall layers (which are consists of microfibrils, a thread like units forming from the cellulose chains located in a hemicellulose and lignin matrix) differ in their thickness and their microfibril orientation within the tree.

Therefore, the mechanical properties of wood strongly get affected, especially due to the difference in the microfibril angles in the radially and tangentially oriented cell-walls. For instance, an increase in radial stiffness and a decrease in radial shrinkage may be resulted because of the larger microfibril angles in the radial cell walls. In addition, the ray cells aligned in the radial direction act as a reinforcement which also enhance the stiffness of the wood structure in that direction. On the contrary, the tangential direction in which the cells are shaped in disorganized pattern has lower stiffness than the radial one in which the cells are shaped in straight rows due to the difference in cell arrangement (Holmberg, Persson and Petersson, 1999).

Wood is a highly anisotropic material due to the growth way of the tree and the wood cells alignment within the stem. However, wood can be considered locally as an orthotropic material that can distinguish three directions: longitudinal (L), radial (R), and tangential (T) (see Figure 2). Therefore, to simulate the deformations in wood numerically, proper constitutive models are required. The model depends on both, the loading conditions and the environmental effects, such as moisture and temperature variations. For instance, short-term loading condition and small variations in moisture content may be sufficient for employing linear elastic model. In other cases, plasticity and fracturing must be considered under long-term loading condition such as creep effects (Holmberg, Persson and Petersson, 1999; Dassault Systèmes Simulia, 2013; Sandhaas and Van de Kuilen, 2013).

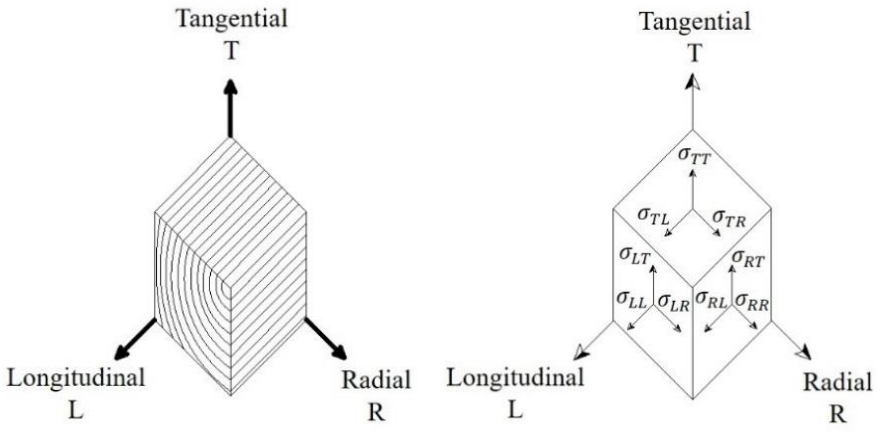

Figure 2 Stress components and material directions

Orthotropic elastic material model can be assumed for the timber material. Linear elasticity in an orthotropic material can be defined by giving nine-independent elastic stiffness parameters (or nine-damage variables) (Dassault Systèmes Simulia, 2013; Sandhaas and Van de Kuilen, 2013). Hooke's generalized law for an orthotropic material like wood can be written as follow:

$$\sigma_{ij} = D_{ijkl}\ \varepsilon_{kl} \qquad [1]$$

Where,

The D_{ijkl} is the material stiffness parameters which can be defined by the engineering constants for an orthotropic material; the 9-elastic stiffness parameters D_{ijkl} in orthotropic constitutive equations are comprised of 3-young's moduli (E_L, E_R, E_T), 6-poisson's ratios $(\nu_{LR}, \nu_{LT}, \nu_{RT}, \nu_{TR}, \nu_{RL}, \nu_{TL})$, and 3-shear moduli (G_{LR}, G_{RT}, G_{TL}) as shown in the following matrix:

$$\begin{Bmatrix}\sigma_{LL}\\ \sigma_{RR}\\ \sigma_{TT}\\ \sigma_{LR}\\ \sigma_{LT}\\ \sigma_{RT}\end{Bmatrix} = \Gamma \begin{bmatrix} E_L(1-\nu_{RT}\nu_{TR}) & E_L(\nu_{RL}-\nu_{TL}\nu_{RT}) & E_L(\nu_{TL}-\nu_{RL}\nu_{TR}) & 0 & 0 & 0 \\ E_R(\nu_{LR}-\nu_{TR}\nu_{LT}) & E_R(1-\nu_{LT}\nu_{TL}) & E_R(\nu_{TR}-\nu_{LR}\nu_{TL}) & 0 & 0 & 0 \\ E_T(\nu_{LT}-\nu_{LR}\nu_{RT}) & E_T(\nu_{RT}-\nu_{RL}\nu_{LT}) & E_T(1-\nu_{LR}\nu_{RL}) & 0 & 0 & 0 \\ 0 & 0 & 0 & G_{LR} & 0 & 0 \\ 0 & 0 & 0 & 0 & G_{LT} & 0 \\ 0 & 0 & 0 & 0 & 0 & G_{RT} \end{bmatrix} \begin{Bmatrix}\varepsilon_{LL}\\ \varepsilon_{RR}\\ \varepsilon_{TT}\\ \gamma_{LR}\\ \gamma_{LT}\\ \gamma_{RT}\end{Bmatrix}$$

Where, $$\Gamma = \frac{1}{1-\nu_{LR}\nu_{RL}-\nu_{RT}\nu_{TR}-\nu_{TL}\nu_{LT}-2\nu_{RL}\nu_{TR}\nu_{LT}} \qquad [2]$$

Therefore, in order to define the properties of the adherent orthotropic material, determining the engineering constants E, ν, G are required through the standard tests. Then, substituting using the above matrix formula to obtain the nine-material stiffness parameter D_{ijkl} in normal, radial and tangential directions.

3.1.2. Properties and modeling of adhesive

A wide spectrum of adhesives comprising of various chemicals is available for the manufacture and strengthening of laminated timber structures. These adhesives must have a set of important properties: good compatibility with wood components (cellulose), good adhesion on wood, high bond strength, water and heat resistance, high creep resistance, gap filling properties (a glue line is usually 0.1 mm but with some wood structural elements, glue lines can be as thick as 1 to 1.3 mm), resistance to micro-organisms and fungi (Christophe Morel Fourrier, 1999).

The glue-line performance can be expressed by a Cohesive Zone Model (CZM) to evaluate the progressive failure. The response of cohesive elements in numerical simulation may be

based on a continuum description of the material or a traction-separation description of the interface. The continuum description is used when the actual interface thickness is being modeled. On the contrary, the traction-separation description is used when the interface thickness can be considered to be zero which is the case in this study (Liu, 2006).

Generally, three-cohesive parameters characterizing traction-separation relationship must be determined, including the initial stiffness, damage initiation (described by the interface strength), and damage evolution (described by the interface fracture toughness W). The three-parameters can be determined using experimental techniques with appropriate analysis of standardized test. However, the fracture toughness (or the critical energy release rate) is still difficult to obtain. Therefore, it is available in literature or handbooks for many material systems (Liu, 2006; Sandhaas, 2012; Tran, Oudjene and Meausoone, 2014; Tran, Oudjene and Méausoone, 2015).

For cohesive elements used to model bonded interfaces, the initial stiffness coefficient (K_{nn}, K_{ss}, K_{tt}) in normal, and two local shear directions respectively were required. That was defined as the ratio of traction vector stress to strain with the strain being defined as the ratio of separation δ to the initial constitutive thickness T_0, i.e. $(\varepsilon = \delta/T_0)$. In contrast with the most literature, the stiffness of cohesive elements K' was defined as the ratio of traction-stress $\bar{t}$ to separation-displacement δ (Liu, 2006; Dassault Systèmes Simulia, 2013). Thus,

$$K' = \frac{\bar{t}}{\delta} = \frac{\bar{t}}{\varepsilon . T_0} = \frac{K}{T_0} \qquad [3]$$

The value of K not K' were required in the modeling process and both K and K' were identical when the initial constitutive thickness T_0 was specified as 1.0. Therefore, the elasticity definition offered in Abaqus could be expressed directly in terms of the nominal tractions and nominal strains (Dassault Systèmes Simulia, 2013).

Moreover, from the traction-separation relationship, the stiffness was defined in terms of fracture energy (W), separation-displacement at final failure (δ_f), and the damage initiation ratio $(\delta_{ratio} = \delta_0 / \delta_f)$ as follows:

$$K = \frac{2W.T_0}{\delta_{ratio}.\delta_f^2} = \frac{2W.T_0}{\delta_0.\delta_f} \qquad [4]$$

Subsequently, to specify damage evolution, both the values of fracture energy, and the critical cohesive strengths in the normal and the two local shear directions (Normal, Shear-1, and Shear-2) were required. Therefore, the initial stiffness K was expressed in a 3-D as follows:

$$t = \begin{Bmatrix} t_n \\ t_s \\ t_t \end{Bmatrix} = \begin{bmatrix} K_{nn} & K_{ns} & K_{nt} \\ K_{ns} & K_{ss} & K_{st} \\ K_{nt} & K_{st} & K_{tt} \end{bmatrix} \begin{Bmatrix} \varepsilon_n \\ \varepsilon_s \\ \varepsilon_t \end{Bmatrix} = \boldsymbol{K.\varepsilon} \qquad [5]$$

Where $t_n, t_s,$ and t_t represent the nominal tractions in the normal and two local shear directions with respect to the crack plane, respectively; while $\varepsilon_n, \varepsilon_s$ and ε_t were the corresponding nominal separation strains which defined respectively as $\varepsilon_n = \delta_n / T_0$, $\varepsilon_s = \delta_s / T_0$ and $\varepsilon_t = \delta_t / T_0$ being δ_n, δ_s and δ_t as the separation displacements between corresponding points at the interface, and T_0 was the constitutive thickness of the cohesive element (Fortino *et al.*, 2012; Dassault Systèmes Simulia, 2013).

In this study, the off-diagonal stiffness terms were set to zero for the uncoupled behavior between normal and two local shear components. Moreover, the same elastic properties where used for the two local shear directions for the cohesive element.

3.2. Verification and validation

A verification strategy was followed to validate and assess the Abaqus model by comparing the numerical 3-D finite element results with experimental data. The verification was divided into two parts according to adherent and adhesive. The first part was to verify the model with the wood adherent properties which was spruce in this study. Then, second part was to verify the model with the glue properties which was melamine-urea-formaldehyde (MUF) adhesive. A total of 3-specimens for each part were tested experimentally under four-point loading according to the standard test requirements of NLGA-SPS1. The ambient temperature was 20ºC at the time of the tests. The deflection was measured with a linear variable differential transformer (LVDT), a displacement transducers which can convert the rectilinear motion to a corresponding electrical signal, placed at the mid-span of the specimen recorded the deflection versus the applied load. The finite element type was C3D8R (8-node brick elements with reduced Integrations). Also, FJ FEA was expressed based on CZM using traction-separation law to model the interface.

3.2.1. Validation of adherent properties

A total of 3-specimens without FJ of actual dry dimensions 38 x 89 x 1000 mm^3 were tested to measure the deflection using LVDT placed at the mid-span, see Figure 3, 4. The spruce mechanical properties data were identified based on a previous standard tests which are

performed and presented in (Fortino *et al.*, 2012; Sandhaas, 2012; Sandhaas and Van de Kuilen, 2013) where, the studies had specified approximately the same mechanical properties of the spruce wood as orthotropic material in the longitudinal, radial, and tangential directions (see table 1).

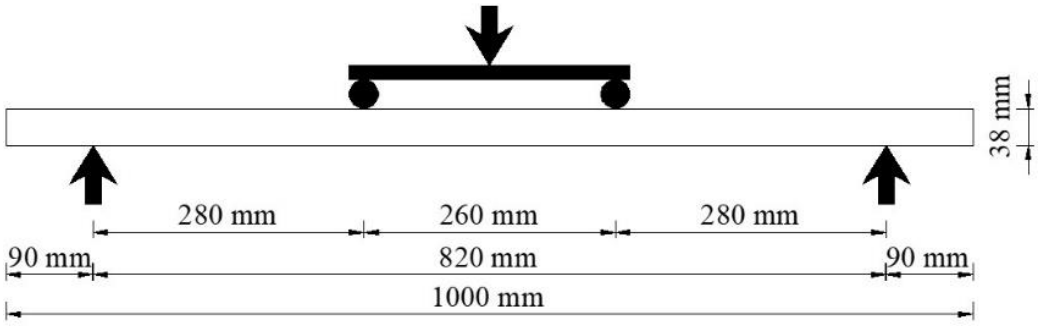

Figure 3 Schematic illustration of the control specimen used in the test

Table 1 Mechanical properties used for the analysis of the specimens

E_L (N/mm^2)	11000
E_R (N/mm^2)	370
E_T (N/mm^2)	370
G_{RL} (N/mm^2)	690
G_{RT} (N/mm^2)	50
G_{TL} (N/mm^2)	690
ν_{LR}	0.430
ν_{LT}	0.530
ν_{RT}	0.420
ν_{TR}	0.240
ν_{RL}	0.019
ν_{TL}	0.013

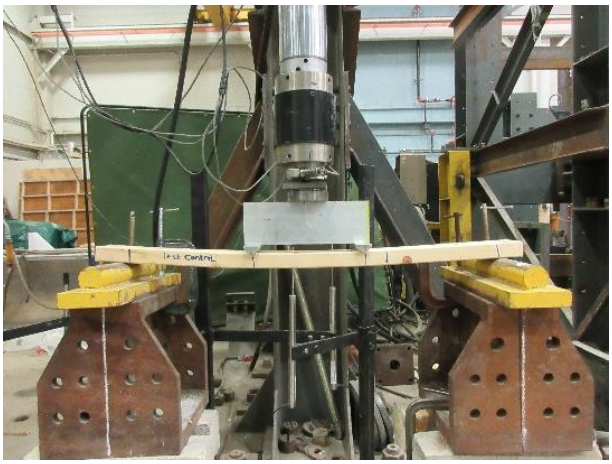

Figure 4 Experimental test of control spruce specimen (without FJ)

A model in Abaqus 6.14 was developed by identifying the nine-independent stiffness parameters D_{ijkl} using the above mechanical properties of spruce, which defined the spruce orthotropic material properties directly. By substituting in the previous stiffness matrix we got the nine-parameters as followed:

$$D_{ijkl} = \begin{bmatrix} 9891.2 & 255.59 & 259.34 & 0 & 0 & 0 \\ 255.59 & 367.45 & 142.15 & 0 & 0 & 0 \\ 259.34 & 142.15 & 366.97 & 0 & 0 & 0 \\ 0 & 0 & 0 & 690 & 0 & 0 \\ 0 & 0 & 0 & 0 & 690 & 0 \\ 0 & 0 & 0 & 0 & 0 & 50 \end{bmatrix} \text{(MPa)} \qquad [6]$$

Note: For the symmetry of the stiffness matrix, an average values were calculated due to the error observed from the data. Therefore, these data were directly required to define the spruce mechanical properties in Abaqus software.

Wood failure, according to NLGA-SPS-4, is a type of failure induced on the glue bond in which the FJ is failed by the tearing away of wood fibre from one and / or the other side of the FJ of the two pieces that have been glued. If the fingers break off at the base or away from the FJ, this is not considered to be wood failure.

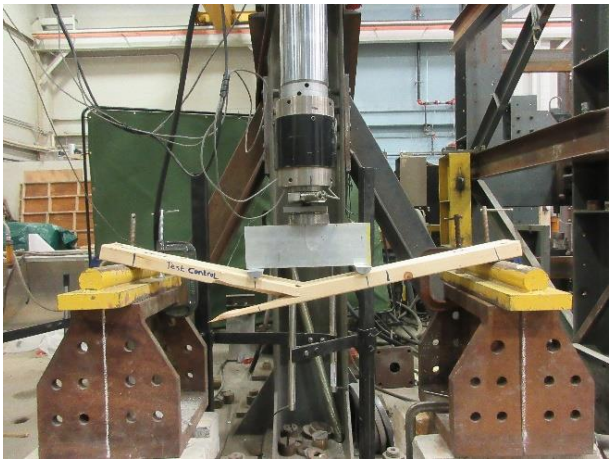

Figure 5 Failure of the experimental control spruce specimen (without FJ)

Figure 5 showed the failure mode of the control specimen which was classified to be wood bending failure accompanied by splitting in the wood fibres. On the other side, Figure 6 and Figure 7 showed a contour diagram of the stresses that occurred due to the simulation of the four point loading test using numerical FEA model.

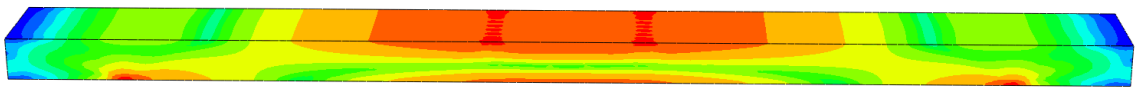

Figure 6 Typical numerical analysis of the control specimen (without FJ)

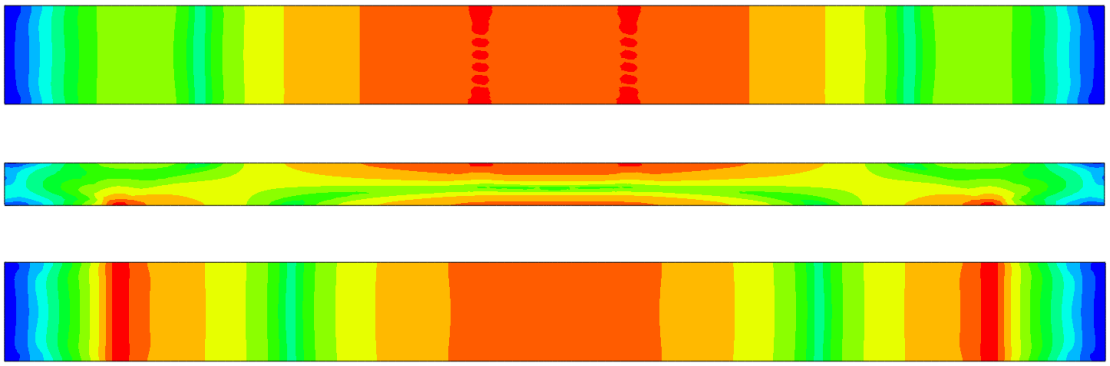

Figure 7 Typical contour showed numerical analysis for the control specimen from upper, side and lower views

Figure 8 showed the load-displacement curves for the 3-specimens without FJ obtained from experimental results and that obtained from the finite element model to make a comparison between experimental data and numerical model data. The curves showed a close agreement between both data which validate the model for the spruce properties.

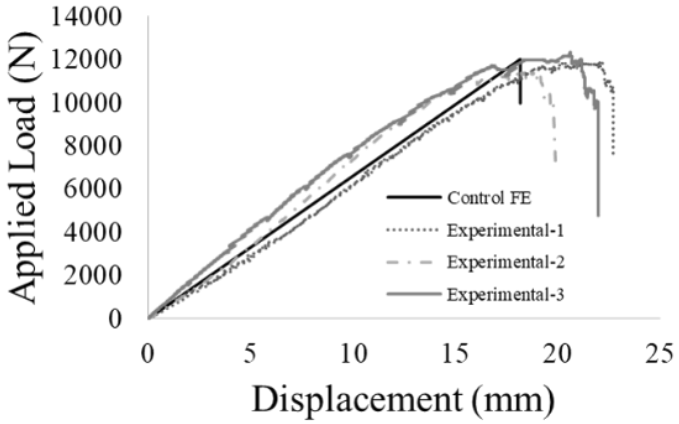

Figure 8 Comparison between experimental and numerical load-displacement curves for control spruce specimens (without FJ)

3.2.2. Validation of adhesive properties

A total of 3-specimens with FJ of actual dry dimensions 38 x 89 x 1000 mm^3 were tested to measure the deflection to validate the numerical 3-D finite element FJ model, see Figures 9, 10, 11. Each specimen was consisted of one-FJ at the mid-span in which, the FJ-length was 28.27 mm, the pitch was 6.33 mm, and the finger-tip width (tip thickness) was 0.76 mm. FJs were assembled with a one face glue using melamine-urea-formaldehyde (MUF) adhesive of constitutive thickness $T_0 = 0.30$ mm. The FJ pieces were pressed at 20° C with a constant end pressure for 24 hours. Then, the specimens were tested after 24 hours of curing at room temperature. The MUF properties data have been identified based on a previous standard tests for mode I (DCB test) and mode II, III (shear test) which are performed and presented in (Fortino *et al.*, 2012; Tran, Oudjene and Meausoone, 2014; Tran, Oudjene and Méausoone, 2015) (see Table 2).

Table 2 Melamine-urea-formaldehyde (MUF) properties for modes I, II and III

Mode I		Mode II		Mode III	
Normal Stiffness K_{nn} N/mm^2	Normal Strength σ_{nn} N/mm^2	Shear-1 Stiffness K_{ss} N/mm^2	Shear-1 strength σ_{ss} N/mm^2	Shear-2 Stiffness K_{tt} N/mm^2	Shear-2 strength σ_{tt} N/mm^2
1.35	1.6	9.0	9.7	9.0	9.7

Also, the initial stiffness K used in this study can be represented in the following matrix:

$$t = \begin{bmatrix} 1.35 & 0 & 0 \\ 0 & 9 & 0 \\ 0 & 0 & 9 \end{bmatrix} \boldsymbol{\varepsilon} \qquad [7]$$

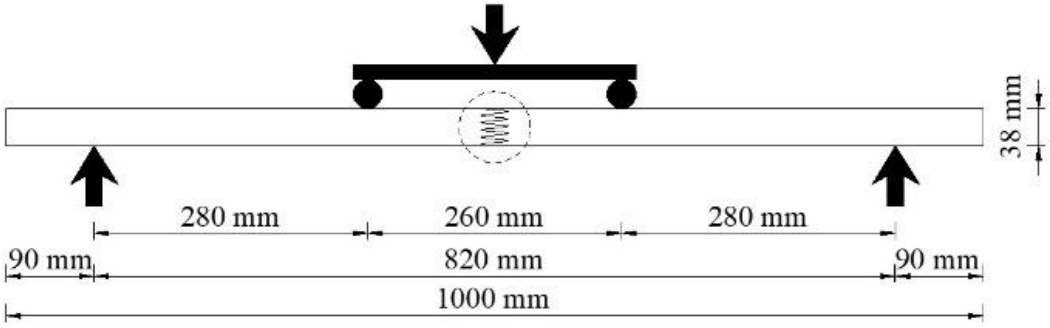

Figure 9 Schematic illustration of the test specimen with FJ at mid-span

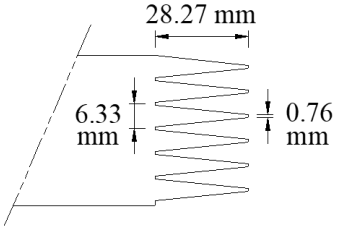

Figure 10 Cross-section showed the FJ specimen geometry dimensions

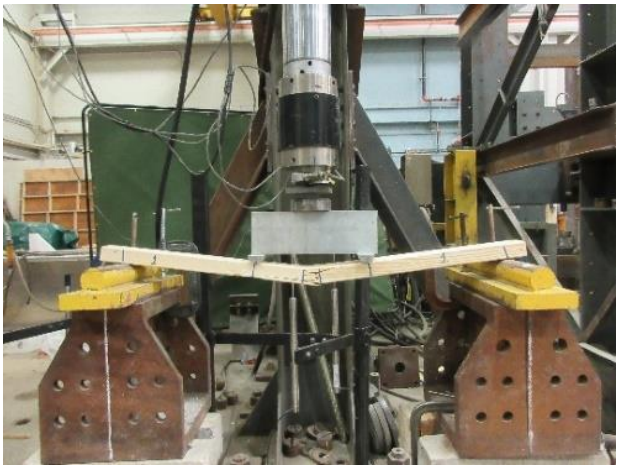

Figure 11 Experimental test of spruce specimen with FJ

Figure 12 Failure of the experimental spruce specimen with FJ

According to the NLGA-SPS-4, 2014 standards, the quality of the glue line may be assessed by assessing the wood failure developed in the FJ. Wood failure shall mean that the joint fails in a wood layer next to the glue line. The difficulty in testing FJ with a wood failure test procedure is a tendency for some of the fingers to break off at the base rather than pull out of the joint. Such failure are not considered wood failure, but are indeterminate and that because of the glue line under the finger was not stressed in shear parallel to the glue line.

Figure 13 Failure profile of the spruce specimen with FJ

Figure 12 and Figure 13 showed that failure was along the joint profile accompanied with failure at the FJ-tips which was classified as Failure Mode 3 according to NLGA-SPS-4.

The failure modes occurring in FJ specimens based on ASTM D4688 were classified into six modes as followed: (NLGA-SPS-4, 2014)

- Failure mode 1, along the bond line surfaces of the joint profile with poor wood failure of any kind.
- Failure mode 2, along the bond line surfaces of the joint profile with good wood shear failure.
- Failure mode 3, along the joint profile but with some failure at the finger roots or scarf tips. In addition, good overall wood shear failure along joint profile surfaces.
- Failure mode 4, tensile wood failure at FJ roots or scarf tips. Little failure of any kind along the joint profile.
- Failure mode 5, beginning at the joint and continuing away from the joint due to a stress riser. This is 100% wood failure.
- Failure mode 6, occurring away from the joint, not influenced by the joint. This is all wood failure.

Figure 14 and Figure 15 showed the contour failure of spruce specimen with FJ due to stresses from numerical FEA analysis.

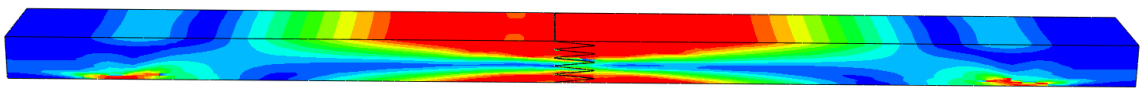

Figure 14 Typical numerical analysis of the spruce specimen with FJ

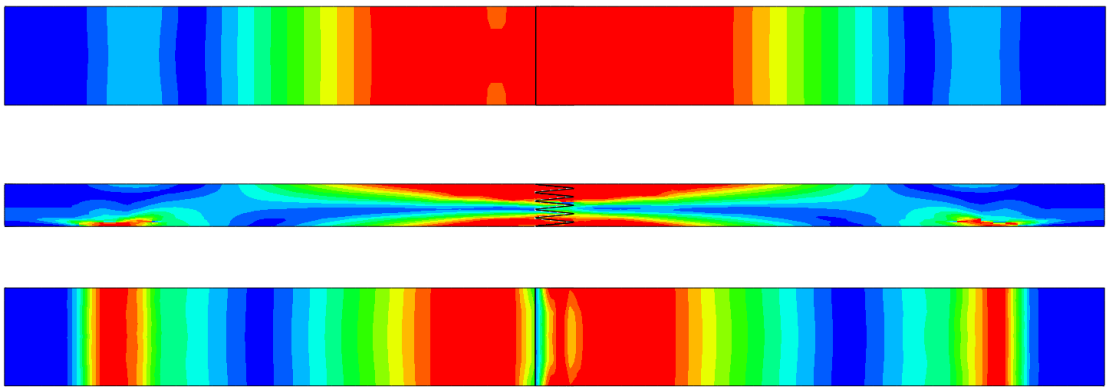

Figure 15 Typical contour showed numerical failure for the spruce specimen with FJ from upper, side and lower views

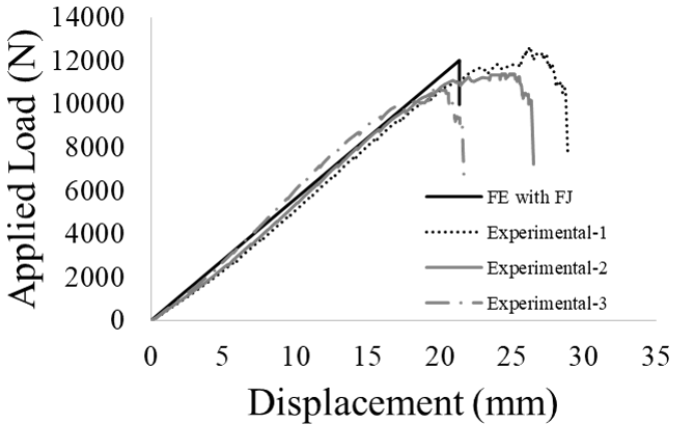

Figure 16 Comparison between experimental and numerical load-displacement curves for spruce specimen with FJ

The load-displacement curves in Figure 16 were obtained for the 3-specimens with FJ from experimental results and from the FEA model to make a comparison between them. The curves showed a close agreement between both experimental and numerical model data which validated the model for adhesive properties with the spruce adherent used.

Chapter 4

Optimization of finger-joined spruce lumber

The optimization process is aimed at maximizing or minimizing some functions relative to some criteria, in order to determine alternatives with the most effective cost and performance under the given constraints. Information was needed to manage process inputs to optimize the outputs. Therefore, statistical design of experiment (DOE) was used to determine the relationship between constraints (factors or parameters) affecting a process and the responses of that process. In other words, it was used to find cause-and-effect relationships.

In this part, the objective was to use the previously experimentally verified numerical 3-D FE combined with DOE methodology as a tool to investigate the factors affecting the stiffnesses values of spruce lumber as a function of the geometry of FJ configuration. The 3-D FE Model provided accurate results observed from the close agreement between model and experiments corresponding to the actual specimens. The numerical 3-D FE was established to obtain responses (stiffnesses) for the statistical designed experiments.

The study were divided into eight parts according to:

- FJ orientation (horizontal and vertical), See Figures 17, 18.
- FJ slope position measured from the vertical axis (Normal: 0°; Inclined: 30°, 45° and 60°),
- FJ geometry configuration (FJ-length, FJ-pitch and FJ-tip) as follows:
    1. Optimization of Normal 0° slope FJ Spruce Lumber in horizontal orientation,
    2. Optimization of Normal 0° slope FJ Spruce Lumber in vertical orientation,

3. Optimization of Inclined 30° slope FJ Spruce Lumber in horizontal orientation,
4. Optimization of Inclined 30° slope FJ Spruce Lumber in vertical orientation,
5. Optimization of Inclined 45° slope FJ Spruce Lumber in horizontal orientation,
6. Optimization of Inclined 45° slope FJ Spruce Lumber in vertical orientation,
7. Optimization of Inclined 60° slope FJ Spruce Lumber in horizontal orientation,
8. Optimization of Inclined 60° slope FJ Spruce Lumber in vertical orientation.

For simplicity, the following notations were used:

Normal 0° slope (N), Inclined 30° slope (I-S-30°), Inclined 45° slope (I-S-45°), Inclined 60° slope (I-S-60°), Horizontal orientation (Hz) and Vertical orientation (VL). Hence, for instance, Optimization of Normal 0° slope FJ Spruce Lumber in vertical orientation can be expressed by (N-FJ-VL) and also Optimization of Inclined 45° slope FJ Spruce Lumber in horizontal orientation can be expressed by (I-S-45°-FJ-Hz). See Table 3.

Table 3 Summarized the Models used for obtaining the optimal FJ-Configurations

#	Item	Position	Slope	Orientation	Wood Type
1	N-FJ-Hz	Normal	0°	Horizontal	Spruce
2	N-FJ-VL	Normal	0°	Vertical	Spruce
3	I-S-30°-FJ-Hz	Inclined	30°	Horizontal	Spruce
4	I-S-30°-FJ-VL	Inclined	30°	Vertical	Spruce
5	I-S-45°-FJ-Hz	Inclined	45°	Horizontal	Spruce
6	I-S-45°-FJ-VL	Inclined	45°	Vertical	Spruce
7	I-S-60°-FJ-Hz	Inclined	60°	Horizontal	Spruce
8	I-S-60°-FJ-VL	Inclined	60°	Vertical	Spruce

The first two Items 1 and 2 are covered in chapter 4, optimization of Normal 0° slope FJ Spruce Lumber in horizontal / vertical orientations. Items 3 to 6 are covered in chapter 5, Optimization of Inclined FJ Spruce Lumber in horizontal / vertical orientations.

4.1. Optimization of normal finger-joined spruce lumber

Normal FJ is the most popular joint used in wood industry. Normal means that FJ is at 0° slope position measured from the vertical axis. Normal FJ is made in both horizontal and vertical orientations. Hence, in this study, Normal FJ joint were divided to two parts according to its orientation (horizontal and vertical). Optimization of each part was carried out to optimize the configuration of the normal FJ and to produce guidelines to achieve structural behaviour of FJ elements that approaches non-finger-joined (NFJ) lumber. The optimum configurations improved the structural properties which impact the behaviour and capacity of finger-joined elements at the serviceability and ultimate limit states.

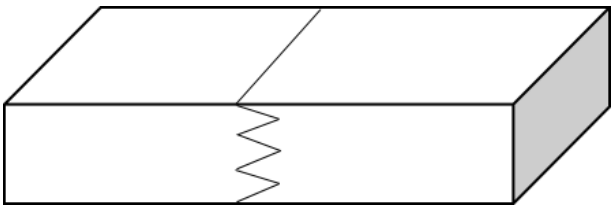

Figure 17 FJ in the Normal horizontal orientation

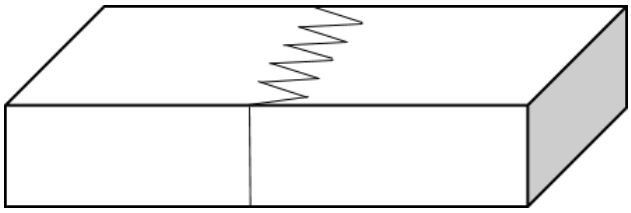

Figure 18 FJ in the normal vertical orientation

Vertical Finger-Joint (VL-FJ) according to (NLGA-SPS-4, 2014) means a profile formed so that an image of the fingers appears on the wide face of the lumber.

Optimization process was performed to specify the optimal geometry of FJ configuration in the two different orientations using a modified response surface model provided from Design-Expert software (version 10). A response surface models (RSM) is a combination between the variations of the simple linear regression with the second order effects of non-linear relationships. RSM is a popular optimization technique to specify the best possible combinations of variables (factors and their interactions) to determine a specific response to a phenomenon (Minimum / maximum / saddle point). In addition, RSM is useful to understand the relationship between multiple predictor variables. There are a multiple benefits of using the RSM such as: determine the optimum combination of factors that yield a desired response and describes the response near the optimum. RSM is also used to determine how specific response is affected by changes in the level of the factors over the specified level of interest. The other use of RSM is to achieve a quantitative understanding of the system behavior over the region tested and to find robust condition for process stability (insensitive spot). Last but not least, RSM is used to replace a more complex model with a much simpler second order regression model for use within a limited range e.g. replace FEM with a simple regression model (Montgomery, 2012).

RSM techniques and statistical optimization plays a key role in industries (Rajan, 2018). Traditional optimization techniques such as the OFAT (one-factor-at-a-time) or the COST (Changing-one-single-thing) techniques are misguided in computing the optimum as they do not take into account factor interactions. Additionally, in real life scenarios, changes in

multiple factors impact a specific response. Design limits, minimum and maximum, must be entered first for numeric factors and exact settings for categorical parameters. In addition, constraints can be added to historical data designs to limit the analysis to a specific part of the data.

In this part, three factors or parameters each at two levels (a high and a low) were chosen for the design of experiment (DOE): A: FJ-length, B: FJ-pitch, and C: FJ-tip width (tip thickness) as shown in Table 4; in which were determined pursuant to the vast values used in previous studies. A modified response surface model (RSM) design was established to assess the effect of the three factors and their interactions on the stiffnesses which affects both modulus of elasticity (MOE) and modulus of rupture (MOR). A regression prediction model was then developed to create prediction equations for the different FJ orientations which can predict the stiffness value for any other desired FJ configuration. A validation for the prediction equations were performed with the numerical 3-D FEM. Hence, this regression equations is useful to determine the stiffness for any FJ geometry directly without the need to use a trial and error approach.

A total of 40-numerical models, 20-models per each FJ orientation, were established to obtain the load-displacement curves per each case using Abaqus FEA software. The applied-load was defined in terms of the maximum bending force obtained from four-point bending tests which was specified to be equal to 12 KN for NFJ spruce specimen, and the corresponding stiffness for the control NFJ was equal to 660.5 N/mm.

4.1.1. Optimization of Hz-finger-joint spruce lumber at normal position

4.1.1.1. DOE for normal FJ in Hz orientation (N-FJ-Hz)

A total of 20-numerical models were established to obtain the load-displacement curves using traction separation law technique under the CZM for the horizontal orientation.

Table 4 Run parameters of 20-models design variables for N-FJ-Hz

Run	A: FJ-length mm	B: FJ-pitch mm	C: FJ-tip mm	Response: stiffness N/mm
1	7	5.7	1.5	527.90
2	21	7.6	0.5	501.85
3	35	7.6	1.0	584.67
4	35	3.8	1.0	596.50
5	21	3.8	1.5	561.98
6	35	5.7	0.5	588.59
7	7	3.8	1.0	556.23
8	21	3.8	0.5	573.29
9	21	7.6	1.5	564.37
10	35	5.7	1.5	615.67
11	7	7.6	1.0	496.49
12	7	5.7	0.5	466.78
13	7	3.8	0.5	465.66
14	35	3.8	0.5	527.48
15	7	7.6	0.5	435.67
16	35	7.6	0.5	560.96
17	7	3.8	1.5	515.18
18	35	3.8	1.5	578.85
19	7	7.6	1.5	490.71
20	35	7.6	1.5	564.66

A modified RSM design type model (a combination of a 2-level factorial design with center points together with a uniform design) was carried out to study the effect of the chosen variables and their interactions. Table 4 showed the stiffnesses values that were achieved within the studied ranges (from 435.67 N/mm to 615.67 N/mm).

Three variables factors were chosen, each of two levels (a high and a low) plus a center point of each factor were added in order to cover all the ranges in between and to predict the changes that could occur in the design model. The added center points aimed to determine the linearity / non-linearity of the model. The parameter's values were A: FJ-length (low 7.0mm, CP 21.0mm and high 35.0mm), B: FJ-pitch (low 3.8mm, CP 5.7mm and high 7.6mm) and C: FJ-Tips (low 0.5mm, CP 1.0mm and high 1.5mm). The obtained results demonstrated clearly the potential of increasing the finger-joint resistance by optimizing its geometry. In addition, the model seemed to be non-linear (quadratic type) from the cube diagram and contour 3-D plot diagram (See Figure 37 and Figure 38). From Figure 26 to Figure 34 show contour graphs obtained from statistical analysis of the relation between A: FJ-length, B: FJ-pitch, and C: FJ-Tips.

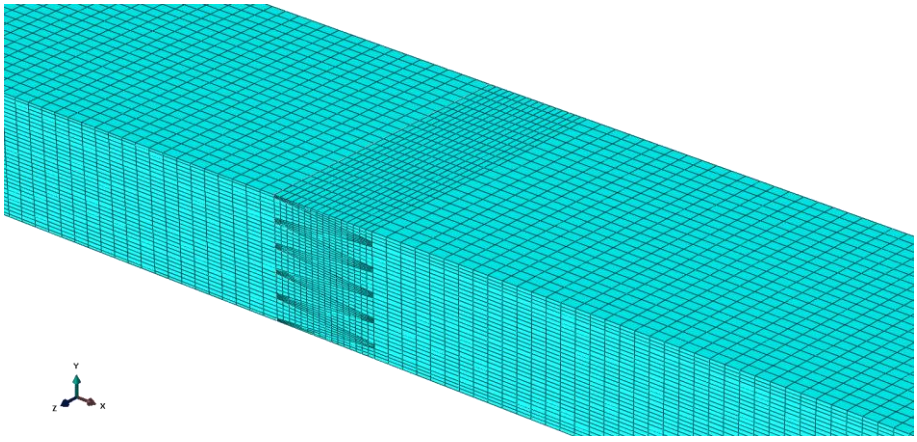

Figure 19 Typical meshed FE model of spruce specimen in N-FJ-Hz

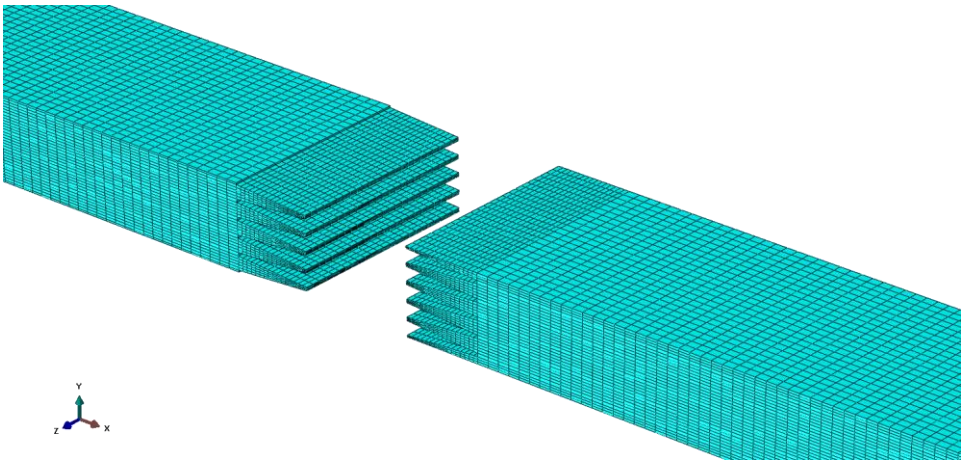

Figure 20 Typical meshed cross-section of the N-FJ-Hz before interlocking

Figure 19 and Figure 20 showed a typical meshed finite element numerical 3-D model of normal FJ in the horizontal orientation. The meshed elements (mesh refinement) at the interface were finer than other parts because higher stresses were expected at these regions. The other parts would not expected to carry peak stresses at least under a four-point static load test, and a relatively slow variation of stresses in these regions were safely assumed. See Figure 21, 22.

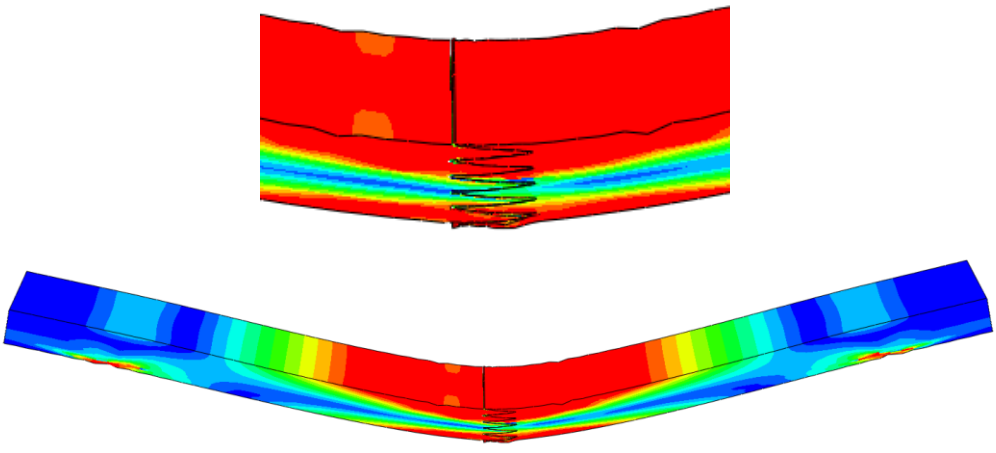

Figure 21 Typical FEA stress contour for failure of FJ spruce specimen in N-FJ-Hz

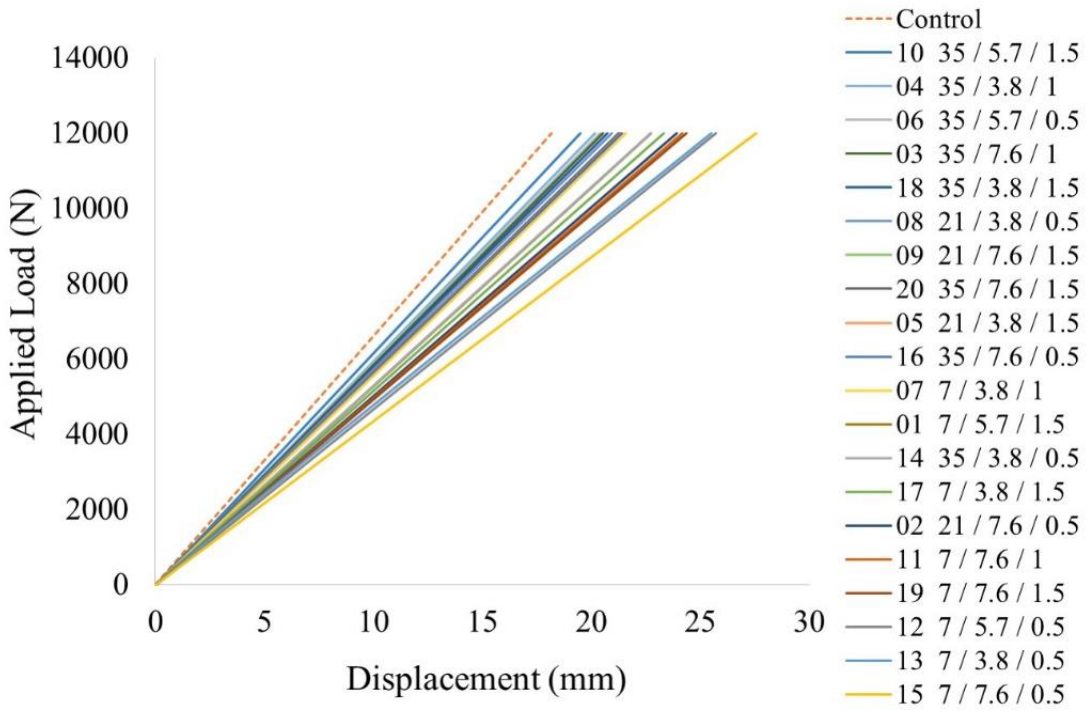

Figure 22 Numerical load-displacement curves show comparison between the control and different FJs geometries of spruce specimens in N-Hz orientation

* The legend for instance [18 35 / 3.8 / 1.5] refers to:

[Run number FJ Length / FJ pitch / FJ tip] respectively.

4.1.1.2. ANOVA for normal FJ in Hz orientation (N-FJ-Hz)

The analysis of variance (ANOVA) for a second-order response surface model for the normal FJ in Hz-orientation showed the model F-value of 16.19 implied that the model was significant as shown in Table 5. There was only a 0.01% chance that an F-value this large could occur due to noise.

Table 5 ANOVA for RSM second-order model for N-FJ-Hz

Source	Sum of Squares	df	Mean Square	F - Value	P - Value Prob > F	
Model	41200.28	6	6866.71	16.19	< 0.0001	Significant
A	27453.18	1	27453.18	64.72	< 0.0001	
B	1931.38	1	1931.38	4.55	0.0525	
C	5589.06	1	5589.06	13.18	0.0031	
A^2	2899.82	1	2899.82	6.84	0.0214	
B^2	2788.79	1	2788.79	6.57	0.0236	
C^2	4499.36	1	4499.36	10.61	0.0062	
Residual	5514.18	13	424.17			
Cor Total	46714.46	19				

From the previous table, Values of "Prob > F" less than 0.05 indicated model terms were significant. In this case, A, C, A^2, B^2, C^2 were the significant model terms. Values greater than 0.1 indicated the model terms were not significant. However, the model required to add insignificant model terms such as B here to support hierarchy. The model had a sample standard deviation equal 20.60 which indicated the measure of the dispersion of the set of the data from its mean which equal 538.67 N/mm. The standard deviation was calculated as the square root of the variance by determining the variation between each data point relative to the mean. So, if the data points were further from the mean, there was higher deviation within the data set.

Three-model summary statistics were calculated to validate the adequacy of the model and could be illustrated as follow:

1. R-squared (R^2) indicates how well the model fits the data (the higher the R^2, the better the model fits the data). In other words, R^2 is a statistical measure of how

close the data are to the fitted regression line. It is also known as the coefficient of determination or the coefficient of multiple determination for multiple regression. The R^2 is always between (0 – 100%) in which 0% indicates that the model explains none of the variability of the response data around its mean. On the contrary, 100% indicates that the model explains all the variability of the response data around its mean. The R^2 removes the proportion of total variability explored by the model. Nonetheless, it cannot be relied on because it increases as factors are added to the model, even if these factors are not significant (Montgomery, 2012).

2. Adjusted R-squared (R^2_{adj}) is a measure of the amount of variation about the mean expressed by the model. The R^2_{adj} increases only if the new term improves the model more than would be expected by chance and it decreases when a predictor improves the model by less than expected by chance. It also compares the explanatory power of regression models that contain different number of predictors. Therefore, R^2_{adj} is a modified version of R^2 that has been adjusted for the number of predictors in the model and it is always lower than R^2 (Montgomery, 2012).

3. Predicted R-squared (R^2_{Pred}) is a measure of how the model fits each point in the design or how well a regression model predicts responses for new observations. To calculate R^2_{Pred}, a model is used to estimate each point using all of the design points except the one being estimated. In other words, R^2_{Pred} can be calculated by systematically removing each observation from the data set, then estimating the regression equation and determining how well the model predicts the removed observation. A good model has a high R^2_{Pred} (Montgomery, 2012).

Table 6 Model summary statistics for N-Hz

Source	Standard Deviation	R-squared (R^2)	Adjusted R^2 (R^2_{adj})	Predicted R^2 (R^2_{Pred})	
Linear	27.09	0.75	0.70	0.60	
Quadratic	19.01	0.92	0.85	0.69	Suggested
Cubic	22.63	0.97	0.79	-0.49	Aliased

Table 6 showed the model summary statistics for the Normal FJ in horizontal orientation. The results demonstrated that a Modified Quadratic design type was chosen. The model statistics $R^2_{adj} = 0.85$ and $R^2_{Pred} = 0.69$ were in a reasonable agreement; the model with the $R^2_{Pred} = 0.69$ had a good chance of making reasonable prediction.

Validation of the basic assumptions of the ANOVA and model adequacy were investigated by the examination of residuals. The residuals are the deviation of observed data from the predicted value. The residuals, which are the estimation of the error terms in the model, were assumed to be structureless and to be normally distributed with a mean zero and a constant standard deviation. There were three-model assumptions checks:

- Checks for the normality assumption, (see, Figure 23),
- Checks for the homogeneous variance assumption, (see, Figure 24), and
- Checks for independence assumption (see, Figure 25).

Figure 23 displayed a Design-Expert normal probability plot of the studentized residuals. All the values were well distributed around the mean. This plot resembles a straight line, all the values seemed to lie on the straight line, which means that the underlying error distribution is normal. It was noticed that some of the residuals seemed to be skewed, but that skewed seemed to be very little. So, the first assumption of ANOVA was satisfied.

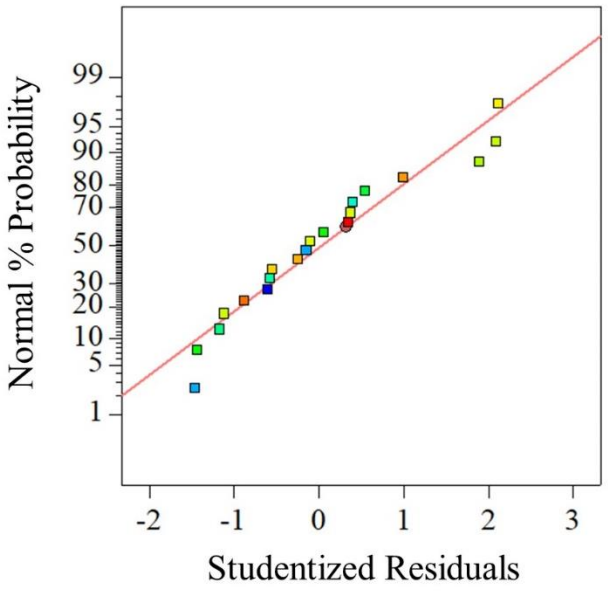

Figure 23 Normal probability plot of residuals for N-FJ-Hz

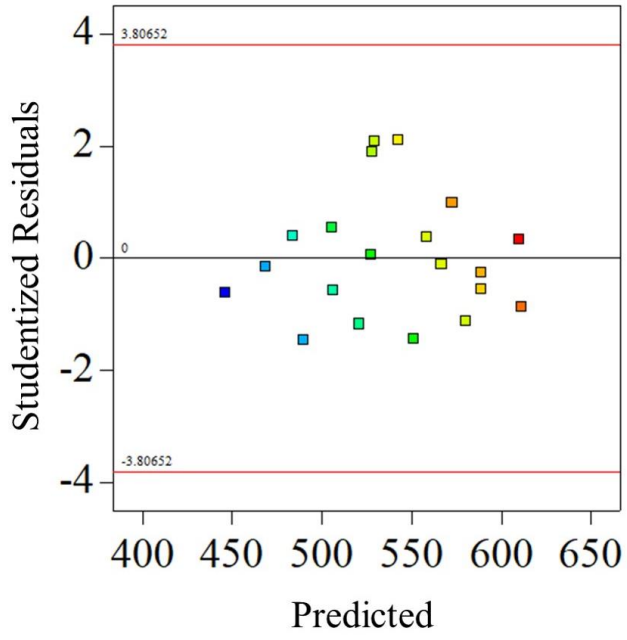

Figure 24 Plot between residuals and predicted for N-FJ-Hz

Figure 24 displayed a Design-Expert plot of studentized residuals versus predicted values. The plot showed that the distribution between the residuals and predicted values were random, and there was no obvious pattern in it. There was no behavior which mean that the residuals appeared to be independent of the size of the fitted values and had constant variance. This indicated that the second ANOVA assumption was satisfied.

Figure 25 displayed a Design-Expert plot of studentized residuals versus run order. This plot was used to detect the correlation between the residuals that might accrued as a result of improper randomization of the experiments. There was no tendency for positive or negative residuals in the plot and this implied that there was no independence among the treatments. In addition, the treatments were properly randomized. Therefore, since all the assumptions were valid, the model provided an adequate fit to the observed data.

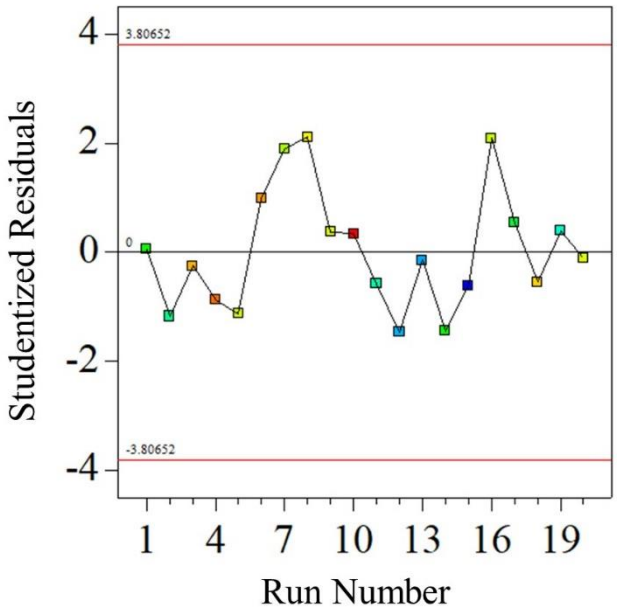

Figure 25 Plot between residuals and run for N-FJ-Hz

Then, for studying the effect of the treatments and their interactions on the stiffness, a contour graphs were drawn between two factors at the different levels of the third remaining factor. See from Figure 26 to Figure 34.

The graphs showed that FJ geometry had a significant effect on the stiffnesses values which consequently affect the values of MOE and MOR. The observations from curves were as follow:

Figure 26 to Figure 28 showed the interaction effect between factors A: FJ-length and B: FJ-pitch on the stiffness value with changing the value of factor C: FJ-tip from minimum to maximum. The figures showed that the stiffness value was increasing with the increase of C: FJ-tip until a value of C between its mid and maximum limits (around 1.20 mm) and then decreasing again at maximum C of 1.5mm.

Figure 29 to Figure 31 showed the interaction effect between factors A: FJ-length and C: FJ-tip on the stiffness value with changing the value of factor B: FJ-pitch from minimum to maximum. The graphs showed an increasing in the stiffness value with the increase of B: FJ-pitch until approximately its mid value then the stiffness decreased again.

Figure 32 to Figure 34 showed the interaction effect between factors B: FJ-pitch and C: FJ-tip on the stiffness value with changing the value of factor A: FJ-length from minimum to maximum. It was demonstrated that with the increase of A until maximum, the stiffness increased. This was due to the increasing of the interface surface between the two adherent parts.

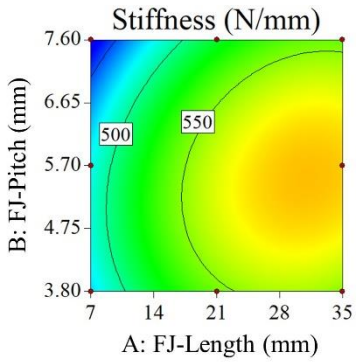

Figure 26 Contour shows interaction between A and B at min C = 0.5 mm

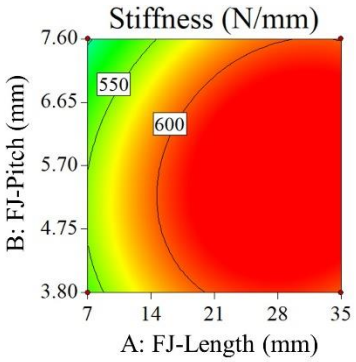

Figure 27 Contour shows interaction between A and B at mid C = 1.0 mm

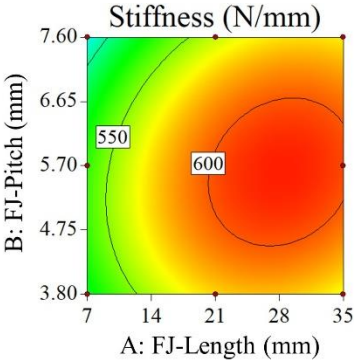

Figure 28 Contour shows interaction between A and B at max C = 1.5 mm

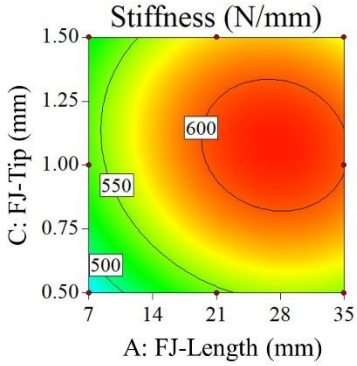

Figure 29 Contour shows interaction between A and C at min B = 3.8 mm

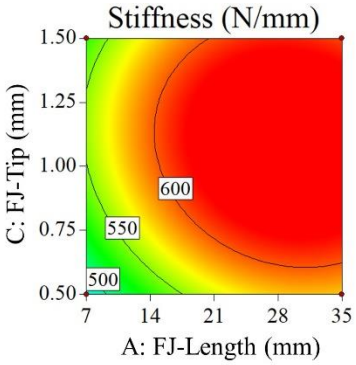

Figure 30 Contour shows interaction between A and C at mid B = 5.7 mm

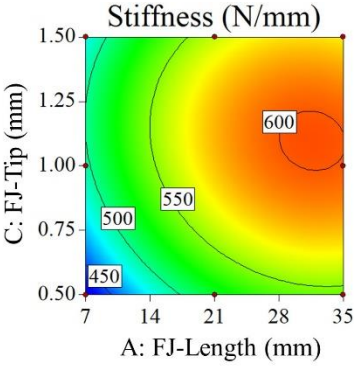

Figure 31 Contour shows interaction between A and C at max B = 7.6 mm

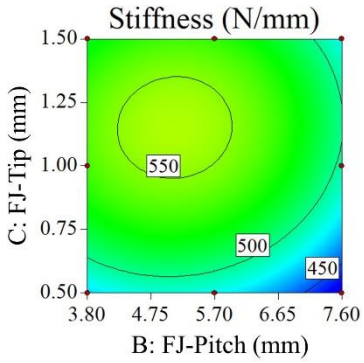

Figure 32 Contour shows interaction between B and C at min A = 7.0 mm

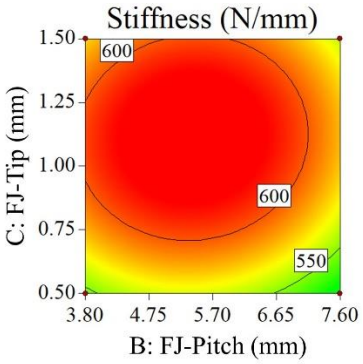

Figure 33 Contour shows interaction between B and C at mid A = 21.0 mm

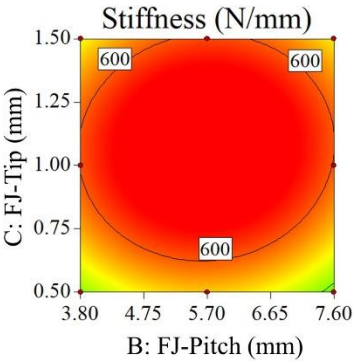

Figure 34 Contour shows interaction between B and C at max A = 35.0 mm

Table 7 Optimization for N-FJ-Hz

Factors	Lower	Upper	Optimal N-FJ-Hz
A: FJ-Length (mm)	7.0	35.0	29.80
B: FJ-Pitch (mm)	3.80	7.60	5.40
C: FJ-Tips (mm)	0.50	1.50	1.11
Stiffness (N/mm)	435.67	615.67	639.85

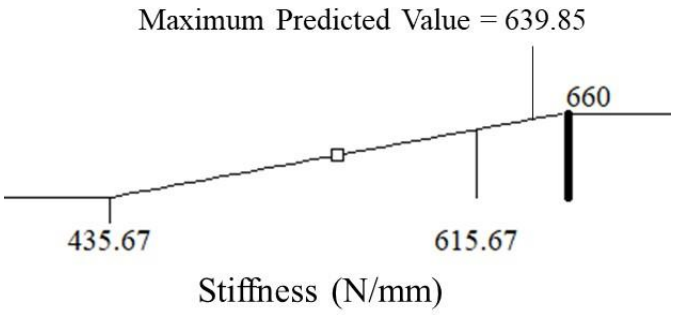

Figure 35 Schematic diagram for optimal predicted maximum N-FJ-Hz value

Table 7 and Figure 35 showed the maximum stiffness that was reached from the studied ranges of the data was equal to 639.85 N/mm, which is a close value to the control one. Other purpose of that study was to find a relation from using regression analysis that could predict the stiffness value. That predicted equation will save time, money, and material (wood and glue) compared to the trial and error approach to determine the FJ geometry that approaches NFJ lumber:

$$Stiffness = 27.68 + 10.03A + 96.34B + 365.99C - 0.17A^2 - 8.96B^2 - 164.30C^2 \quad [8]$$

Where,

Stiffness in (N/mm), A: FJ-length in (mm), B: FJ-pitch in (mm), and C: FJ-tips in (mm).

A verification was established for the horizontal regression equation in terms of the factors and their interactions to make it be used for prediction of stiffness within the factor's levels. Extra points were added due to the number of errors (lack of fit) in the statistical model.

Hence, seven-random FJ-geometries values within the specified ranges were chosen and 3-D FE models were established for all, in order to compare stiffnesses values through a predicted-model relationship curve to validate the equation. See Table 8 and Figure 36.

Table 8 Stiffnesses from predicted equation versus model – N-FJ-Hz

Run Number	A	B	C	Predicted stiffness (N/mm)	Model stiffness (N/mm)	Agreement (%)	Tolerance (%)
1	9.58	7.04	0.63	507.34	452.49	89.19	10.81
2	14.0	5.43	1.50	573.36	539.22	94.05	5.95
3	17.83	7.43	0.54	523.05	483.49	92.44	7.56
4	21.0	5.7	1.0	623.79	549.27	88.05	11.95
5	23.0	7.47	0.53	536.98	521.30	97.08	2.92
6	30.71	6.12	1.06	634.32	562.45	88.67	11.33
7	33.0	4.23	0.50	564.44	574.92	98.18	1.82

* A: FJ-length, B: FJ-pitch, and C: FJ-Tips

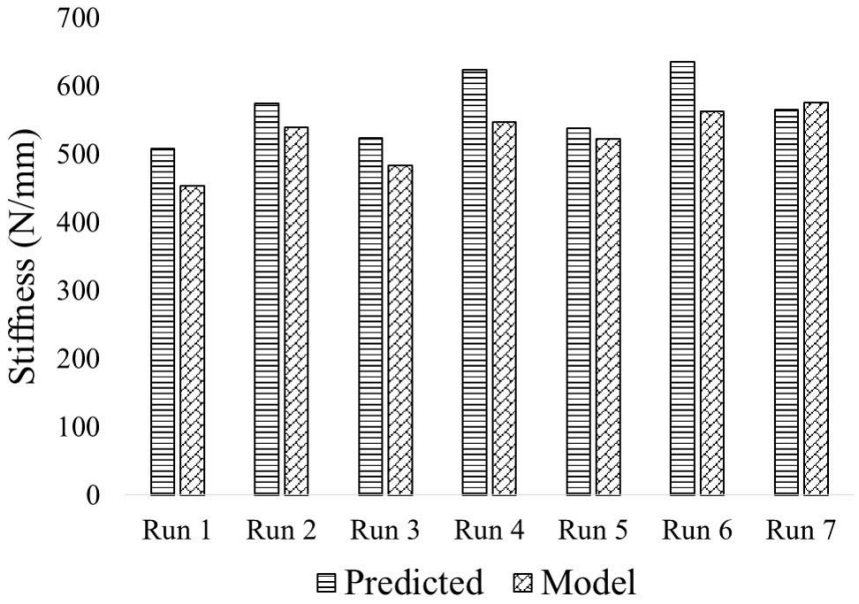

Figure 36 Graph showed predicted stiffnesses versus model values – N-FJ-Hz

Table 8 and Figure 36 showed the stiffnesses values from regression predicted equation versus stiffnesses from model numerical simulation. The tolerance did not exceed 12%

error which was an acceptable error with using numerical simulation, also putting into consideration that wood is a natural resource that is difficult to control. Hence, the predicted regression equation can predict the stiffness value for the corresponding FJ-geometry within the specified ranges.

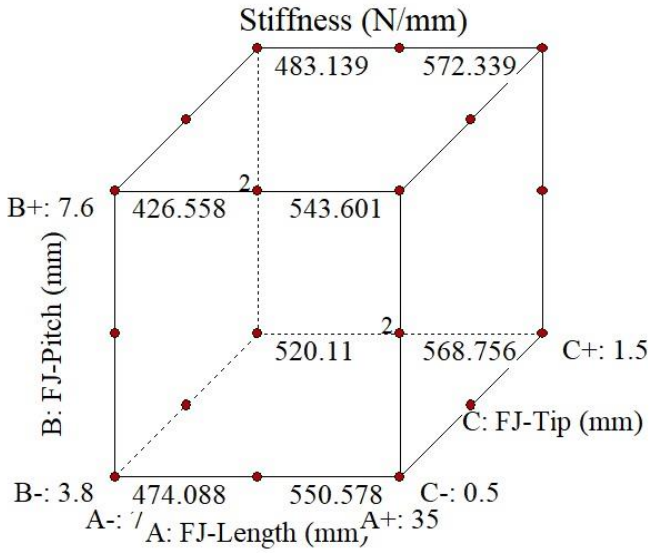

Figure 37 Cube simulate the second-order model – N-FJ-Hz

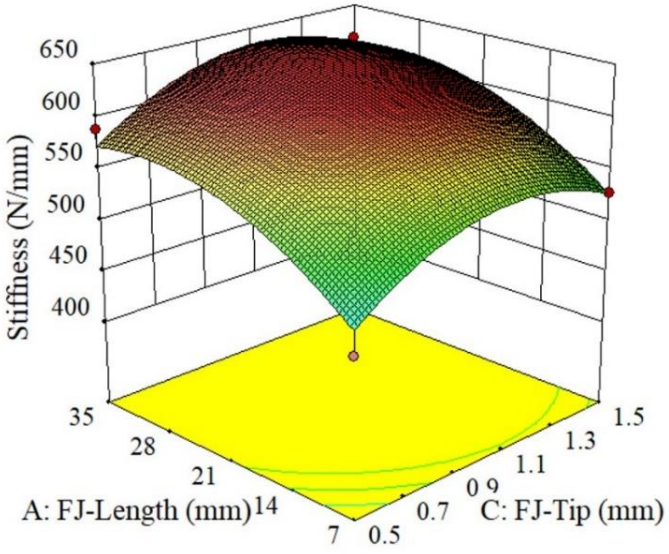

Figure 38 3-D surface simulated the statistical second-order model –N-FJ-Hz

4.1.2. Optimization of VL-finger-joint spruce lumber at normal position

4.1.2.1. DOE for normal FJ in VL orientation (N-FJ-VL)

A total of 20-numerical models were carried out to obtain the load-displacement curves using traction separation law technique under CZM for vertical orientation. A modified RSM design type model was established to study the effect of the chosen variables.

Table 9 Run parameters of 20-models design variables for N-FJ-VL

Run	A: FJ-length mm	B: FJ-pitch mm	C: FJ-tip mm	Response: stiffness N/mm
1	7	11.12	1.5	530.99
2	21	17.8	0.5	520.24
3	35	17.8	1.0	565.03
4	35	4.45	1.0	613.61
5	21	4.45	1.5	613.99
6	35	11.12	0.5	562.02
7	7	4.45	1.0	580.65
8	21	4.45	0.5	617.64
9	21	17.8	1.5	536.73
10	35	11.12	1.5	600.28
11	7	17.8	1.0	507.74
12	7	11.12	0.5	535.59
13	7	4.45	0.5	453.59
14	35	4.45	0.5	606.94
15	7	17.8	0.5	408.84
16	35	17.8	0.5	524.76
17	7	4.45	1.5	451.28
18	35	4.45	1.5	619.08
19	7	17.8	1.5	422.74
20	35	17.8	1.5	486.94

Table 9 showed the stiffnesses values that were achieved within the studied ranges (from 408.84 N/mm to 619.08 N/mm). Three parameters or factors were chosen as same as the previous study for the horizontal orientation, each of two levels (a high and a low). An additional points (a center point in between each two levels per each factor) were added to determine the linearity / non-linearity and to predict the changes that could occur in the design model. The parameter's values were A: FJ-length (low 7.0mm, CP 21.0mm and high 35.0mm), B: FJ-pitch (low 4.45mm, CP 11.13mm and high 17.8mm) and C: FJ-Tips (low 0.5mm, CP 1.0mm and high 1.5mm). The obtained results showed clearly the potential of increasing the finger-joint resistance by optimizing its geometry. In addition, the model seemed to be non-linear (quadratic type) from the cube figure and contour 3-D plot diagram (See Figure 57 and Figure 58). From Figure 46 to Figure 54 show contour graphs obtained from statistical analysis of the relation between A: FJ-length, B: FJ-pitch, and C: FJ-Tips.

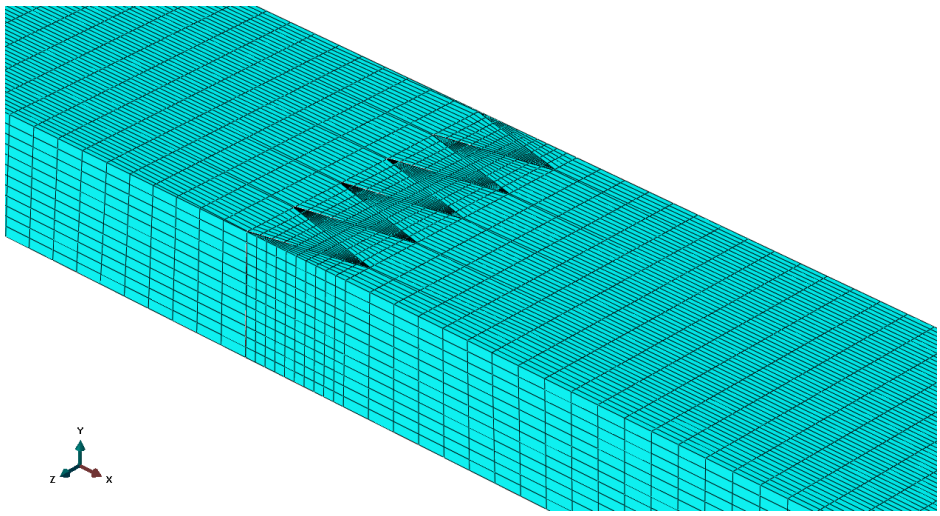

Figure 39 Typical meshed FE model of Spruce Specimen in N-FJ-VL

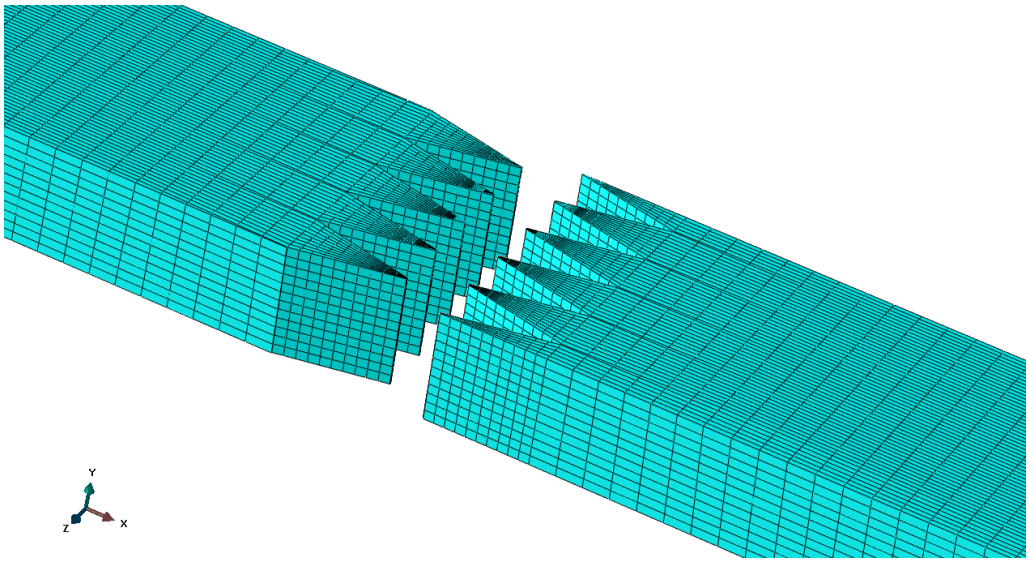

Figure 40 Typical meshed Cross-section of the N-FJ-VL before interlocking

Figure 39 and Figure 40 showed a typical meshed FEA numerical 3-D model of normal FJ in the vertical orientation. The meshed elements at the interface were finer than other parts because higher stresses were expected at these regions. See Figure 41.

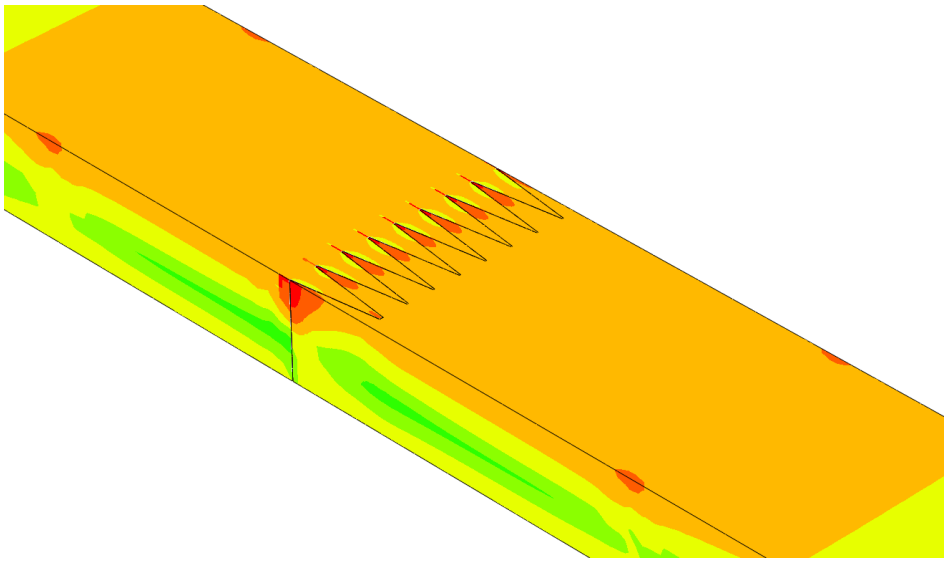

Figure 41 Typical FEA stress contour for failure of FJ spruce specimen in N-FJ-VL

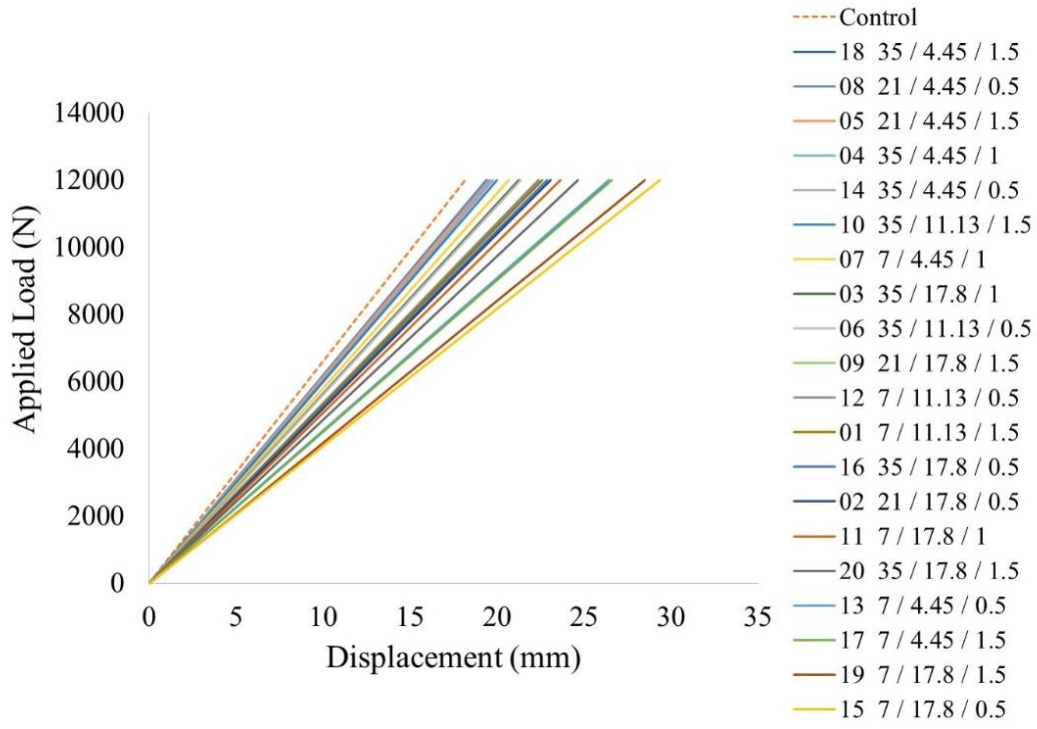

Figure 42 Numerical load-displacement curves show comparison between the control and different FJs geometries of spruce specimens in N-VL orientation

* The legend for instance [18 35 / 4.45 / 1.5] refers to:

[Run number FJ Length / FJ pitch / FJ tip] respectively.

4.1.2.2. ANOVA for normal FJ in VL orientation (N-FJ-VL)

The analysis of variance for the modified response surface second-order model for the normal FJ in VL orientation is shown in Table 10. The results showed the model F-value of 14.71 implied that the model was significant. There was only a 0.01% chance that an F-value this large could occur due to noise.

Table 10 ANOVA for RSM second-order model for N-FJ-VL

Source	Sum of Squares	df	Mean Square	F - Value	P - Value Prob > F	
Model	73967.01	6	12327.84	14.71	<0.0001	Significant
A	29477.46	1	29477.46	35.17	<0.0001	
B	21333.52	1	21333.52	25.46	0.0002	
C	67.61	1	67.61	0.081	0.7809	
A^2	15176.01	1	15176.01	18.11	0.0009	
B^2	9763.49	1	9763.49	11.65	0.0046	
C^2	13083.94	1	13083.94	15.61	0.0017	
Residual	10894.39	13	838.03			
Cor Total	84861.40	19				

From the previous table, Values of "Prob > F" less than 0.05 indicated model terms were significant. In this case, A, B, A^2, B^2, C^2 were the significant model terms. Values greater than 0.1 indicated the model terms were not significant. However, the model required to add insignificant model terms such as C here to support hierarchy. The model had a sample standard deviation equal 28.95 which indicated the measure of the dispersion of the set of the data from its mean which equal 537.91 N/mm.

Table 11 showed the model summary statistics for the Normal FJ in vertical orientation. The results showed that a Modified Quadratic design type was selected. The model statistics $R^2_{adj} = 0.81$ and $R^2_{Pred} = 0.71$ were in a reasonable agreement; the model with the $R^2_{Pred} = 0.71$ had a good chance of making reasonable prediction.

Table 11 Model summary statistics for N-VL

Source	Standard Deviation	R-squared (R^2)	Adjusted R^2 (R^2_{adj})	Predicted R^2 (R^2_{Pred})	
Linear	46.09	0.60	0.53	0.35	
Quadratic	31.20	0.89	0.78	0.52	Suggested
Cubic	28.03	0.97	0.82	-0.26	Aliased

Validation of the basic assumptions of the ANOVA and model adequacy were investigated by the examination of residuals. The residuals, which are the estimation of the error terms in the model, were assumed to be normally distributed with a mean zero and a constant standard deviation. Three-model assumptions checks were verified:

- Checks for the normality assumption, (see, Figure 43),
- Checks for the homogeneous variance assumption, (see, Figure 44), and
- Checks for independence assumption (see, Figure 45).

Figure 43 displayed a Design-Expert normal probability plot of the studentized residuals. All the values were well distributed around the mean and seemed to lie on the straight line, which means that the underlying error distribution is normal. Hence, the first assumption of ANOVA was satisfied.

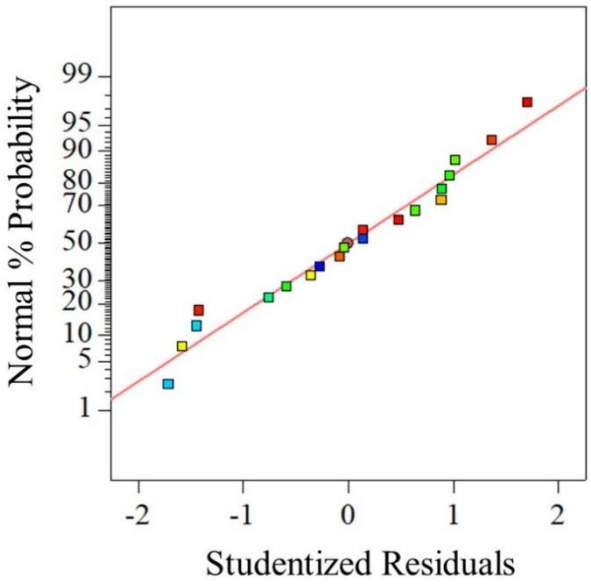

Figure 43 Normal probability plot of residuals for N-FJ-VL

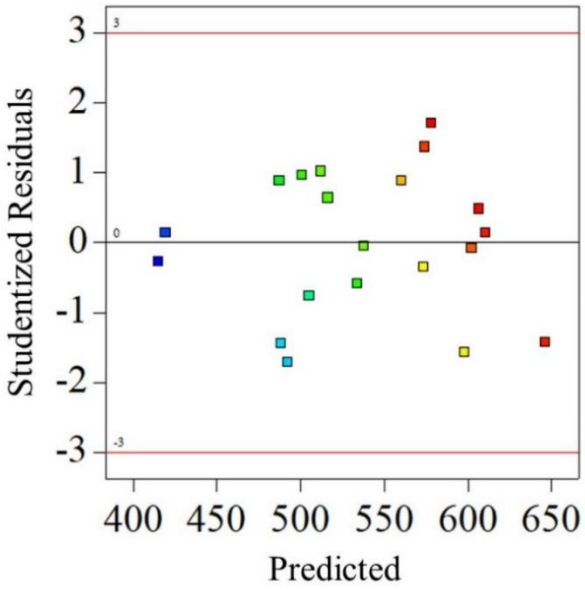

Figure 44 Plot between residuals and predicted for N-FJ-VL

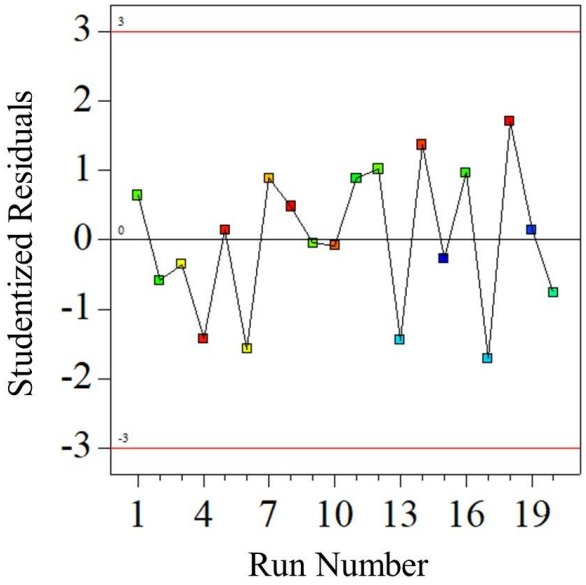

Figure 45 Plot between residuals and run for N-FJ-VL

Figure 44 displayed a Design-Expert plot of studentized residuals versus predicted values. The plot showed that the distribution between the residuals and predicted values were random, and there was no obvious pattern in it which mean that the variance was constant. Hence, this indicated that the second ANOVA assumption was satisfied.

Figure 45 displayed a Design-Expert plot of studentized residuals versus run order. There was no tendency for positive or negative residuals in the plot and this implied that there was no independence among the treatments. In addition, the treatments were properly randomized. Since all the assumptions of that adequate model were valid, therefore, the model provided an adequate fit to the observed data.

A contour graphs were drawn between two factors at the different levels of the third remaining factor for studying the effect of the treatments and their interactions on the stiffness. See from Figure 46 to Figure 54. The graphs showed that FJ geometry had a significant effect on the stiffnesses values. The following observations can be made:

Figure 46 to Figure 48 showed the interaction effect between factors A: FJ-length and B: FJ-pitch on the stiffness value with changing factor C: FJ-tip from minimum to maximum. Even though factor C was not significant in the model, nevertheless, the figures showed that the stiffness value was increasing with the increase of C until the mid-value of C then decreasing again until reach to maximum of 1.5mm.

Figure 49 to Figure 51 showed the interaction effect between factors A: FJ-length and C: FJ-tip on the stiffness value with changing factor B: FJ-pitch from minimum to maximum. The graphs showed an increasing stiffness value with the increase of B until its mid value then the stiffness decreased.

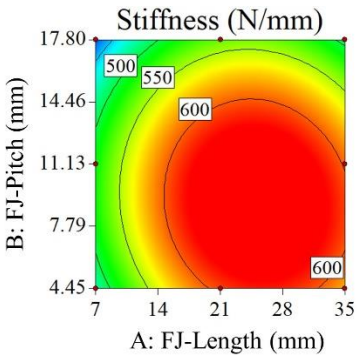

Figure 46 Contour shows interaction between A and B at min C = 0.5 mm

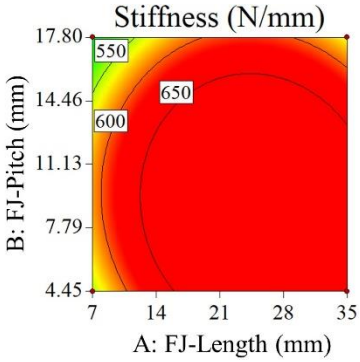

Figure 47 Contour shows interaction between A and B at mid C = 1.0 mm

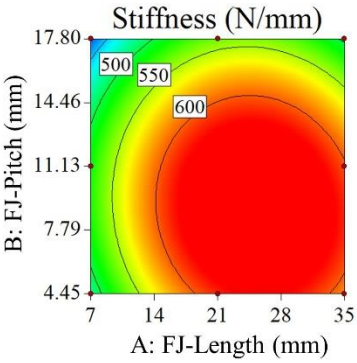

Figure 48 Contour shows interaction between A and B at max C = 1.5 mm

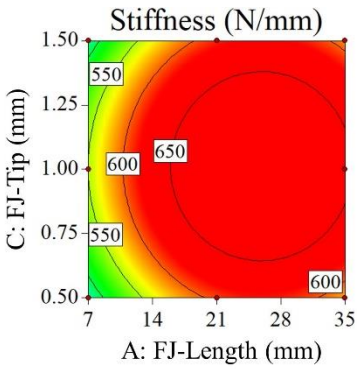

Figure 49 Contour shows interaction between A and C at min B = 4.45 mm

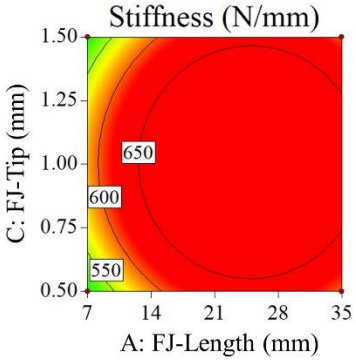

Figure 50 Contour shows interaction between A and C at mid B =11.13 mm

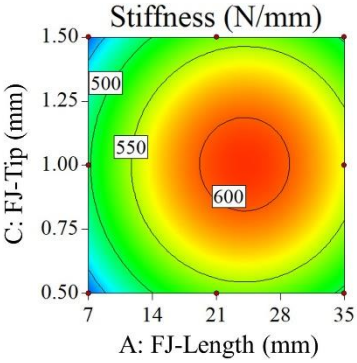

Figure 51 Contour shows interaction between A and C at max B = 17.8 mm

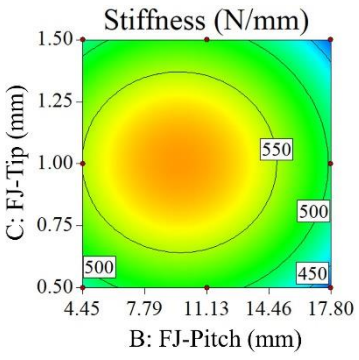

Figure 52 Contour shows interaction between B and C at min A = 7.0 mm

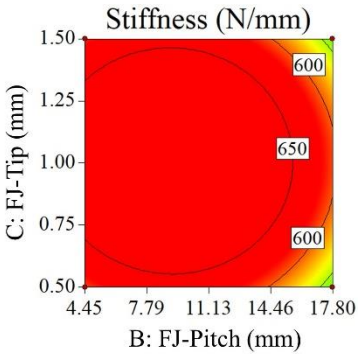

Figure 53 Contour shows interaction between B and C at mid A = 21.0 mm

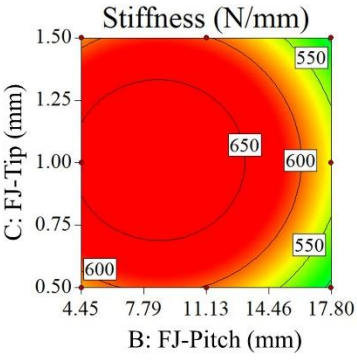

Figure 54 Contour shows interaction between B and C at max A = 35.0 mm

Figure 52 to Figure 54 showed the interaction effect between factors B: FJ-pitch and C: FJ-tip on the stiffness value with changing factor A: FJ-length from minimum to maximum. It was demonstrated that with the increase of A until a value between mid and maximum (around A=25.0mm), the stiffness increased and reached to its maximum, then it decreased after that value.

It was clearly observed that A: FJ-length, B: FJ-pitch and C: FJ-tip had a greater effect on the stiffnesses values. The optimum within the ranges used in the study was achieved by selecting A: FJ-Length value between mid and maximum, also select value for both B: FJ-pitch and C: FJ-Tips around their mid-limits to achieve a higher stiffness value. Therefore, the predicted optimal FJ geometry for the study was shown in the following table for VL-orientation which was obtained from statistical analysis using Design Expert software.

Table 12 Optimization for N-FJ-VL

Factors	Lower	Upper	Optimal N-FJ-VL
A: FJ-Length (mm)	7.0	35.0	23.80
B: FJ-Pitch (mm)	4.45	17.80	5.80
C: FJ-Tips (mm)	0.50	1.50	1.40
Stiffness (N/mm)	408.84	619.08	655.56

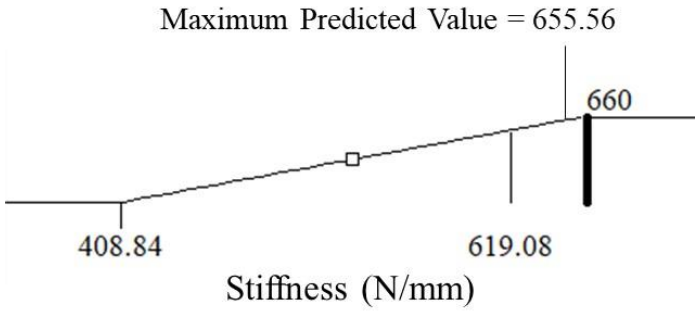

Figure 55 Schematic diagram for optimal predicted maximum N-FJ-VL value

The maximum stiffness that was reached from the studied ranges of the data was equal to 655.56 N/mm, which was too close to the control one value (660.50 N/mm). Other purpose of that study was to find a relation from using regression analysis that could predict the stiffness value corresponding to the trial and error approach to determine the FJ geometry that approaches NFJ lumber:

$$Stiffness = 77.07 + 19.23A + 24.75B + 564.48C - 0.385A^2 - 1.36B^2 - 280.19C^2 \quad [9]$$

Where,

Stiffness in (N/mm), A: FJ-length in (mm), B: FJ-pitch in (mm), and C: FJ-tips in (mm).

A verification was carried out for the vertical regression equation in terms of the factors and their interactions to be used for predictions of stiffness within the factor's levels. More extra points were added due to the number of errors (lack of fit) in the statistical model. Therefore, seven-random FJ-geometry values within the specified ranges were chosen and 3-D FEM models were established for all, in order to compare the stiffnesses values through a predicted-model relationship curve to validate the equation. See Table 13 and Figure 56.

Table 13 Stiffnesses from predicted equation versus model – N-FJ-VL

Run Number	A	B	C	Predicted stiffness (N/mm)	Model stiffness (N/mm)	Agreement (%)	Tolerance (%)
1	11.94	12.64	0.73	610.62	553.14	90.59	9.41
2	15.0	14.83	0.50	559.03	511.25	91.45	8.55
3	19.0	6.06	0.62	645.77	587.64	90.99	9.0
4	21.0	11.13	1.0	650.59	601.47	92.45	7.55
5	23.12	15.63	1.43	605.73	555.62	91.73	8.27
6	29.67	15.09	1.37	617.96	578.02	93.54	6.46
7	35.0	10.0	1.50	606.29	543.56	89.65	10.35

* A: FJ-length, B: FJ-pitch, and C: FJ-Tips.

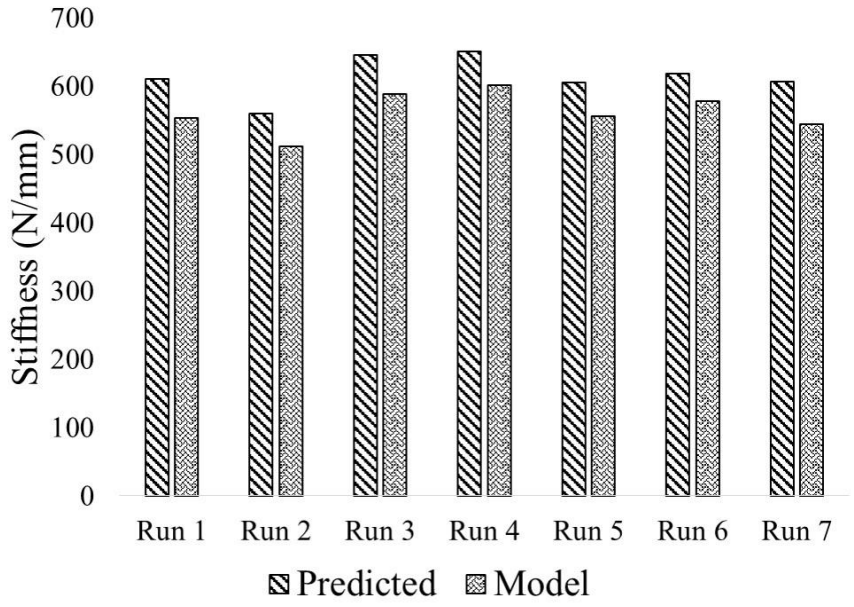

Figure 56 Graph showed predicted stiffnesses versus model values – N-FJ-VL

From Table 13 and Figure 56, showed stiffnesses obtained from regression predicted equation versus stiffnesses obtained from model numerical simulation. The tolerance did not exceed 12% error which was an acceptable error with using numerical analysis simulation, also putting into consideration that wood is a natural resource that is difficult to control. Hence, the predicted regression equation can predict the stiffness value for the corresponding FJ-geometry.

The goal was to optimize the FJ geometry towards the improvement of its structural properties. The results showed that FJs in the vertical orientation perform better performance than in the horizontal orientation.

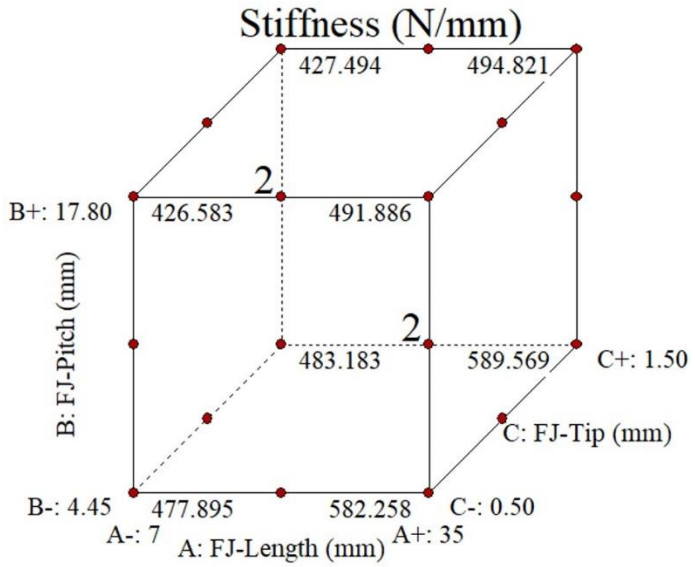

Figure 57 Cube simulate the second-order model – N-FJ-VL

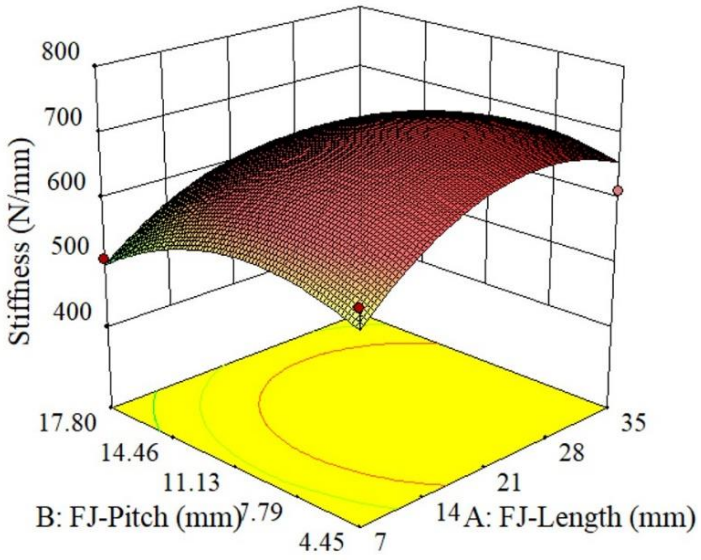

Figure 58 3-D surface simulated the statistical second-order model – N-FJ-VL

Chapter 5

Optimization of inclined finger-joined spruce lumber

5.1. Optimization of Finger-Joint in slope position

Inclined finger-joint is not a popular joint used in wood industry due to no more studies around its significance. There are a few research papers for that category of finger-Joint. Inclined Joint means that FJ is at different slope position rather than Normal Joint which indicates that FJ is at 0° slope position measured from the vertical axis. Inclined FJ is made in both horizontal and vertical orientations. Therefore, in this part, Inclined FJ joint were divided into two parts according to its orientation (horizontal and vertical). See Figure 59 and Figure 60Figure 59.

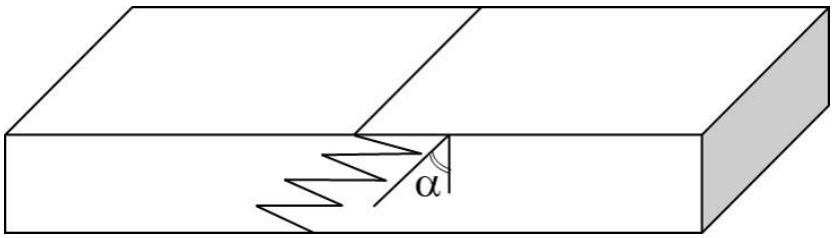

Figure 59 FJ at α^{o} slope position – Hz orientation

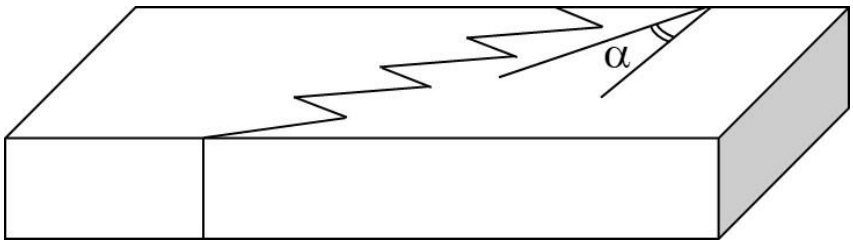

Figure 60 FJ at α^{o} slope position – VL orientation

Optimization modelling of each part were established to optimize the configuration of the inclined FJ and produce guidelines to analyze the relation of slope positions of FJ-length and FJ-tips regarded to the stiffnesses of spruce lumber. In addition to obtaining the optimum configurations to improve the structural properties which impact the behaviour and capacity of FJ elements at the serviceability and ultimate limit states. Other target was to achieve structural behaviour of FJ elements that approaches non-finger-joined (NFJ) lumber.

In this part, four numeric factors affect the response (stiffness), three of the factors were of two levels each (a high and a low) and the last factor was of three levels. The three-numeric factors were chosen for the design of experiment (DOE): A: FJ-length, B: FJ-pitch, and C: FJ-tip width (tip thickness), while the last factor was α^{o} slope position.

The objective was to use the previously verified numerical 3-D FEM combined with DOE methodology as a tool to investigate the effect of slope positions of FJ-length and FJ-tips (Inclined: 30°, 45° and 60°) on the stiffnesses values of spruce lumber. The numerical 3-D FE was used to obtain the responses (stiffnesses) for the statistical experiments. A total of 48-numerical models, 24-models per each FJ orientation, were carried out to obtain the load-displacement curves per each case. The applied-load was defined in terms of the maximum bending force obtained from four-point bending tests which was specified in chapter 3 to be equal to 12 KN for NFJ spruce specimen, and the corresponding stiffness for the control NFJ was equal to 660.5 N/mm.

This chapter will cover the following categories:

(Category 1 and 2 were covered in Chapter 4)

3. Optimization of Inclined 30° slope FJ Spruce Lumber in horizontal orientation,
4. Optimization of Inclined 30° slope FJ Spruce Lumber in vertical orientation,
5. Optimization of Inclined 45° slope FJ Spruce Lumber in horizontal orientation,
6. Optimization of Inclined 45° slope FJ Spruce Lumber in vertical orientation,
7. Optimization of Inclined 60° slope FJ Spruce Lumber in horizontal orientation,
8. Optimization of Inclined 60° slope FJ Spruce Lumber in vertical orientation.

5.1.1. Optimization of Hz-FJ spruce lumber at different slope positions

5.1.1.1. DOE for inclined FJ in Hz orientation (I-S-FJ-Hz)

A total of 24-numerical models were founded to obtain the load-displacement curves using traction separation law technique under the CZM. A modified RSM design type model was established to investigate the effect of the variables and their interactions. Four-factors, three-numeric each of two levels (a low and a high) and one-numeric of three levels, were selected. The three-numeric parameter's values were A: FJ-length (low 7.0mm and high 35.0mm), B: FJ-pitch (low 3.8mm and high 7.6mm) and C: FJ-Tips (low 0.5mm and high 1.5mm), while the last numeric parameter's values were: Inclined: 30°, 45° and 60° slope positions. The obtained results demonstrated the potential of increasing the FJ resistance by optimizing its geometry at different slope positions of FJ. Table 14 showed the 24 design variables models at different slope positions of VL-Orientation and the corresponding stiffnesses values that can be achieved through FEM (from 489.68 N/mm to 653.29 N/mm).

Table 14 Run parameters of 24-models design variables – I-S-FJ-Hz

Run	A: FJ-length mm	B: FJ-pitch mm	C: FJ-tip mm	D: slope position α^o	Response: stiffness N/mm
1	7	3.8	0.5	30	548.69
2	35	3.8	0.5	30	558.32
3	7	7.6	0.5	30	504.11
4	35	7.6	0.5	30	514.33
5	7	3.8	1.5	30	568.59
6	35	3.8	1.5	30	575.06
7	7	7.6	1.5	30	517.67
8	35	7.6	1.5	30	542.08
9	7	3.8	0.5	45	551.92
10	35	3.8	0.5	45	608.41
11	7	7.6	0.5	45	514.54
12	35	7.6	0.5	45	525.31
13	7	3.8	1.5	45	584.67
14	35	3.8	1.5	45	628.38
15	7	7.6	1.5	45	528.36
16	35	7.6	1.5	45	550.32
17	7	3.8	0.5	60	564.00
18	35	3.8	0.5	60	602.96
19	7	7.6	0.5	60	489.68
20	35	7.6	0.5	60	576.27
21	7	3.8	1.5	60	562.09
22	35	3.8	1.5	60	653.29
23	7	7.6	1.5	60	521.52
24	35	7.6	1.5	60	599.21

Where,

* (I-S-FJ-Hz): Inclined-Slope-Finger Joined-Horizontal

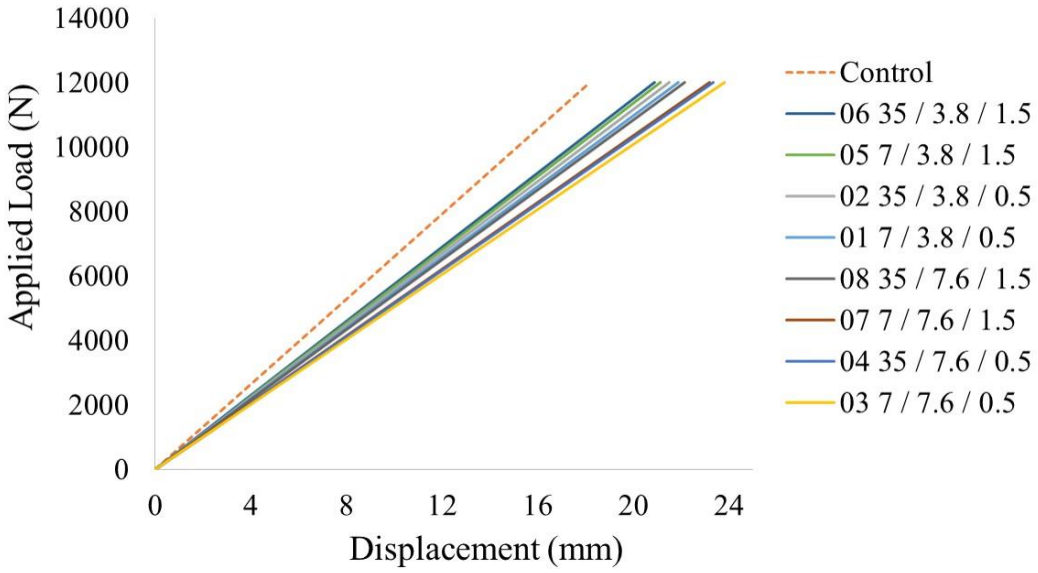

Figure 61 Numerical load-displacement curves for I-S-30°-FJ-Hz

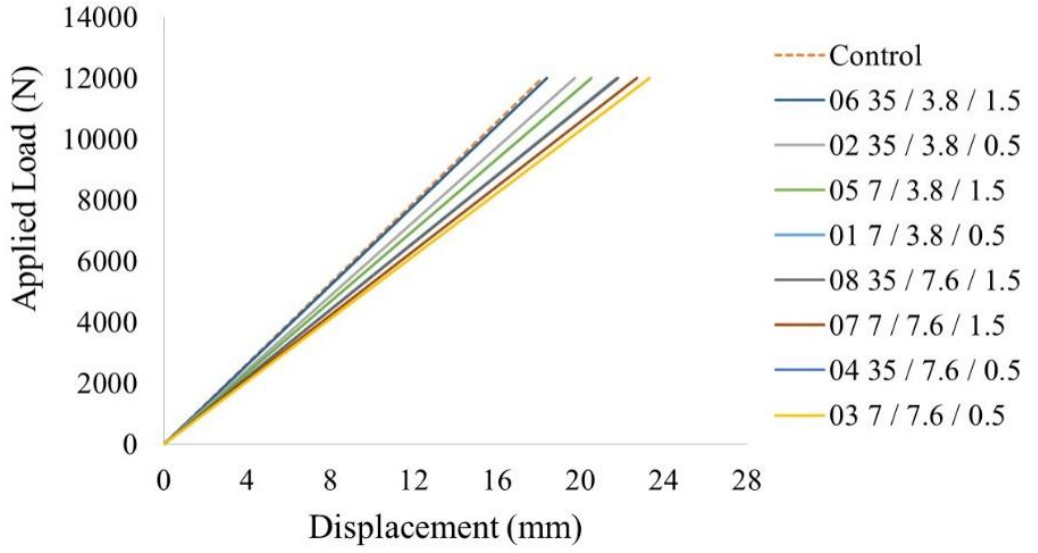

Figure 62 Numerical load-displacement curves for I-S-45°-FJ-Hz

* The legend for instance [06 35 / 3.8 / 1.5] refers to:

[Run number FJ Length / FJ pitch / FJ tip] respectively.

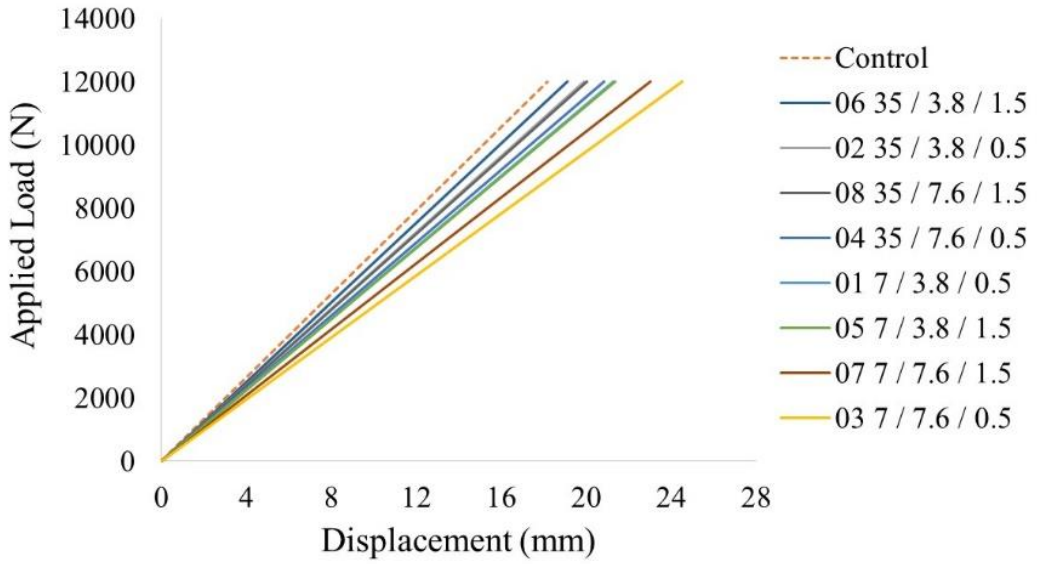

Figure 63 Numerical load-displacement curves for I-S-60°-FJ-Hz

* The legend for instance [06 35 / 3.8 / 1.5] refers to:

[Run number FJ Length / FJ pitch / FJ tip] respectively.

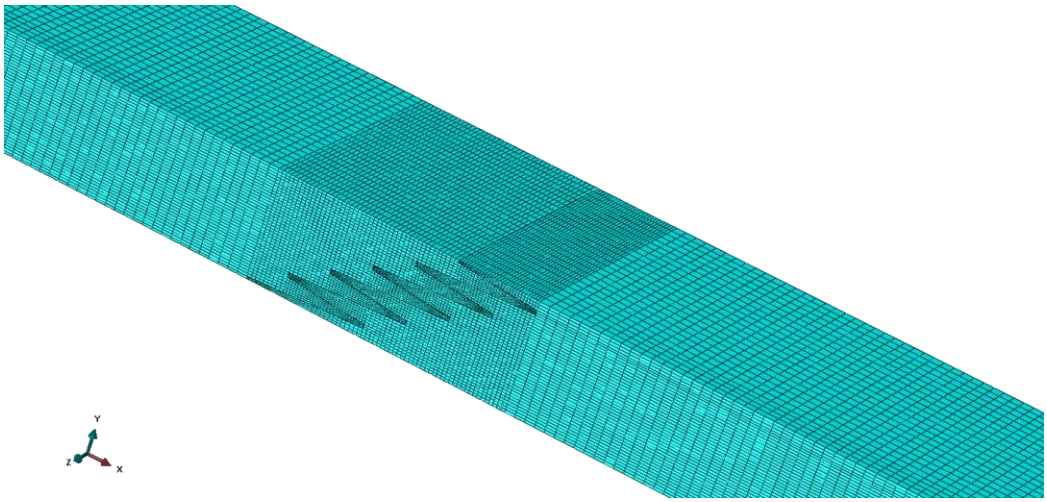

Figure 64 Typical meshed FE of Hz-FJ specimen at α^{o} slope

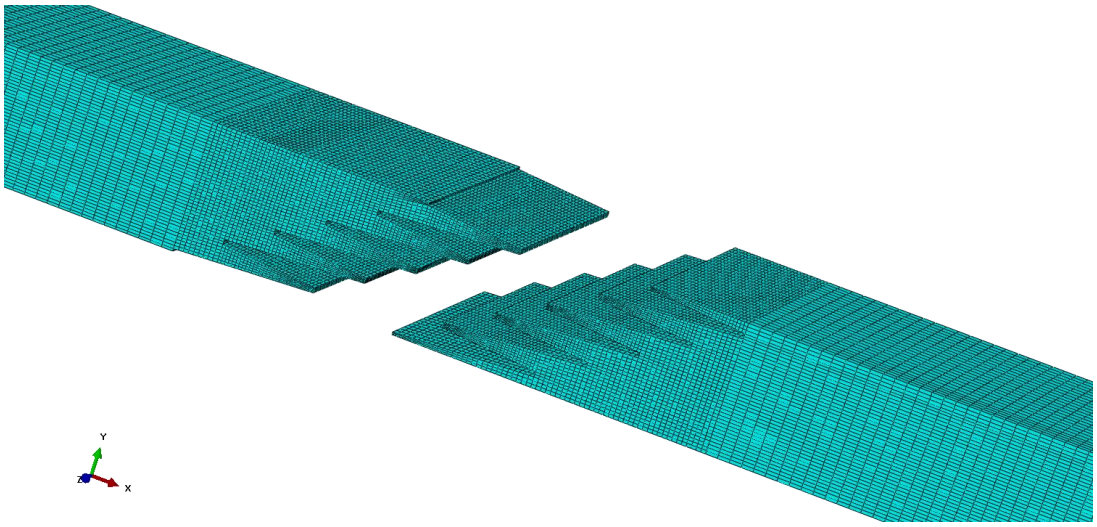

Figure 65 Typical meshed cross-section of Hz-FJ at α^{o} slope before interlocking

Figure 64 and Figure 65 showed a typical meshed FEA numerical 3-D model of inclined FJ in the Hz-orientation. The mesh refinement at the interface were finer than other parts because of the higher stresses at these regions. A contour diagram of stresses obtained from the numerical analysis was showed in Figure 66.

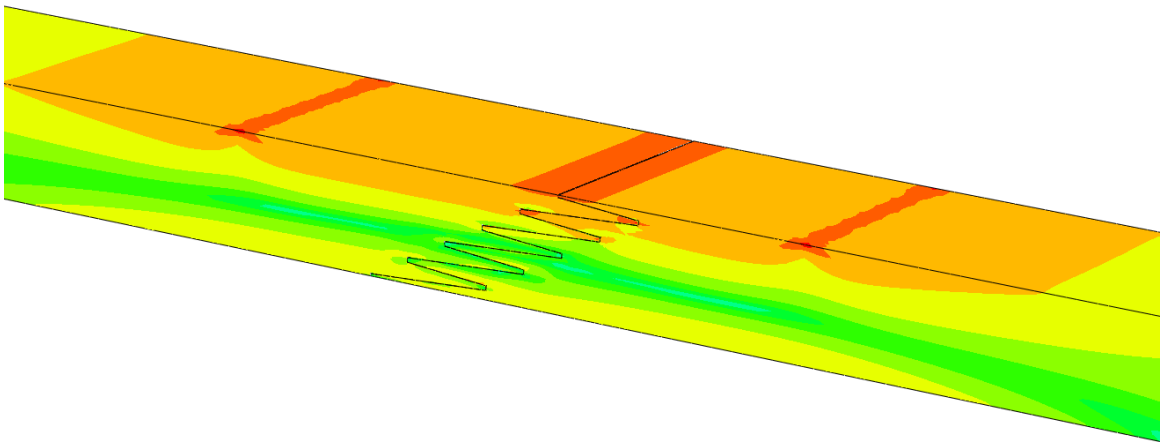

Figure 66 Typical FEA stress contour for failure at α^{o} of Hz-FJ spruce specimen

5.1.1.2. ANOVA for for inclined FJ in Hz orientation (I-S-FJ-Hz)

A modified response surface design were applied to the model. Table 15 showed the analysis of Variance (ANOVA) for Response Surface Reduced Linear Model for the Inclined FJ in the vertical orientation. Values of "Prob > F" less than 0.05 indicated model terms were significant. In this case, A, B, C, D, AD were the significant model terms. The model had a sample standard deviation equal 11.53 which indicated the measure of the dispersion of the set of the data from its mean which equal 557.91 N/mm.

Table 15 ANOVA for RSM for I-S-FJ-Hz

Source	Sum of Squares	df	Mean Square	F - Value	P - Value Prob > F	
Model	36110.97	5	7222.19	54.34	<0.0001	Significant
A	9524.15	1	9524.15	71.66	< 0.0001	
B	16171.00	1	16171.00	121.67	<0.0001	
C	3098.55	1	3098.55	23.31	0.0001	
D	3605.10	1	3605.10	27.12	<0.0001	
AD	3712.16	1	3712.16	27.93	<0.0001	
Residual	2392.42	18	132.91			
Cor Total	38503.39	23				

Where,

* A: FJ-length, B: FJ-pitch, C: FJ-tips and D: FJ-slope degree.

Table 16 showed the model summary statistics for the Inclined FJ in horizontal orientation. The results demonstrated that a Modified 2FI (Two-Factor Interaction) statistics design type was suggested. A Modified 2FI had a model statistics $R^2_{adj} = 0.92$ and $R^2_{Pred} = 0.89$

were in a reasonable agreement; the model of R^2_{Pred} = 0.89 had a good chance of making reasonable prediction.

Table 16 Model summary statistics for I-S-FJ-Hz

Source	Standard Deviation	R-squared (R^2)	Adjusted R^2 (R^2_{adj})	Predicted R^2 (R^2_{Pred})	
Linear	17.92	0.84	0.81	0.74	
2FI	12.99	0.94	0.89	0.81	Suggested
Quadratic	13.04	0.95	0.89	0.79	Aliased

Validation of ANOVA basic assumptions and model adequacy were investigated through the examination of the residuals. The residuals, which are the deviation of observed data from the predicted value, were assumed to be normally distributed with a mean zero and a constant standard deviation.

Three-model assumptions checks were verified as follow:

- Checks for the normality assumption, (see, Figure 67),
- Checks for the homogeneous variance assumption, (see, Figure 68), and
- Checks for independence assumption (see, Figure 69).

Figure 67 displayed a Design-Expert normal probability plot of the studentized residuals. All the values were well distributed around the mean. All the values seemed to lie on the straight line, which means that the underlying error distribution is normal. Therefore, the first assumption of ANOVA was satisfied.

Figure 68 displayed a Design-Expert plot of studentized residuals versus predicted values. The plot showed that the distribution between the residuals and predicted values were

random, and there was no obvious pattern in it, which mean that the variance was constant. This indicated that the second ANOVA assumption was satisfied.

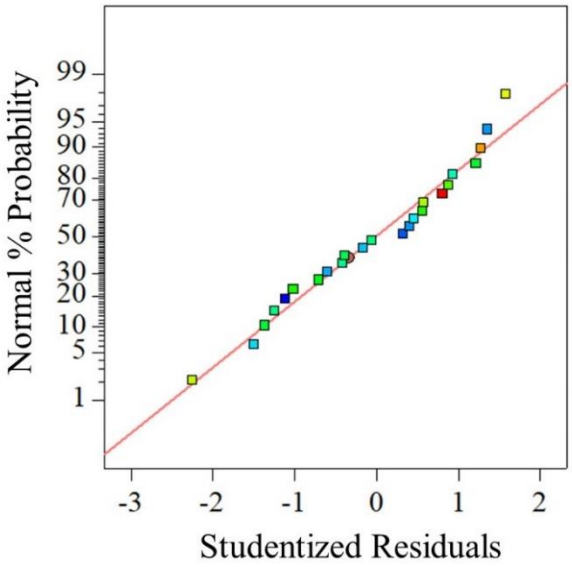

Figure 67 Normal probability plot of residuals for I-S-FJ-Hz

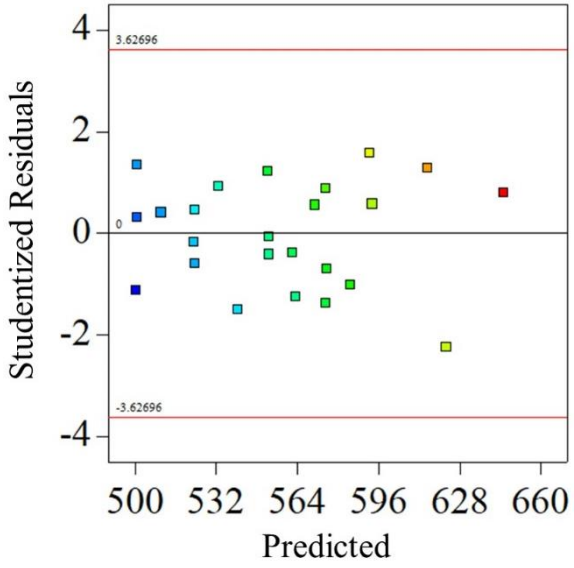

Figure 68 Plot between residuals and predicted for I-S-FJ-Hz

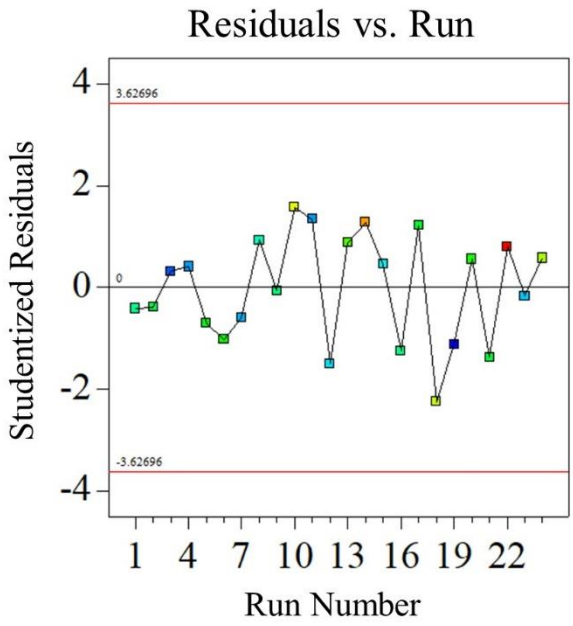

Figure 69 Plot between residuals and run for I-S-FJ-Hz

Figure 69 displayed a Design-Expert plot of studentized residuals versus run order. This plot implied that there was no independence among the treatments. Therefore, the model provided an adequate fit to the observed data since all the assumptions were valid.

A contour graphs were drawn between two factors at the different levels of the other two remaining factors for studying the effect of the treatments and their interactions on the stiffness. See from Figure 70 to Figure 78.

Figure 70 to Figure 72 showed the interaction effect at minimum C: FJ-tip of 0.5 mm between factors A: FJ-length and D: FJ-slope degree on the stiffness value with changing the value of factor B: FJ-pitch from minimum to maximum.

Figure 73 to Figure 75 showed the interaction effect at minimum C: FJ-tip of 1.0 mm between factors A: FJ-length and D: FJ-slope degree on the stiffness value with changing the value of factor B: FJ-pitch from minimum to maximum.

Figure 76 to Figure 78 showed the interaction effect at minimum C: FJ-tip of 1.5 mm between factors A: FJ-length and D: FJ-slope degree on the stiffness value with changing the value of factor B: FJ-pitch from minimum to maximum.

The graphs showed that FJ geometry had a significant effect on the stiffnesses values. It was observed that the stiffness value was increasing with the increase of C until its maximum of 1.5mm at the different values of factor B. However, stiffness was decreased with the increase of factor B from minimum to maximum.

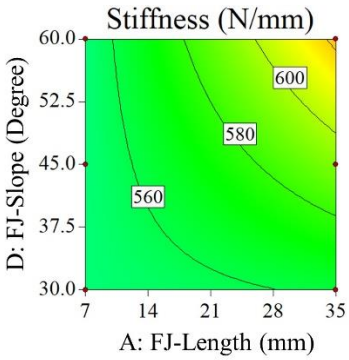

Figure 70 Contour shows interaction between A and D at C=0.5mm and B=3.8mm

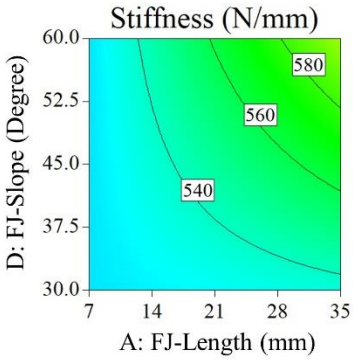

Figure 71 Contour shows interaction between A and D at C=0.5mm and B=5.7mm

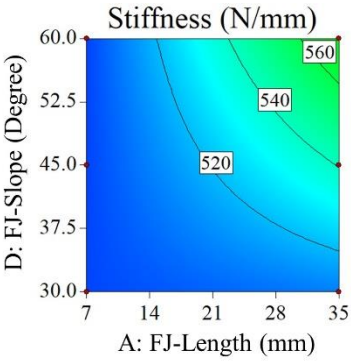

Figure 72 Contour shows interaction between A and D at C=0.5mm and B=7.6mm

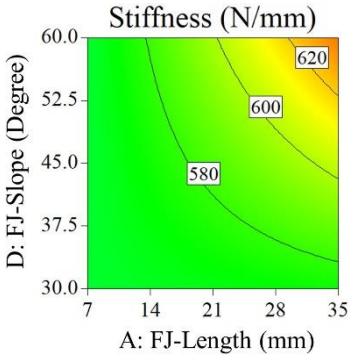

Figure 73 Contour shows interaction between A and D at C=1.0mm and B=3.8mm

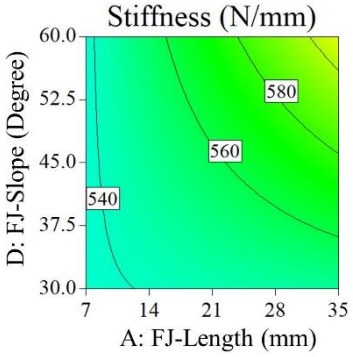

Figure 74 Contour shows interaction between A and D at C=1.0mm and B=5.7mm

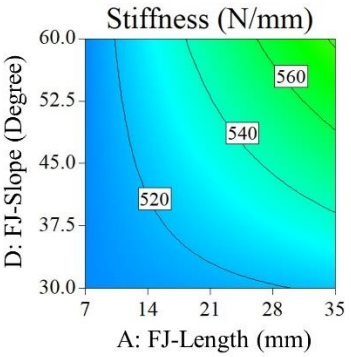

Figure 75 Contour shows interaction between A and D at C=1.0mm and B=7.6mm

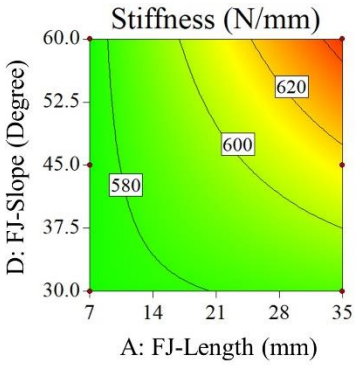

Figure 76 Contour shows interaction between A and D at C=1.5mm and B=3.8mm

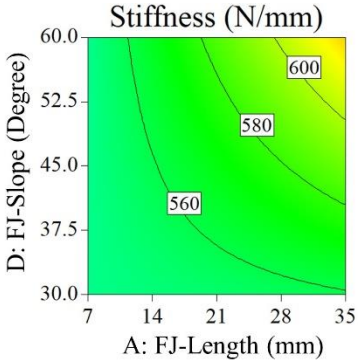

Figure 77 Contour shows interaction between A and D at C=1.5mm and B=5.7mm

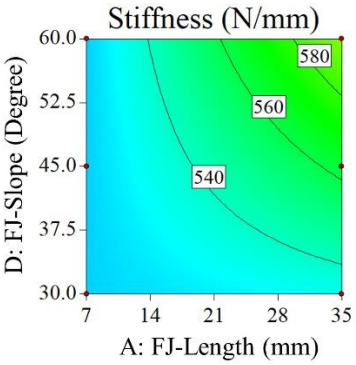

Figure 78 Contour shows interaction between A and D at C=1.5mm and B=7.6mm

The Optimal Stiffness close to the NFJ control specimen could obtained at D: Slope degree 60° by selecting the maximum of both A: FJ-Length and C: FJ-tips with minimum of B: FJ-Pitch. This was due to the increasing of the interface surface between the two adherent parts.

Table 17 Optimization for I-S-FJ-Hz

Factors	Lower	Upper	Optimal I-S-FJ-Hz
A: FJ-Length (mm)	7.0	35.0	35.0
B: FJ-Pitch (mm)	7.60	3.80	3.80
C: FJ-Tips (mm)	0.50	1.50	1.50
D: FJ-Slope (Degree)	60°	60°	60°
Stiffness (N/mm)	489.68	653.29	645.25

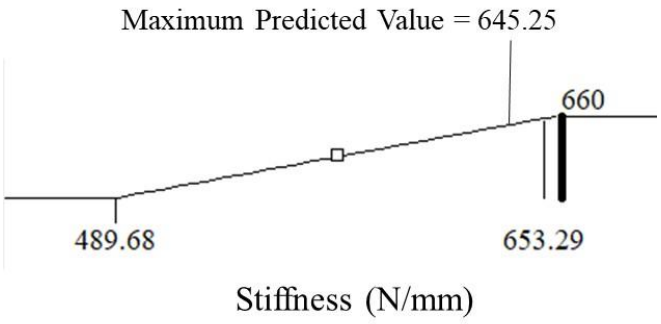

Figure 79 Schematic diagram for optimal predicted maximum I-S-FJ-Hz value

The maximum predicted stiffness that can be reached using RSM Equations was equal to 645.25 N/mm obtained from statistical analysis, which was a close value to the control one.

5.1.2. Optimization of VL FJ spruce lumber at different slope positions

5.1.2.1. DOE for inclined FJ in VL orientation (I-S-FJ-VL)

A total of 24-numerical models were established for the load-displacement curves using traction separation law technique under the CZM in Abaqus FEA software. A similar modified RSM design type model technique was followed to investigate the effect of the selected variables and their interactions.

Same procedure as inclined FJ in the horizontal orientation, Four-factors, three-numeric each of two levels (a low and a high) and one-numeric of three levels, were selected. The three-numeric parameter's values were A: FJ-length (low 7.0mm and high 35.0mm), B: FJ-pitch (low 4.45mm and high 17.8mm) and C: FJ-Tips (low 0.5mm and high 1.5mm). However, the last numeric parameter's values were: Inclined: 30°, 45° and 60° slope positions. The results elaborated that by optimizing the FJ geometry at different slope positions, the potential of FJ resistance was increased. Table 18 showed the 24-models design variables in the slope position of the vertical orientation and also showed the stiffnesses values that can be achieved (from 480.61 N/mm to 658.78 N/mm).

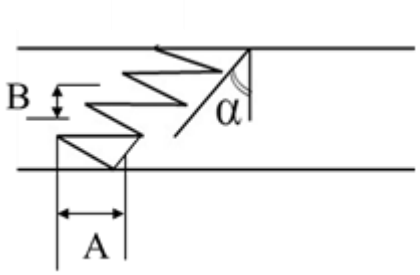

Table 18 Run parameters of 24-models Design variables – I-S-FJ-VL

Run	A: FJ-length mm	B: FJ-pitch mm	C: FJ-tip mm	D: slope position α^o	Response: stiffness N/mm
1	7	4.45	0.5	30	561.20
2	35	4.45	0.5	30	614.65
3	7	17.80	0.5	30	468.56
4	35	17.80	0.5	30	521.55
5	7	4.45	1.5	30	527.58
6	35	4.45	1.5	30	610.66
7	7	17.80	1.5	30	466.02
8	35	17.80	1.5	30	548.47
9	7	4.45	0.5	45	556.79
10	35	4.45	0.5	45	622.81
11	7	17.80	0.5	45	480.61
12	35	17.80	0.5	45	546.09
13	7	4.45	1.5	45	559.42
14	35	4.45	1.5	45	618.33
15	7	17.80	1.5	45	490.35
16	35	17.80	1.5	45	638.58
17	7	4.45	0.5	60	611.22
18	35	4.45	0.5	60	602.96
19	7	17.80	0.5	60	551.46
20	35	17.80	0.5	60	615.80
21	7	4.45	1.5	60	625.71
22	35	4.45	1.5	60	658.78
23	7	17.80	1.5	60	559.48
24	35	17.80	1.5	60	638.58

Where,

* (I-S-FJ-VL): Inclined-Slope-Finger Joined-Vertical

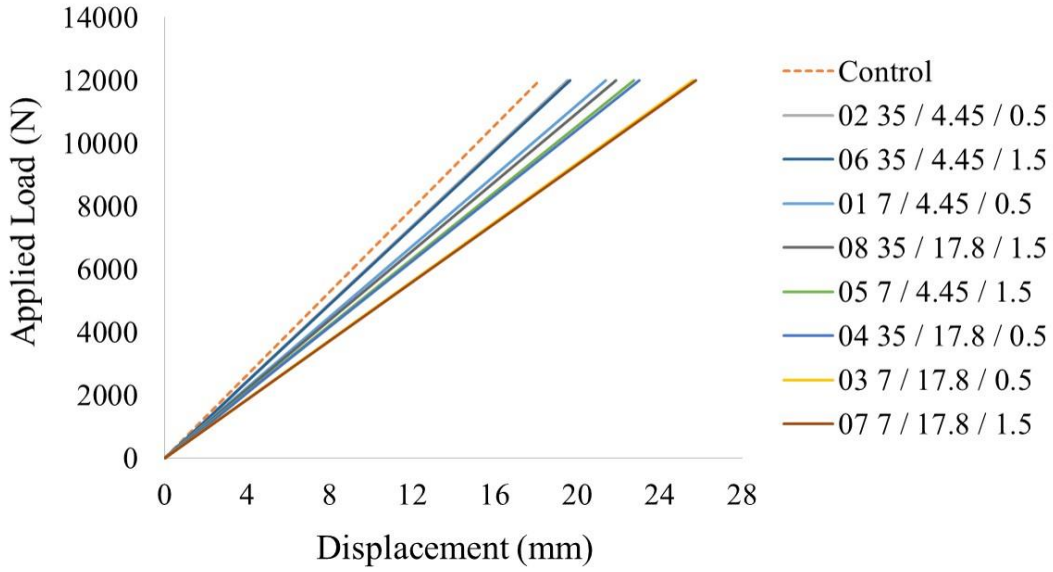

Figure 80 Numerical load-displacement curves at I-S-30°-FJ-VL

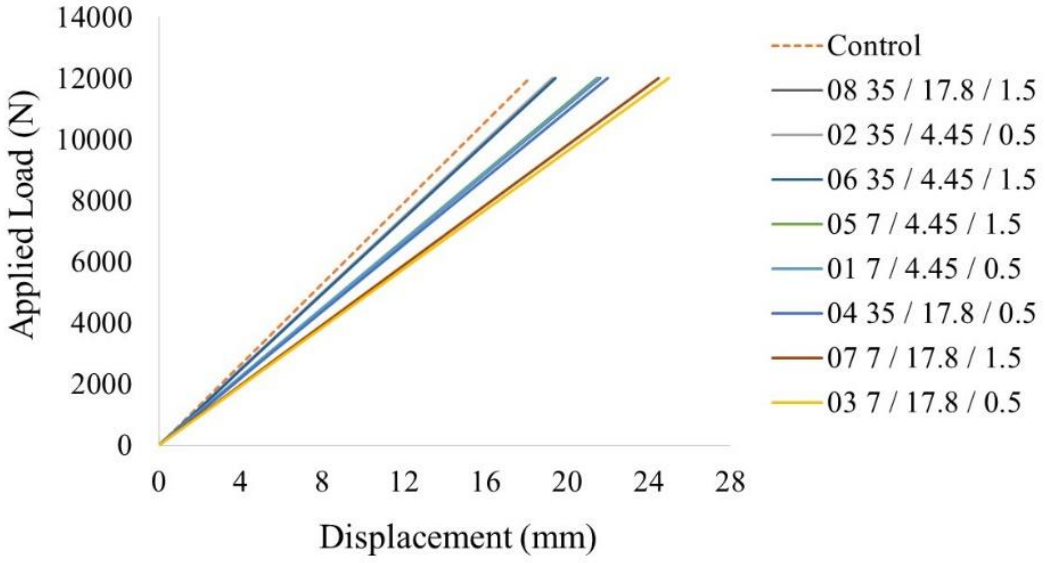

Figure 81 Numerical load-displacement curves at I-S-45°-FJ-VL

* The legend for instance [06 35 / 4.45 / 1.5] refers to:

[Run number FJ Length / FJ pitch / FJ tip] respectively.

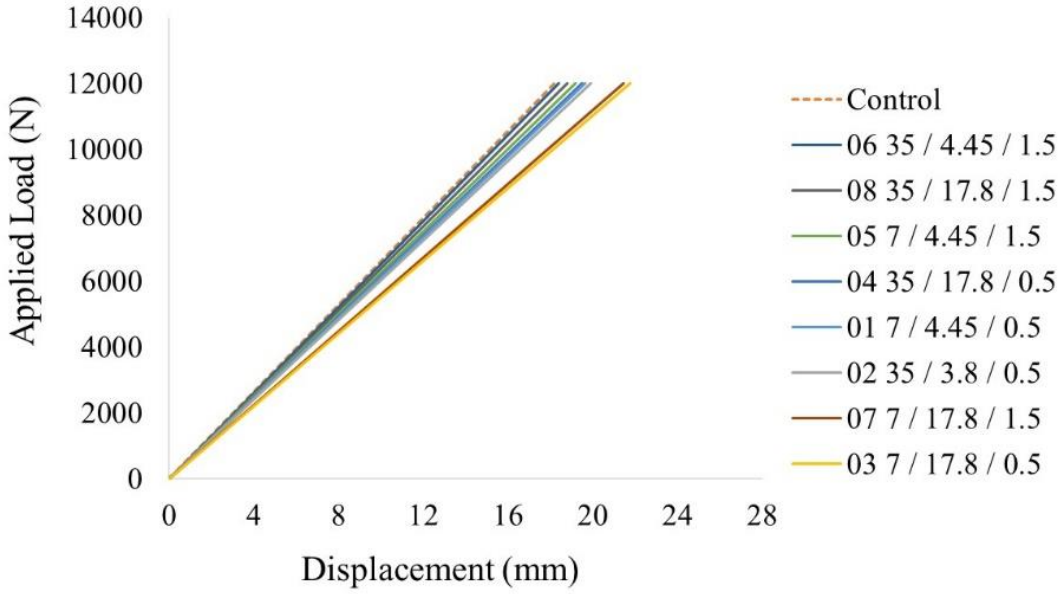

Figure 82 Numerical load-displacement curves at I-S-60°-FJ-VL

* The legend for instance [06 35 / 4.45 / 1.5] refers to:

[Run number FJ Length / FJ pitch / FJ tip] respectively.

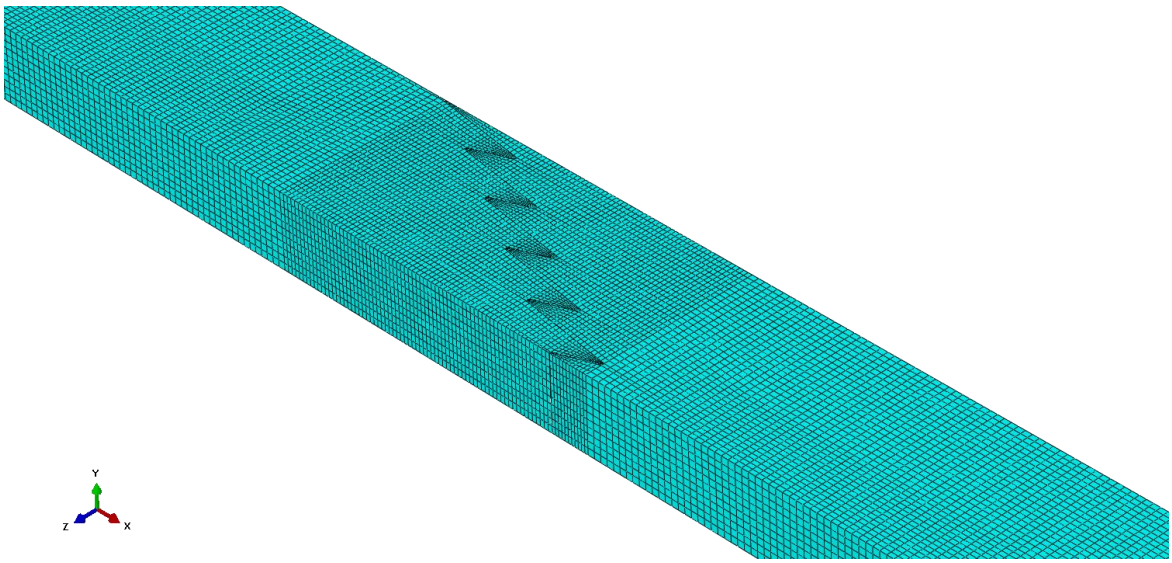

Figure 83 Typical meshed FE of VL-FJ specimen at α^{o} slope

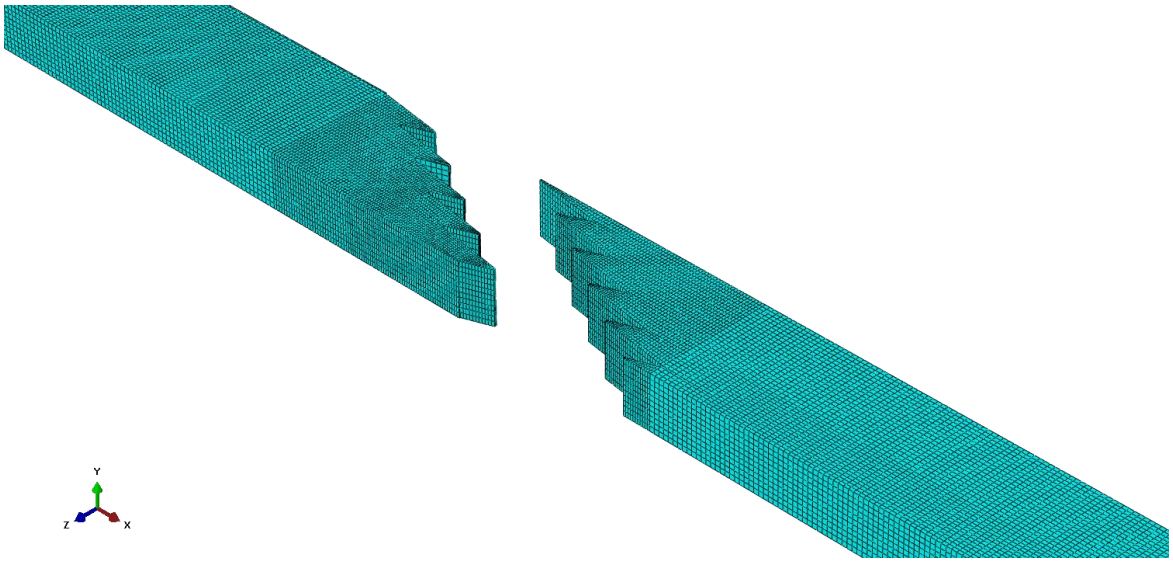

Figure 84 Typical meshed cross-section of VL-FJ at α^{o} slope before interlocking

Figure 83 and Figure 84 showed a typical meshed FEA numerical 3-D model of inclined FJ in the VL-Orientation. Same as previous, the mesh at the interface were finer than other parts because of the higher stresses at these regions. See Figure 85 for the contour diagram of stresses obtained from the numerical analysis.

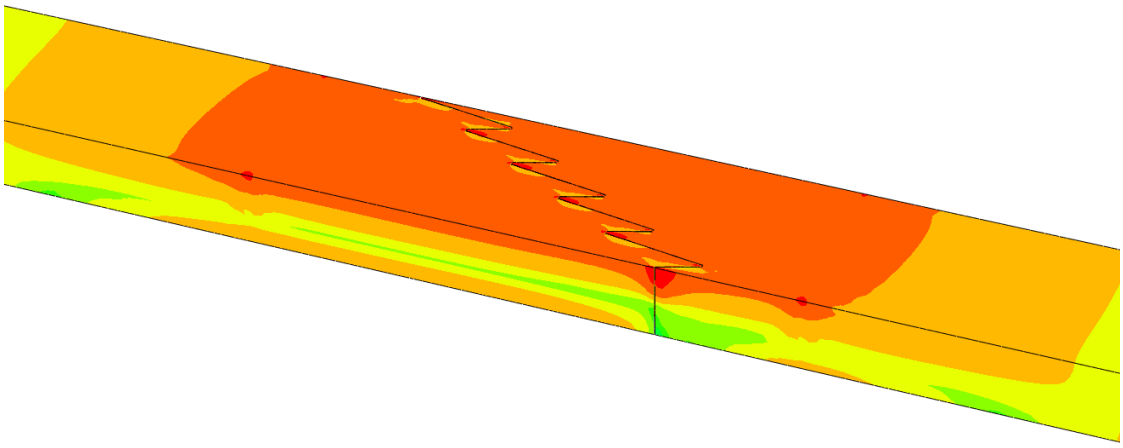

Figure 85 Typical FEA stress contour for failure at slope of VL-FJ Spruce Specimen

5.1.2.2. ANOVA for inclined FJ in VL orientation (I-S-FJ-VL)

A similar modified response surface design were applied to the model. Table 19 showed the analysis of variance (ANOVA) for the response surface reduced linear model for the Inclined FJ in the vertical orientation. Values of "Prob > F" less than 0.05 indicated model terms were significant. In this case, A, B, D were the significant model terms. The model had a sample standard deviation equal 26.74 which indicated the measure of the dispersion of the set of the data from its mean which equal 570.65 N/mm.

Table 19 ANOVA for RSM for I-S-FJ-VL

Source	Sum of Squares	df	Mean Square	F - Value	P - Value Prob > F	
Model	61171.19	3	20390.40	28.51	<0.0001	Significant
A	25275.95	1	25275.95	35.35	< 0.0001	
B	17310.73	1	17310.73	24.21	<0.0001	
D	18584.51	1	18584.51	25.99	<0.0001	
Residual	14302.13	20	715.11			
Cor Total	75473.32	23				

Where,

* A: FJ-length, B: FJ-pitch and D: FJ-slope degree.

Table 20 Model summary statistics for I-S-FJ-VL

Source	Standard Deviation	R-squared (R^2)	Adjusted R^2 (R^2_{adj})	Predicted R^2 (R^2_{Pred})	
Linear	25.98	0.83	0.79	0.73	
2FI	20.45	0.93	0.87	0.76	Suggested
Quadratic	20.26	0.94	0.88	0.75	Aliased

Table 20 showed the model summary statistics for the Inclined FJ in vertical orientation. The results demonstrated that a Modified 2FI (Two-Factor Interaction) statistics design type was suggested. A Modified 2FI had a model statistics $R^2_{adj} = 0.78$ and $R^2_{Pred} = 0.73$ were in a reasonable agreement; the model of $R^2_{Pred} = 0.73$ had a good chance of making reasonable prediction.

Validation of ANOVA basic assumptions and model adequacy were investigated through the examination of the residuals. Three-model assumptions checks were verified as follow:

- Checks for the normality assumption, (see, Figure 86),
- Checks for the homogeneous variance assumption, (see, Figure 87), and
- Checks for independence assumption (see, Figure 88).

Figure 86 displayed a Design-Expert normal probability plot of the studentized residuals. All the values were well distributed around the mean. All the values seemed to lie on the straight line, which means that the underlying error distribution is normal. Therefore, the first assumption of ANOVA was satisfied.

Figure 87 displayed a Design-Expert plot of studentized residuals versus predicted values. The plot showed that the distribution between the residuals and predicted values were random, and there was no obvious pattern in it, which mean that the variance was constant. This indicated that the second ANOVA assumption was satisfied.

Figure 88 displayed a Design-Expert plot of studentized residuals versus run order. This plot implied that there was no independence among the treatments. Therefore, the model provided an adequate fit to the observed data since all the assumptions were valid.

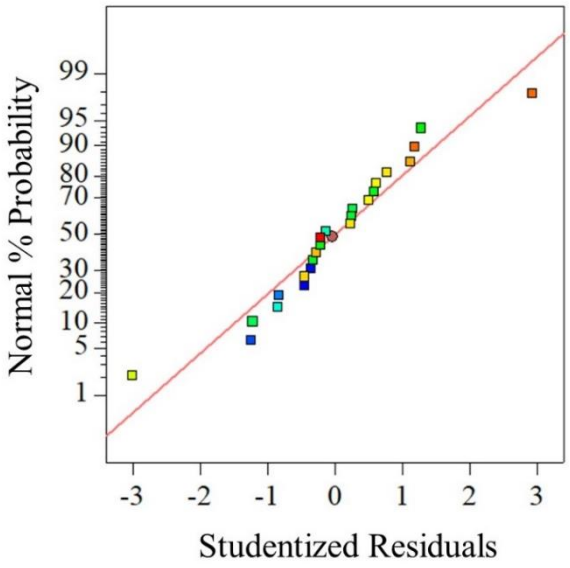

Figure 86 Normal probability pot of residuals for I-S-FJ-VL

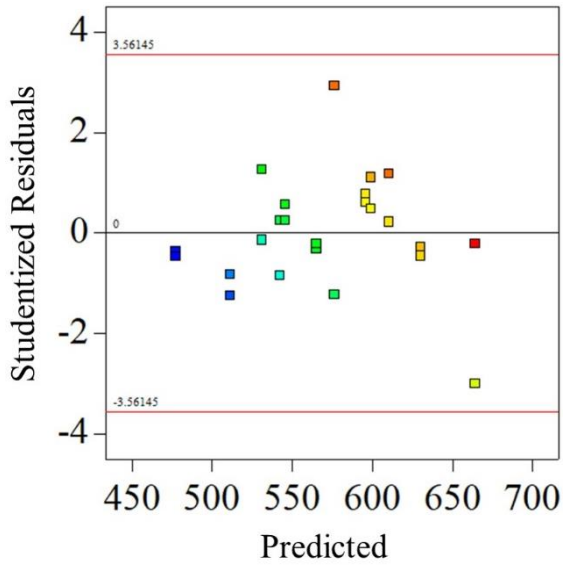

Figure 87 Plot between residuals and predicted for I-S-FJ-VL

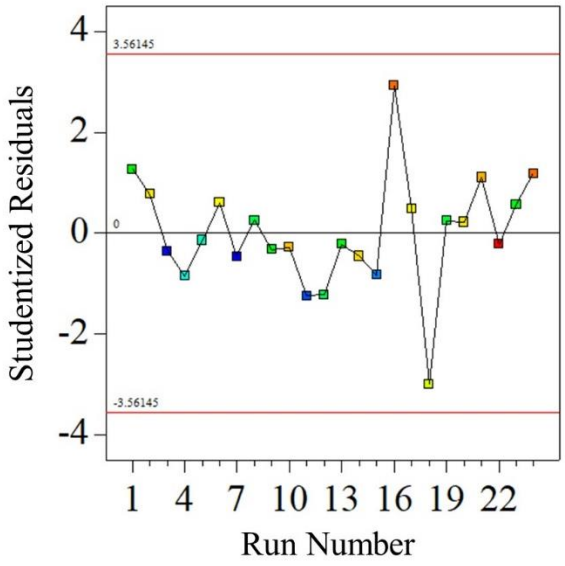

Figure 88 Plot between residuals and run for I-S-FJ-VL

It was noticed that C: FJ-tip had no significant in that case of inclined FJ in horizontal orientation. A contour graphs were drawn between two factors at the different levels of the other two remaining factors for studying the effect of the treatments and their interactions on the stiffness. See from Figure 89 to Figure 97.

Figure 89 to Figure 91 showed the interaction effect at minimum C: FJ-tip of 0.5 mm between factors A: FJ-length and B: FJ-pitch on the stiffness value with changing the value of factor D: FJ-slope degree from minimum to maximum.

Figure 92 to Figure 94 showed the interaction effect at mid C: FJ-tip of 1.0 mm between factors A: FJ-length and B: FJ-pitch on the stiffness value with changing the value of factor D: FJ-slope degree from minimum to maximum.

Figure 95 to Figure 97 showed the interaction effect at maximum C: FJ-tip of 1.5 mm between factors A: FJ-length and B: FJ-pitch on the stiffness value with changing the value of factor D: FJ-slope degree from minimum to maximum.

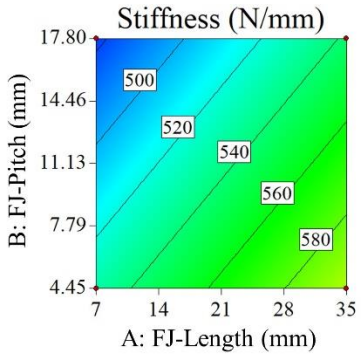

Figure 89 Contour shows interaction between A and B at min C=0.5mm and D=30°

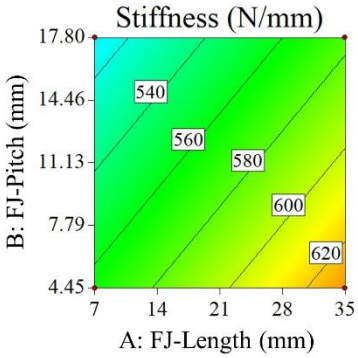

Figure 90 Contour shows interaction between A and B at min C=0.5mm and D=45°

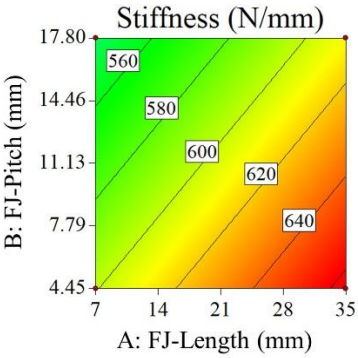

Figure 91 Contour shows interaction between A and B at min C=0.5mm and D=60°

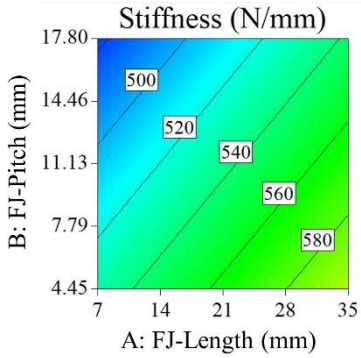

Figure 92 Contour shows interaction between A and C at mid C=1.0mm and D=30°

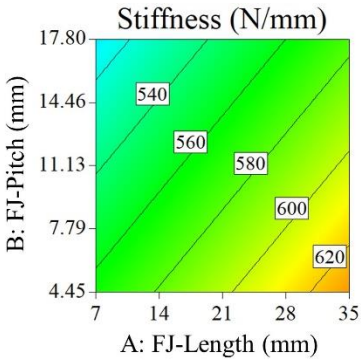

Figure 93 Contour shows interaction between A and C at mid C=1.0mm and D=45°

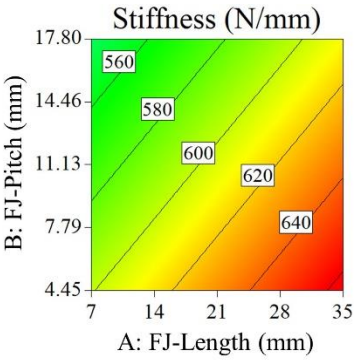

Figure 94 Contour shows interaction between A and C at mid C=1.0mm and D=60°

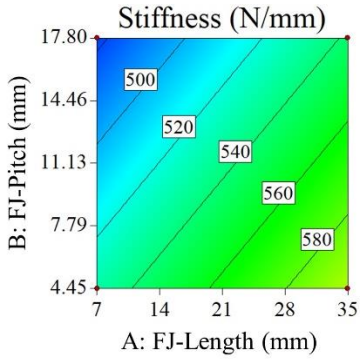

Figure 95 Contour shows interaction between B and C at max C=1.5mm and D=30°

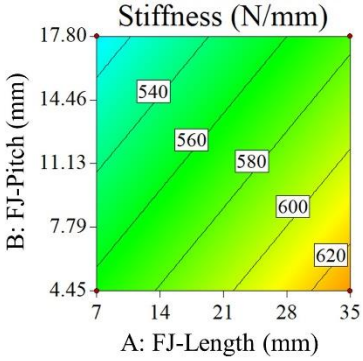

Figure 96 Contour shows interaction between B and C at max C=1.5mm and D=45°

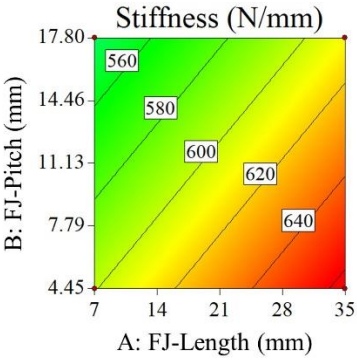

Figure 97 Contour shows interaction between B and C at max C=1.5mm and D=60°

The graphs showed that A: FJ-length, B: FJ-pitch and D: FJ-slope degree had a significant effect on the stiffnesses values. It was noticed from all curves that the stiffness value was increasing with the increase of D. It was clearly shown that C: FJ-tip had no effect at all ranges.

The Optimal Stiffness close to the NFJ control specimen could be obtained at D: Slope degree 60° by selecting maximum of A: FJ-Length with minimum of B: FJ-Pitch. This was due to the increasing of the interface surface between the adherent parts.

Table 21 Optimization for I-S-FJ-VL

Factors	Lower	Upper	Optimal I-S-FJ-VL
A: FJ-Length (mm)	7.0	35.0	34.70
B: FJ-Pitch (mm)	17.80	4.45	4.80
C: FJ-Tips (mm)	1.50	1.50	1.0
D: FJ-Slope (Degree)	30°	60°	60°
Stiffness (N/mm)	466.02	658.78	660.0

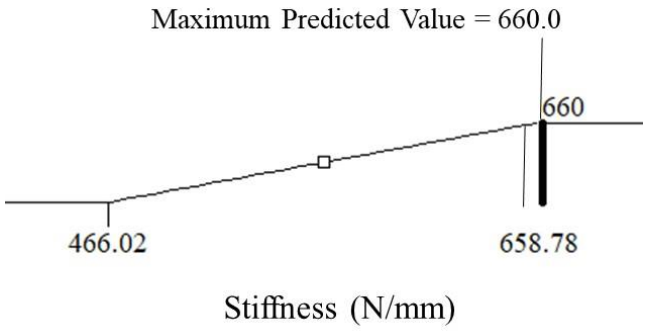

Figure 98 Schematic diagram for optimal predicted maximum I-S-FJ-VL value

The maximum predicted stiffness that was reached using RSM Equations was equal to 660.0 N/mm obtained from statistical analysis, which was as same as the control value.

Chapter 6

6.1. Conclusions

In practice, achieving structural behaviour of FJ elements that approaches non-finger-joined (NFJ) lumber require many trials to generate the data that may identify the optimum FJ geometry configuration. In the present research, numerical 3-D finite element analysis, and statistical design of experiment methodology were applied to optimize FJ geometry configurations instead.

The developed models were also utilized to graphically (contour and trace plots) and numerically (desirability function approach) predicted FJ structural performance, and to optimize the FJ geometry which was the main goal of the statistical optimization method.

The following conclusions can be drawn from the present research.

- Simulation of the FJ lumber using numerical 3-D FEM provide a valuable resource for performing engineering analysis. The 3-D FEM Modeling perform accurate results observed from the close simulation agreement corresponding to the actual specimens. The numerical 3-D FEM was used to obtain the responses (stiffnesses) for the statistical experiments.
- The statistical design of experiment methodology was used effectively to provide a simple and cost-effective approach for designing and optimizing FJ geometry with the lowest possible trial samples.

- A Reduced quadratic model fitted the Normal FJ categories types. While, a modified Two-Factor Interaction (2FI) model was suggested for the Inclined FJ categories. Then, validation were investigated for all basic assumptions of the ANOVA and model adequacy and were valid, therefore, the model provided an adequate fit to the observed data.
- Optimization using statistical analysis was established to assess the effect of the three factors (FJ-length, FJ-pitch, and FJ-tip width) and their interactions on the stiffness. The study were divided into eight parts according to: FJ orientation (vertical and horizontal), FJ slope position measured from the vertical axis (Normal: 0°; Inclined: 30°, 45° and 60°), FJ geometry configuration (FJ-length, FJ-pitch and FJ-tip). The observations per each part were summarized in the following points.
- Chapter 4, Optimization of Normal 0° slope FJ Spruce Lumber; The results demonstrated that:
    - FJs in the N-VL perform better structural performance than FJs in the N-Hz (for N-Hz, the maximum stiffness that was reached equal 639.85 N/mm, while, for N-VL was equal 655.56 N/mm, which was too close to the control value 660.50 N/mm).
    - The Contour graphs for N-Hz elaborated that the stiffness value was increasing with the increase of both B: FJ-pitch and C: FJ-tip until approximately their mid values then the stiffness decreased again. It was also observed that with the increase of A until maximum, the stiffness increased.

- The Contour graphs for N-VL elaborated that the optimum within the ranges used was achieved by selecting values for both B: FJ-pitch and C: FJ-Tips around their mid-limits, and A: FJ-Length value between mid and maximum to achieve a higher stiffness value.
- As a secondary objective, a relation from using regression analysis were concluded and verified to predict the stiffness value. The predicted equation will save time, money, and material (wood and glue).

- Chapter 5, Optimization of Inclined FJ Spruce Lumber; it was observed that the Inclined performed much better than the Normal slope position for both orientations. This was due to the increasing of the interface surface between the two adherent parts.
  - FJs in I-S-VL perform better structural performance than FJs in I-S-Hz (for the I-S-Hz, the maximum stiffness was equal 645.25 N/mm, while, for the I-S-VL was equal 660.0 N/mm, which was as same as the control value).
  - The Contour graphs for I-S-Hz elaborated that the Optimal Stiffness close to the NFJ control specimen could be obtained at D: Slope degree 60° by selecting the maximum of both A: FJ-Length and C: FJ-tips with minimum of B: FJ-Pitch.
  - The Contour graphs for I-S-VL observed that from all curves that the stiffness was increasing with the increase of D: Slope. It was clearly shown that C: FJ-tip had no effect at all ranges. Therefore, Optimal Stiffness could be obtained at D: Slope degree 60° by selecting maximum of A: FJ-Length with minimum of B: FJ-Pitch.

- FJ in vertical orientation can obtain higher performance due to its wider width than the corresponding FJ in horizontal orientation which help in increasing the bond-surface between the two-adherents.
- The regression equations for predicting the stiffness were verified. There was a little bit tolerance (not exceeded 12%) between the stiffness obtained from the equations and the numerical FEA model.

Last but not least, enhancing the existing FJ techniques will provide more efficient use of natural resources which will lead to mitigate the dire consequences from the improper use of nature. FJ technique could play a major role in exploiting the unused and inexpensive wasted short wood pieces which harm the environment. FJ can extend the scraps by joining them together end to end that will benefit both nature and humans.

In addition, these equations can be generalized as a guideline for designing and optimizing FJ spruce lumber. The application of these methods proves to be more sufficient for product design and development time in which data are not available.

Eventually, the development of the existing FJs techniques will lead to a great potential for wider structural applications. This will enable the engineering wood industry to produce a larger variety of the pieces of wood that are fabricated with optimal structural performance.

6.2. Recommendations

Some recommendations that might be helpful for designing a better experimental design space, and for fitting better prediction models, are as follows:

- Select slightly wider components' ranges to draw better interpretation of the results.
- The statistical design model types were selected focusing on the accurate prediction of the models parameters. There is no specific consideration for covering all the design space. Extra care is required to generate a satisfactory distribution of information that covers the entire design space not only part of it.
- The results showed that some models had small R-squared (R^2), Predicted R^2 (R^2_{Pred}) and large standard deviations. To this end, it might be useful to augment the design to increase the accuracy of the models or to fit higher order models.
- From the obtained regression equations, design tables can be established for FJ-geometry for the spruce specimens to make it useful and easy for structural applications such as: structural glulam beam, column, curved, and arched members.
- It would be recommended to do more experimental validation to verify the statistical design models to add more power to the study.
- Manufacture actual finger joints according to the optimized results to verify that the optimized results can be achieved.

REFERENCES

Barboutis, J., Vassiliou, V. and Karastergiou., S. (2005) 'Effect of the finger length on bending strength properties of the finger jointed steamed and unsteamed beech wood', *Second European Conference on Hardwood*, pp. 62–68.

Bustos, C. *et al.* (2003) 'Effects of curing time and end pressure on the tensile strength of finger-joined black spruce lumber', *Forest Products Journal*, 53(11/12), pp. 1–5.

Bustos, C. *et al.* (2011) 'Effects of end-pressure on the finger-joint quality of black spruce lumber: a microscopic analysis', *Maderas. Ciencia y tecnología*, 13(3), pp. 319–328. doi: 10.4067/S0718-221X2011000300007.

Christophe Morel Fourrier (1999) 'Structural Beam Laminations', in *Adhesives in timber systems*, pp. 22–28.

Dassault Systèmes Simulia (2013) 'Abaqus CAE User's Manual'.

Fortino, S. *et al.* (2012) 'A simple approach for FEM simulation of Mode I cohesive crack growth in glued laminated timber under short-term loading', *Rakenteiden Mekaniikka (Journal of Structural Mechanics)*, 45(1), pp. 1–20.

Gao, Y. *et al.* (2015) 'Numerical analysis of the bending properties of cathay poplar glulam', *Materials(1) Y. Gao, Y. Wu, X. Zhu, L. Zhu, Z. Yu, and Y. Wu (2015), 'Numerical analysis of the bending properties of cathay poplar glulam', Materials, 8(10): 7059–7073.*, 8(10), pp. 7059–7073. doi: 10.3390/ma8105362.

Habipi, B. and Ajdinaj, D. (2015) ‘Wood Finger-Joint Strength as Function of Finger Length and Slope Positioning of Tips’, *International Journal of Engineering and Applied Sciences (IJEAS)*, 2(12), pp. 128–132.

Hernández, R. E., Coman, R. and Beauregard, R. (2011) ‘Influence of machining parameters on the tensile strength of finger-jointed high-density black spruce lumber’, *Wood and Fiber Science*, 43(1), pp. 2–10.

Holmberg, S., Persson, K. and Petersson, H. (1999) ‘Nonlinear mechanical behaviour and analysis of wood and fibre materials’, *Computers & Structures*, 72(4–5), pp. 459–480. doi: 10.1016/S0045-7949(98)00331-9.

Kumar, V. S. K., Sharma, C. M. and Gupta, S. (2015) ‘Compression and flexural properties of finger jointed mango wood sections’, *Maderas. Ciencia y tecnología*, 17(ahead), pp. 0–0. doi: 10.4067/S0718-221X2015005000015.

Li, H. T. *et al.* (2016) ‘Flexural performance of laminated bamboo lumber beams’, *BioResources*, 11(1), pp. 929–943. doi: 10.15376/biores.11.1.929-943.

Liu, C. (2006) ‘Selecting Material Parameters in Abaqus for Cohesive Elements Defined in Terms Of Traction-Separation’, *Mechanical Engineering*, pp. 1–2.

Montgomery, D. C. (2012) *Design and Analysis of Experiments, Design*. doi: 10.1198/tech.2006.s372.

NLGA-SPS-1 (2014) ‘Special Products Standards for Finger-Joined Structural Lumber’, *National Lumber Grades Authority*.

NLGA-SPS-4 (2014) ‘Special Products Standards for Finger-Joined Machine Graded Lumber (FJ-MGL)’, *National Lumber Grades Authority*.

Özçifçi, A. and Yapıcı, F. (2008) ‘Structural performance of the finger-jointed strength of some wood species with different joint configurations’, *Construction and Building Materials*, 22(7), pp. 1543–1550. doi: 10.1016/j.conbuildmat.2007.03.020.

Rajan, S. (2018) *Response Surface Methodology , Analysis & Interpretation*.

Sandhaas, C. (2012) *Mechanical Behaviour of Timber Joints With Slotted-in Steel Plates*.

Sandhaas, C. and Van de Kuilen, J. W. G. (2013) ‘Material Model for Wood’, 58(2), pp. 179–200.

Tran, V. D., Oudjene, M. and Meausoone, P. J. (2014) ‘FE analysis and geometrical optimization of timber beech finger-joint under bending test’, *International Journal of Adhesion and Adhesives*. Elsevier, 52, pp. 40–47. doi: 10.1016/j.ijadhadh.2014.03.007.

Tran, V., Oudjene, M. and Méausoone, P. (2015) ‘Experimental and numerical analyses of the structural response of adhesively reconstituted beech timber beams’, *COMPOSITE STRUCTURE*. Elsevier Ltd, 119, pp. 206–217. doi: 10.1016/j.compstruct.2014.08.013.

Tree Canada - Arbres Canada (no date) *Newfoundland & Labrador - Black spruce (Picea mariana)*. Available at: https://treecanada.ca/en/resources/canadas-arboreal-emblems / newfoundland-labrador-black-spruce-picea-mariana/ (Accessed: 30 January 2017).

Yeh, M. C. and Lin, Y. L. (2012) 'Finger joint performance of structural laminated bamboo member', *Journal of Wood Science*, 58(2), pp. 120–127. doi: 10.1007/s10086-011-1233-7.

Zhou, H. Bin and Ren, H. Q. (2012) 'Factors Influencing Structural Performance of Finger-Jointed Chinese Fir Lumber', *Applied Mechanics and Materials*, 174–177, pp. 635–640. doi: 10.4028/www.scientific.net/AMM.174-177.635.